Atmospheric Aqueous Aerosol Interfaces:
Thermodynamic Modeling and Biphasic Microfluidic Flows with Fluid-Fluid Interfaces

A THESIS
SUBMITTED TO THE FACULTY OF THE GRADUATE SCHOOL
OF THE UNIVERSITY OF MINNESOTA
BY

Hallie C. Boyer

IN PARTIAL FULFILLMENT OF THE REQUIREMENTS
FOR THE DEGREE OF
DOCTOR OF PHILOSOPHY

Professor Cari Dutcher, *advisor*

May, 2017

Acknowledgment

Immediately, I must acknowledge my advisor, Professor Cari S. Dutcher, for her incredible mentorship and guidance. Professor Dutcher's capability as a research scientist has first and foremost inspired me; however, in an effort not to overstate, Cari has been a considerate and perceptive advisor. She has mentored me through the struggles and victories of pursuing a PhD. Through Cari's expertise in complex fluids and solution thermodynamics, I was introduced to the disciplines of atmospheric aerosols and microfluidics. A heartfelt thanks to Cari for enabling my graduate career to be as rewarding as it was productive. I look forward to my future work on this path and I cannot thank Cari enough for taking a chance on me as one of her first students. I am honored to be the first PhD graduate in the Dutcher group!

I am grateful to my other excellent mentors: Professors Chris Hogan, Lian Shen and Peter McMurry in Mechanical Engineering and Ilja Siepmann in Chemistry. I have known Professor Hogan since my first week of graduate school. I took his advanced aerosols class, which has helped me greatly in my research by giving context to particle processing in the atmosphere. Professor Shen taught two great classes that I took; one was on thermodynamics of fluid flows and the other, convection. These classes enhanced my understanding in my experimental work with microfluidic flows. Professor Siepmann taught a challenging class on statistical mechanics. This class has been very beneficial to me in my modeling research, since I use statistical mechanics heavily. I would like to especially thank Professors Hogan, Shen and Siepmann for sitting on my PhD committee during my preliminary oral exam and my final defense. Peter McMurry and I have something other than aerosols in common: we were both Peace Corps Volunteers in Africa. In addition to his advice for getting through

graduate school and venturing into a research career, I also really appreciate our discussion on this special experience we both had.

Next, I acknowledge my fellow members of the Dutcher group. Dr. Andrew Metcalf has been a source of support, counsel, knowledge, and encouragement. Much of my work in microfluidics was facilitated by his initial developments at device fabrication and data analysis. His detailed note-taking and coding have benefitted everyone else working on microfluidics. (As a sidenote, his son was born four days ago as I write this, so congrats Andrew and welcome little Nathanael!). To my labmates past and present: Nikolas, Peter, Eric, Lucy, Shweta, Athena, Ellie, and Archit. Peter's and Lucy's codes were really helpful for my first two papers. Lucy, Shweta, and Archit have been marvelous cohorts and a pleasure to work with in the microfluidics side of the lab. Although I have not gotten a chance to work directly with Nick, Athena, or Ellie, I recognize their brilliance and awesomeness as colleagues and as people. I'm going to miss you all when I leave and I wish you all the best of luck in finishing grad school and in your future endeavors.

Of course, my family members have been utterly selfless and understanding, not just as I have been writing this thesis, but for the last five years. I thank my Mom, Dad, Ardie, and Mike, and my new family-in-law, Tammy, Jeff, Jon, Elle, Rome', Amy, and baby Jasey for their love and support for me throughout this program. My husband-to-be, Joe, is an absolute miracle. Thank you to all my family for your love, patience, and support.

Dedication

This thesis is dedicated to my wonderful (soon-to-be) husband, Joe.

Abstract

Surface properties of atmospheric aerosol particles are crucial for accurate assessment of the fates of liquid particles in the atmosphere. Surface tension directly influences predictions of aerosol particle activation to clouds, as well as indirectly acts as a proxy for chemical surface partitioning. Challenges to predicting surface tension are posed by the chemical complexity of particles, which contain mixtures of water soluble compounds of both surface-active organics and inorganic electrolytes. The interface itself is varied in that it may be liquid - vapor, as in the surface of an aerosol particle with the ambient air, or liquid - liquid, as in the interior surfaces that exist in multiphase particles. These surface-based properties and their relevant processes govern atmospheric aerosol particle size, morphology, composition, and growth. This thesis explores aqueous aerosol interfaces through thermodynamic modeling of liquid-vapor surfaces to predict surface tension and biphasic microfluidic measurements of liquid-liquid interfacial tension of atmospheric aqueous aerosols.

Using adsorption isotherms and statistically mechanically derived expressions for entropy and Gibbs free energy, predictive modeling of surface tension as a function of concentration for aqueous solutions containing both water-soluble organic species and inorganic electrolytes is demonstrated for a breadth of atmospherically relevant solutes. Alcohols, polyols, sugars and organic acids represent the organic solutes. Nitrates, sulfates and chlorides represent the electrolytes. A unique feature of the model is the surface partition function, where the solvent molecules (waters) represent adsorption sites, and solute molecules can displace more than one waters either positively or negatively, therefore the model implicitly depends on solute size and surface propensity. For binary solutions, model parameters are eliminated through

strong correlations with solute properties, such as molar volume for organics and surface-bulk partitioning coefficients for electrolytes. A multicomponent model is derived for an arbitrary number of solutes, using no further parametrization beyond the optimized binary cases. For organic and inorganic aqueous mixtures, model predictions agree excellently with available data, including novel measurements made at supersaturated concentrations using optical tweezers. To further complement model predictions, interfacial tensions are measured for liquid-liquid systems using microfluidics.

Microfluidic platforms afford many advantages, including high throughput, rapid prototyping of devices (using soft photolithography), small sample volume and potential for controlled manipulation of thermal, mechanical, and chemical changes. Microfluidics also offers an appropriate lengthscale, where surface forces influence the system far more than gravitational and inertial forces. In this thesis, atmospheric aerosol interfaces are examined using droplet microfluidics, where the droplets chemically represent the aerosol phase dispersed in an immiscible surrounding phase. The droplets consist of either a chemical mimic or a sample obtained from smog chambers that simulate atmospheric chemistries. Interfacial tensions of numerous individidual droplets are measured with low sample volumes.

Surface and interfacial tensions are applicable to industrial, environmental, and biological engineering areas and this work could be valuable to each of these fields. In this thesis, model development and experimental techniques are presented in the context of atmospheric chemistry to facilitate further application to atmospheric processes, such as aerosol-cloud activation.

Contents

List of Tables

List of Figures

Chapter 1

Introduction to Atmospheric Aerosol Fluid-Fluid Interfaces[†]

Mass transfer and chemical reactions occur at aerosol interfaces between particles and the ambient environment, supporting growth processes and heterogeneous chemistry. These surface-based properties and processes govern atmospheric aerosol particle size, morphology, composition, and growth. In aerosol particles, mass exchanges are regulated by ambient conditions, especially temperature and relative humidity, thereby affecting particle water content and solute concentration. Aqueous atmospheric aerosols have been established as chemically complex microenvironments, [1] containing a wide representation of organics, inorganics, neutral molecules, and ions. They also exhibit multiple separated phases, where solids partition from liquids and the aqueous phase partitions from immiscible liquids, [2] creating complex morphologies. Figure 1.1 is a schematic of the chemical thermodynamics of atmospheric aqueous aerosol with equilibrium partitioning, showing the many equilibria present among solids, liquids,

[†]Part of this chapter was submitted recently in Boyer, H.C. and Dutcher, C.S., Atmospheric Aqueous Aerosol Surface Tensions: Isotherm-based Modeling and Biphasic Microfluidic Measurements,*Journal of Physical Chemistry A*, **2017**, Feature Article

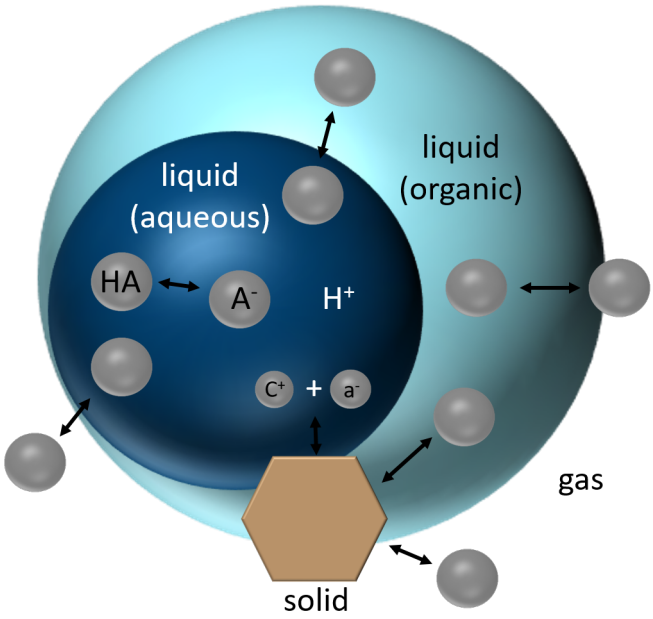

Figure 1.1: Chemical thermodynamics of aerosol particles showing equilibrium molecular partitioning of solids, liquids, and gases, as well as water rich (aqueous) and water poor (organic) liquids. The aqueous phase is partially engulfed in the organic, although complete engulfing and side-by-side separation also may occur, depending on the interfacial energies between the liquids.

and gases.

Atmospheric aerosols play a significant role in our climate regulation, yet it remains a challenge to precisely characterize their direct and indirect effects. Among atmospheric constituents, the largest uncertainty in net solar radiative forcing is attributed to aerosol particles. [3] Due to heightened presence of pollutants, aerosol particles greatly impact cloud albedo, [4–7] which defines their optical properties. Cloud albedo therefore determines the proportion of sunlight that either reflects back into space or gets absorbed and scattered, collectively known as the direct effect. Atmospheric aerosol influence on cloud formation, known as the indirect effect, manifests by particles acting as seeds, or cloud condensation nuclei (CCN). [8–16] To

accurately describe processes leading to CCN activation, classical Köhler theory [17] requires water activity, or the Raoult term, and surface tension [16], or the Kelvin term [18]; otherwise the quantities are parametrized. [11] For predicting CCN activation, the solute term has been well-studied in dilute and concentrated multicomponent aqueous solutions, however the effects of solutes on the surface term remain mostly neglected and, in some cases, simplifed to zero concentration, or pure water. [19, 20] For aqueous aerosol particles, both negative and positive changes in surface tension induced by solutes must be considered.

Water soluble organics typically depress surface tension, [7, 13] lowering the critical supersaturation point above which particles activate to cloud droplets. In order to account for solute surface effects in large-scale aerosol models, surface tensions and surface-bulk partitioning must be considered. Comprehensive thermodynamic treatment of aerosols is necessary in order to consider composition-dependent properties both in solution and at the interface.

In the atmosphere, it has been demonstrated that particles exhibit internal phase separation, [2, 37, 38] leading to instances of non-spherical equilibrium morphologies. Particle morphology can significantly influence the particle's ability to scatter light and interact with water vapor and other ambient chemical species. The internal microphysical structure can be described with equilibrium phase partitioning and interfacial tensions. Interfacial tension measurements inform deviations from spherical particle shapes as well as indicate solute effects at the surface, such as solute surface propensity. In particles containing liquid-liquid phase partitioning, high interfacial tension can result in non-spherical morphologies. [37] Morphological predictions have been previously studied using spreading coefficients, which are a function of surface

and interfacial tensions. [37]

In this thesis, aqueous aerosol interfaces are characterized through measurements of liquid-liquid interfacial tension and modeling of liquid-vapor surface tension. Our results could inform global aerosol models that predict aerosol particle activation to cloud droplets by providing surface tensions as a function of concentration and temperature. Coupled with biphasic microfluidic experiments, the model could provide predictions of multiphase particle morphology, which is traditionally hard to measure in situ.

Introduction to aerosol interface modeling

Recently, Wexler and Dutcher [21] developed a thermodynamic model of surface tension. The theoretical framework was developed in solution using adsorption isotherms and statistical mechanics to predict water activity and solute activity of multi-component aqueous solutions. [22–24] The surface tension model demonstrated that for solutions containing two components, a solute and a solvent, a single expression gives surface tension as a function of solute activity calculated from the multilayer adsorption isotherm. As chapter 2 will outline, model applicability was then extended by parametrizing data sets for single solutes and reducing the parameters through physical interpretation from the work of Boyer, Wexler, and Dutcher. [25] Chapter 3 will discuss a ternary model developed to treat partially dissociating organic acids. [26] Chapter 4 will show the derivation and application of a multicomponent model for an arbitrary number of solutes. [27] It will be shown that the success of the surface tension model for liquid-vapor interfaces complements experimental measurements of liquid-liquid interfacial tension.

The surface tension model is based on the adsorption isotherm in solution. [22–24,

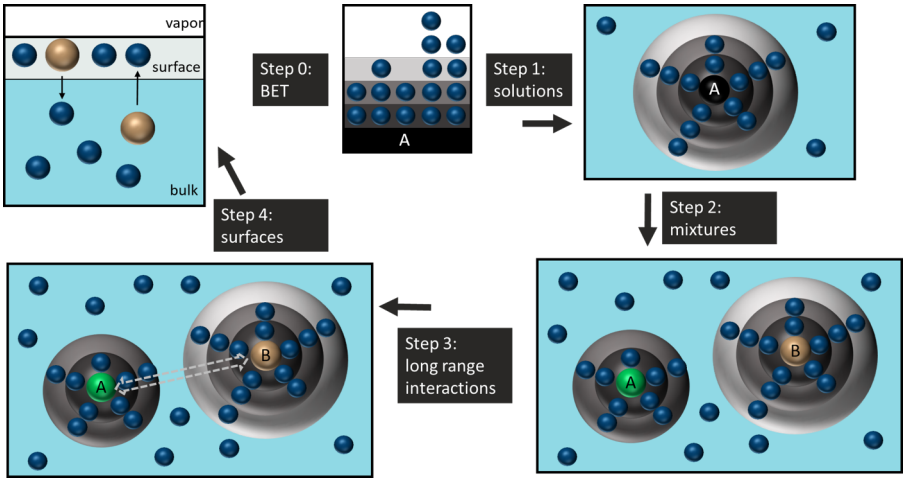

Figure 1.2: Thermodynamic model application of lattice adsorption of gases (BET adsorption isotherm) in solution (steps 1-3) and surfaces (step 4). After step 1, blue circles represent water molecules. Black, green, and orange circles represent solutes. The layers of waters indicate solute hydration and the disordered molecules are in the bulk of the solution.

28, 29] The theoretical framework is outlined schematically in Figure 1.2 for the solution thermodynamic model and in Figure 1.3 for the interface. The first step in Figure 1.2 is monolayer lattice adsorption on planar surfaces originated by Langmuir. [30] Brunauer-Emmett-Teller (BET) theory added a second monolayer, or multilayer, and allowed further numbers of layers with the same associated energy. [31]

The application of adsorption isotherms to solutions was initiated by Stokes and Robinson [32] for concentrated electrolyte aqueous solutions by applying BET theory. In solution, solvent molecules were the adsorbates and solutes were adsorbents. Ally and Braunstein [33] extended the Stokes and Robinson work to accommodate ternary solutions. A modification was presented by Guggenheim, Anderson, and de Boer known as the GAB isotherm in which a second layer was added. [34–36] In the adsorption isotherm developed by Dutcher, Ge, Wexler, and Clegg, [22] a unique energy was assigned to each layer and the number of layers were determined for each

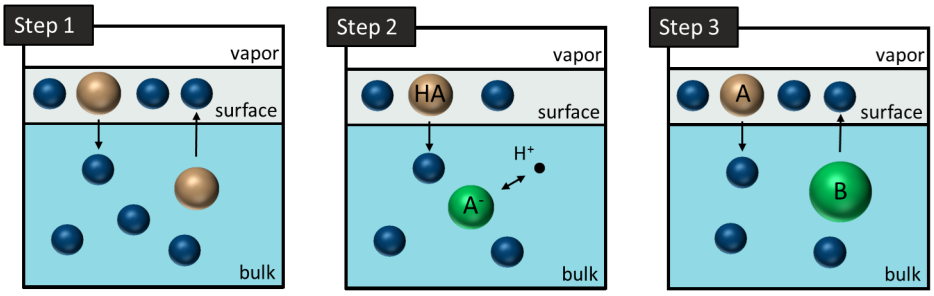

Figure 1.3: Thermodynamic model application to the surface for single solute solutions (step 1), partially dissociating aqueous organic acids (step 2), and multicomponent solutions (step 3). Blue circles represent water molecules. Green and orange circles represent solutes. The waters at the surface are displaced by surface-sorbing molecules or promoted to the surface by bulk-sorbing molecules.

individual solute. Expressions for Gibbs free energy were derived using statistical mechanics and were used to find water activity and solute activity. The model successfully captured activities and osmotic coefficients across the entire concentration range by setting a reference point at pure solute, even for electrolytes. The model was also successfully extended to multicomponent solutions (step 2, Figure 1.2), [24] and included long-range Coulombic interactions to reduce parameters [28], and partial dissociation of organic acids (step 3, Figure 1.2). [29]

The adsorption isotherm used in solution was subsequently introduced to the surface by Wexler and Dutcher [21] to derive a model of surface tension (step 4, Figure 1.2). There were three key distinctions between the solution property model and the surface tension model: 1) the roles of adsorbates and adsorbents were reversed, making solvent molecules the adsorbents and solutes the adsorbates, 2) since the solutes were allowed to adsorb at the surface in the new framework, the monolayer (surface) was separate from the multilayer (bulk), and 3) a single layer was sufficient at the surface to calculate surface tension; however, multilayers could be added if

required. The monolayer represents either the solutes that have adsorbed at the surface and removed solvents (water molecules in the case of aqueous solutions), or solutes that have remained in the bulk and have promoted a number of solvents to the surface. New expressions for Gibbs free energy and entropy were found again using statistical mechanics, where a surface partition function accounts for the available configuration states of the surface and a bulk partition function accounts for solute mixing between the surface and bulk phases.

Introduction to studying interfaces using biphasic microfluidics

At the microscale, surface forces dominate over gravitational and intertial effects. Hudson et al. [42] and Cabral and Hudson [43] developed techniques for measuring interfacial tension in a microfluidic device similar to the design shown in Figure 1.4. Fluid flow of two intersecting fluids occurs upstream, where one fluid becomes the inner dispersed phase and the other becomes the surrounding continuous phase. Downstream, the droplets are carried by the surrounding fluid through a transit channel with constrictions that induce an extensional flow field and cause the droplet to deform. Droplet deformation is highly dependent on interfacial and viscous forces. Interfacial tension is measured using theory based on emulsion studies by G. I. Taylor [40] and J. M. Rallison [41], which uses force balances between the stresses from extensional flow, the material deformation of the interface and the restoring forces trying to keep the droplet spherical.

Knowledge of interfacial tensions can facilitate predictions of particle equilibrium morphology through calculations of spreading coefficients. [37] Our results could therefore apply to aerosol systems where organic lenses or shells cause deviations from spherical shapes that are challenging to observe in situ. In Chapters 5 and

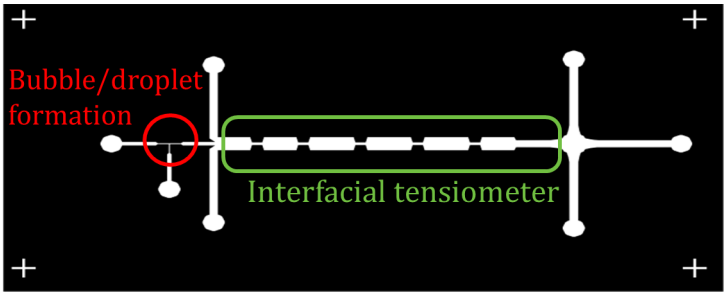

Figure 1.4: Microfluidic devices design for interfacial tensiometry.

6, atmospherically relevant liquid-liquid interfaces are studied using the aforementioned techniques. In particular, aqueous phases are studied containing secondary organic aerosol (SOA), an important and abundant class of particulate matter that are formed through photochemical reactions. [44–46] Characterization of SOA formation processes and equilibrium is poorly characterized and must be studied further to better understand atmospheric aerosol's role in climate and human health. [44, 47] Results are discussed in these chapters for interfacial tensions of SOA particle mimics as well as their implications for particle morphology. [39] Chapter 5 is a study of solute mixtures containing methylglyoxal and formaldehyde, plus an inorganic electrolyte, ammonium sulfate. Aqueous phases with these specific water soluble compounds have been shown to evolve chemically through self-reactions. [48] Chapter 6 includes results for aqueous dicarboxylic acid solutions as well as chamber samples of SOA material extracted in methanol. For the organic acids, both their binary aqueous solutions and their ternary solutions with ammonium sulfate are studied.

Discussions on the use of surface tension model predictions and measurements to calculate spreading coefficients are presented in the subsequent chapters. The microfluidic experimental work in conjuction with modeling of aqueous surfaces offers insight into the influence of solute on aerosol particle morphologies. The next chapter

focuses on the binary surface tension model, its application to aqueous electrolytes and organics, and a reduction of parameters, towards fully predictive surface tension modeling.

Chapter 2

Parameter Interpretation and Reduction for a Unified Statistical Mechanical Surface Tension Model[†]

Predictive models of surface tension as a function of solute concentration are vital to numerous environmental, biological and industrial processes. In atmospheric aerosol sciences, for example, models of surface tension are needed in order to predict homogenous nucleation, growth of these nanoparticles to cloud condensation nuclei (CCN), activation of CCN to clouds, aerosol particle morphology, and other aerosol properties that influence weather, climate and health. However, atmospheric aerosol microenvironments are composed of highly complex chemical solutions, comprising both electrolytes and organic compounds. Limited composition data for aerosol particles are available from a combination of field and laboratory measurements [49–52] and model predictions [53, 54], yielding only indicators of the organic composition (e.g., oxygen to carbon ratios, structural groups present) [55, 56]. The challenge for

[†]Part of this chapter was carried out in collaboration with Anthony Wexler in Boyer, H.C.; Wexler, A.; and Dutcher, C.S., Parameter Interpretation and Reduction for a Unified Statistical Mechanical Surface Tension Model, *Journal of Physical Chemistry Letters*, **2015**, *6*, 3384-3389.

models of surface tension relevant to atmospheric particles is predicting surface tension from only indications of composition.

There has been extensive research in the literature relating surfactant properties of molecules to their group composition and structure. Quantitative Structure Property Relationships (QSPR) for surfactants have been employed to relate properties of molecules to pure compound surface tension, the critical micelle concentration, the cloud point, and hydrophilic-lipophilic balance [57]. These correlations use a few key molecular properties such as the Kier and Hall zeroth order connectivity index [58], the second order structural information index [59], the relative number of oxygen and nitrogen atoms (relevant to the surface activity of amines and related compounds), and the dipole moment [60]. These correlations and others suggest that simple relationships may exist between surface tension and organic compound moieties in atmospheric particles and other applications.

Recently, Wexler and Dutcher [21] used statistical mechanics of multilayer sorption to develop a surface tension model where the surface sorbs a single layer of solute molecules. This model was successful over the full range of concentrations from pure solvent to pure solute, and worked equally well for organics and electrolytes in aqueous solutions. Therefore, the model has important implications for many fields, where surface properties are important over a large concentration range. The goal of the current work is to identify model parameter values for a breadth of solutes, relate them to solute physical properties, and demonstrate a parameter free, fully predictive surface tension modeling for single solute aqueous solutions. Literature values for surface tension (see Wang et al, 2011 [61] for one compendium) and solute molecular properties are used to develop relationships for the parameters in the Wexler and

Dutcher surface tension model.

Methods

Wexler and Dutcher [21] employ statistical mechanics to derive an expression that relates solution surface tension to solute activity. An expression for the Gibbs free energy, G ≈ E – TS, was derived, where the energy term includes solute molecular energies in the surface and bulk, and the entropy is found from Boltzmann's formula, S = kLnΩ, and partition functions for surface and bulk. In this framework, the Gibbs dividing surface is implicitly defined by assuming single layer adsorption is sufficient to describe the surface tension as a function of composition. Evaluating the system in the limit of pure solvent gives the surface tension of the solvent alone, assumed to be water in this work (σ_W). The solution surface tension was found to be

$$\sigma = \sigma_w + \frac{kT}{rS_w} Ln\Big(\frac{1 - Ka_s}{1 - Ka_s(1 - C)}\Big) \tag{2.1}$$

where k is Boltzmann's constant, T is temperature, S_W is the surface area occupied by one solvent molecule, and a_S is the solute activity. The remaining quantities (r, K, and C) are model parameters, where r is the average number of water molecules each solute molecule displaces from the surface, and K and C are related to the sorption energies. Specifically, K ≡ exp(ε_{SB}/kT) and C ≡ exp((ε_{SS}-ε_{SB})/kT), where ε_{SB} and ε_{SS} are the energies of each solute molecule in the bulk and surface, respectively.

Wang and coworkers [61] also developed a single solute surface tension model as a function of solute activity. Equation 2.1 can be rearranged to $\sigma = \sigma_W - (kT/rS_W)Ln(1 + KCa_S/(1 - Ka_S)$, comparable to equation 13 of the Wang model, $\sigma = \sigma_W + kT\Gamma^{\sigma,0}Ln(1 - Ka_S/(1 - Ka_S))$ in which K has the same meaning in both models, and surface excess $\Gamma^{\sigma,0}$ has a similar role to r in equation 2.1. Note that the

Wang model does not use an equilibrium solute partitioning C parameter. Pegram and Record [62] developed a thermodynamic analysis that treats individual ionic contributions to surface tension increments (their equations 1 and 3) for dilute aqueous electrolyte solutions. Separating single ion effects lead to their calculations of ion solute-bulk partitioning and, by addition, electrolyte partition coefficients, denoted as K_P. It will be shown in this work that K_P strongly correlates with the C parameter in our model, which represents equilibrium partitioning of the solute between surface and bulk.

Equation 2.1 can be solved for pure solute obtaining an expression for C in terms of the pure solvent and solute σ_S surface tensions:

$$C = 1 - \frac{\left[1 - (1 - K)exp\left\{(\sigma_W - \sigma_S)\frac{kT}{rS_W}\right\}\right.}{K} \tag{2.2}$$

which can be used to eliminate one of the three free parameters from equation 2.1 when pure solute surface tension is known. For liquid solutes, such as many liquid organics, solute surface tension data are widely available. For electrolyte salts, most of which are solid at 298 K, σ_S values can be predicted using the method described in Dutcher and coworkers [63] by extrapolating high-temperature molten salt surface tension to 298 K using a slope and intercept based on melting temperature, cation radius, and molar volume.

As shown by Wexler and Dutcher [21], equation 2.1 has a limiting case for compounds where partitioning to the surface is strongly preferred, such as alcohols, for

which $\varepsilon_{SB} \rightarrow -\infty$ causing K$\rightarrow$ 0. In this case, equation 2.1 reduces to

$$\sigma = \sigma_w - \frac{kT}{rS_w} Ln(1 + Ka_s) \tag{2.3}$$

a form of the Szyszkowski equation [64]. If the pure solute and solvent surface tensions are known, parameter K' can be found by evaluating equation 2.3 in the limit of $a_S \rightarrow 1$,

$$Ln(K' + 1) = \frac{rS_w(\sigma_W - \sigma_S)}{kT} \tag{2.4}$$

leaving r as the single fit parameter. In this work, solute activity values, a_S, in the above equations were calculated from solvent activity or molality data using the solution thermodynamics model of Dutcher and co-workers [22–24], who extended the monolayer adsorption isotherms of Brunauer -Emmett -Teller (BET) [31], Guggenheim-Anderson- deBoer (GAB) [34–36], and Ally and Braunstein [33] to multiple monolayer formulation. The surface tension model fit parameter values are identified by minimizing the root mean squared error, rmse $=\sqrt{\Sigma_1^{n_p}(\sigma_{fit} - \sigma_{data})^2/n_p}$

Organics

Surface tension predictions using equations 2.1 or 2.3 are shown in Figure 2.1 for representative aqueous solutions containing water-soluble organic compounds (see supplemental material for organics not shown in this figure). In the dilute range, surface tension depression is clearly steeper for surface active compounds that displace more waters from the surface reflected in larger values of the model parameter r. For example, referring to Table 2.1, r = 2.58, 3.00, and 4.56 for methanol, ethanol, and isopropanol, respectively, showing an increase in value with number of methyl groups. Since methyl groups increase molecular volume, it is expected that K', a function of

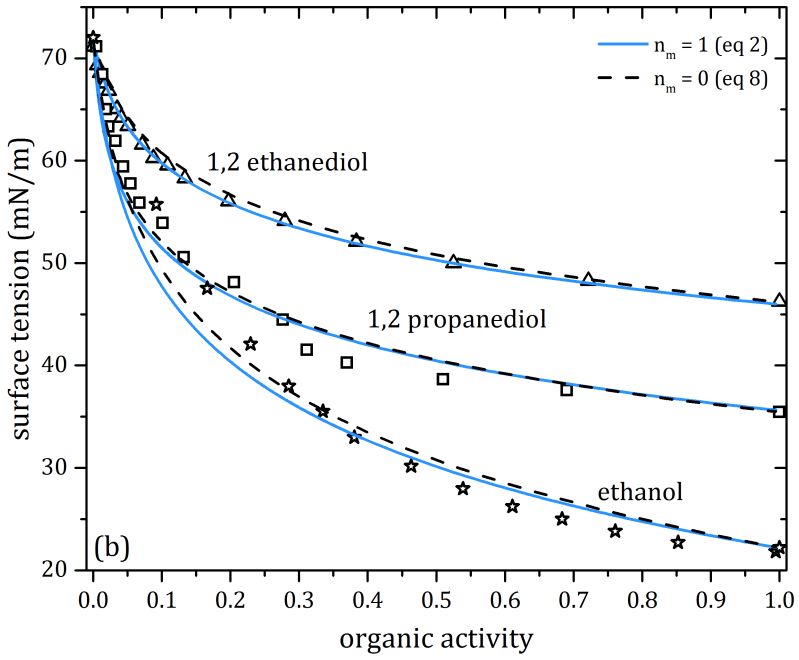

Figure 2.1: Surface tension as a function of solute activity for representative alcohols. Solid lines are model predictions using a single parameter and dashed lines use zero model parameters. There is a single parameter needed since sigmas is known for alcohols and C is not necessary in equation 2.3; K' is eliminated through the relationship with molar volume, v, (K'=$e^{(0.067v))} - 1$).

r through equation 2.4, depends on solute volume.

Figure 2.2 shows the relationship between K' and solute molar volume v for simple alcohols with one hydroxyl group (black circles) and glycols with two hydroxyl groups (blue circles). Size dependence is observed for both classes of alcohols because of the competing effects from hydroxyl groups increasing bulk solubility and methyl groups increasing surface preference. A regression following the functional form of eq 4 gives ln(K'+1)=0.067v.

Solute	r (fit)	K (calc.)	σ_S	$C^{a,b}$	$rmse$	n_P^c	x_{max}^c	$ref.^c$
$methanol$	2.58	22.32	22.0	-	1.21	14^e	1	H.C.B.
$ethanol$	3.00	69.19	22.2	-	3.48	15	1	[65]
$2-propanol$	4.30	291.2	21.0	-	2.74	14	1	[65]
$1,2ethanediol$	6.42	57.79	46.2	-	0.341	18	1	[66]
$1,2propanediol$	5.82	173.6	35.5	-	1.880	18	1	[66]
$1,3butanediol$	6.77	326.7	37.0	-	1.24	18	1	[66]
$1,4butanediol$	7.47	322.6	43.8	-	0.816	18	1	[66]
$sorbitol^d$	20.3	334.4	60.2	-	0.197	7	0.041	[67]
$glycerol^a$	33.1	0.91	62.0	331.7	0.0969	11	1	[68]
$sucrose^b$	-34.7	0.99	121	2.932	0.0468	5	0.16	[69]

Table 2.1: Summary of model parameters and data references for organic solutes. The activity sources are from adsorption isotherm DGWC, [22–24] with energy of multilayer adsorption parameters derived by a power law fit for glycerol and Coulombic potential interaction [28] for the rest of the solutes. The limiting case fit equation 2.3, and a single adjustable parameter, r, was used for all compounds except sorbitol, glycerol, and sucrose. For all equation 2.3 fits, the value of K' was obtained with equation 2.4. [a]For glycerol, the full form of the model (equation 2.1) was used, with r and K as adjustable parameters. [b]For sucrose, the full model (equation 2.1) was used, with r, K, and σ_s as adjustable parameters. A calculated value for C is supplied for both full model equation 2.1 cases. [c]Number of data points, n_p, given in listed reference (ref.), with a maximum mole fraction, x_{max}. [d]For sorbitol, the pure solute surface tension is not known, so the limiting case equation 2.3 fit was used with 2 parameters, r and σ_s. [e]Methanol surface tension measurements were taken by the author with a Wilhemy plate method.

Combining equations 2.3 and 2.4 to eliminate r gives

$$\sigma = \sigma_W - (\sigma_W - \sigma_S)\frac{Ln(1+K'a_S)}{Ln(1+K')} \tag{2.5}$$

Since K' is only a function of v, equation 2.5 is a parameter-free model of surface tension for certain organic solutes as long as the pure solute surface tension and specific volume are known. Figure 2.1 shows excellent agreement among three treatments: the full model (equation 2.1) with 2 fit parameters, the limiting case model (2.3) with

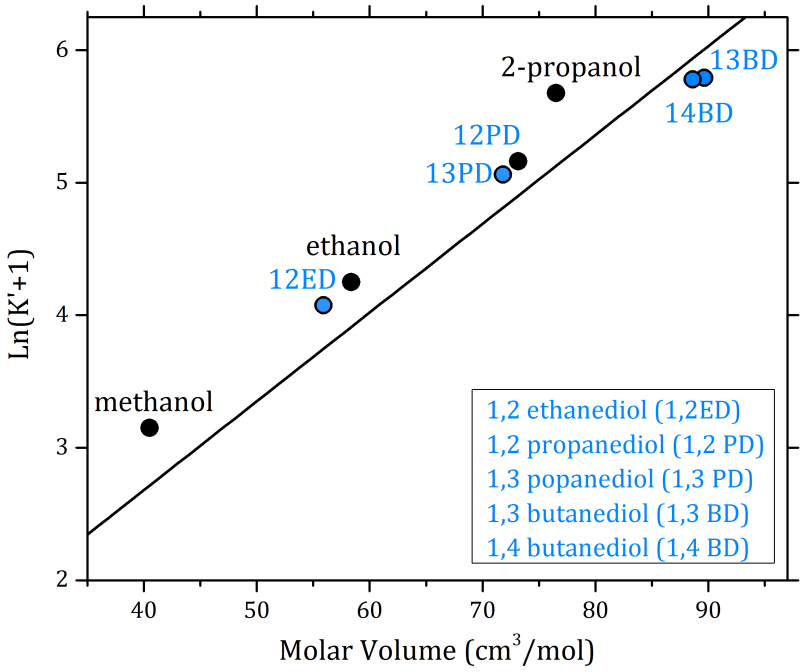

Figure 2.2: ln(K'+1) versus molar volume (cm^3/mol for alcohols with two hydroxyl groups and one hydroxyl group. The linear regression is ln(K'+1)=0.067v.

1 fit parameter, and the volume-based model (2.5) with no fit parameters.

Electrolytes

Whereas the surface tension of many surface active organics in aqueous solutions can be modeled by equation 2.3, the full three parameter model (equation 2.1) is needed for predicting surface tension for electrolyte solutions. In equations 2.1 and 2.2, there are three independent variables among r, K, C, and σ_S. A hypothetical value of pure solute surface tension, σ_S, at 298 K can be estimated using the methods of Dutcher et al. [63], thereby eliminating a parameter. Fitting r and K with the aqueous electrolyte surface tension data yields values of K similar for nearly all electrolytes addressed here. By treating K as a constant equal to 0.99, r is the only remaining fit

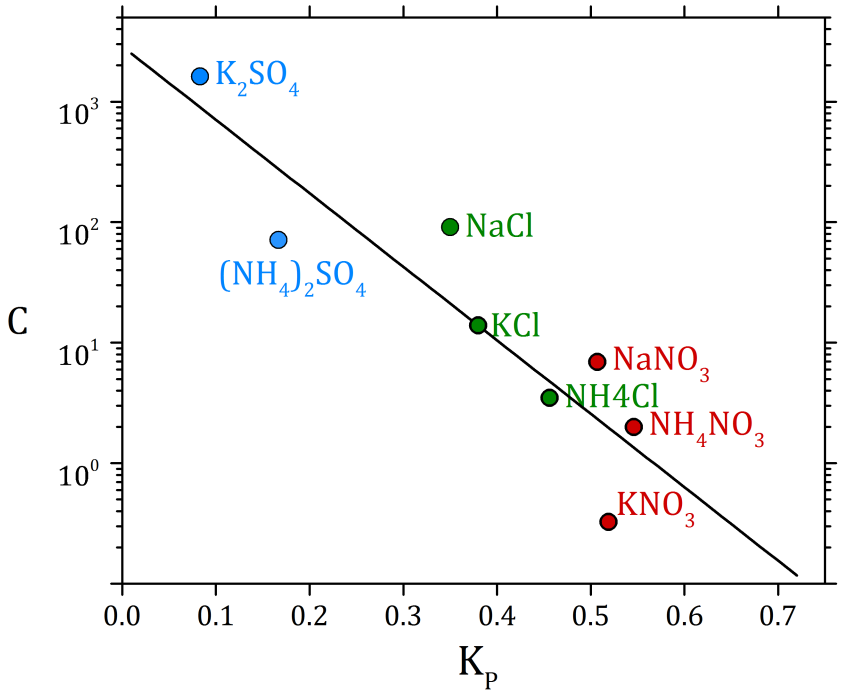

Figure 2.3: C versus partitioning coefficient K_P from Pegram and Record [62]. C values are found using an estimate for σ_S from Dutcher et al [63] and constant K = 0.99, leaving r as the only adjustable parameter. The exponential regression is C=$(2.878 * 10^4)e^{-14.0K_P}$.

parameter. Note that for surface active organics, values of K' are in the range of 30 to 200 since they partition to the surface much more readily than the electrolytes.

Equation 2.3 can be used to replace the remaining parameter, r, with the parameter C. Figure 2.3 shows the relationship between C and the partitioning coefficients K_P of Pegram and Record [62]. An important physical observation from this trend is that the propensity of specific ions to adsorb at the surface is dominated by anions, as shown by the clearly grouped electrolyte species in Figure 2.3. Also, a series of anion families emerges in order of most to least surface active, beginning

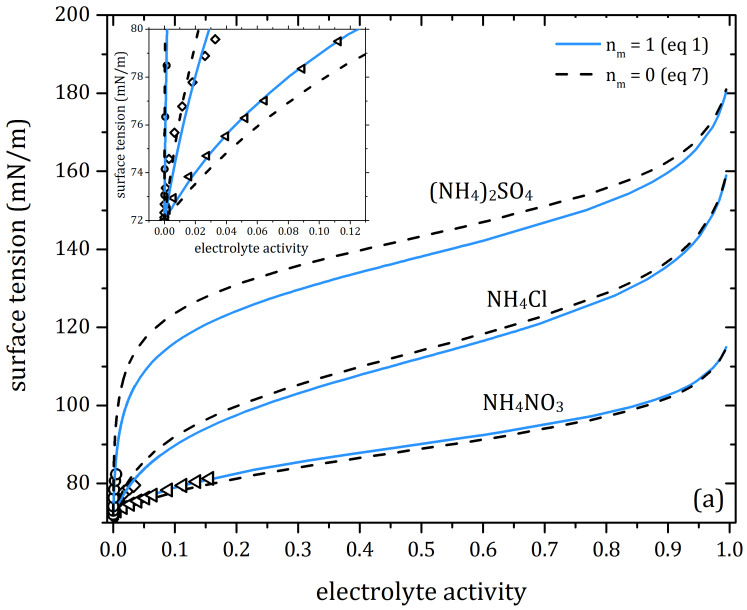

Figure 2.4: Surface tension as a function of electrolyte activity for ammonium sulfate, ammonium chloride, and ammonium nitrate. For all curves, pure solute surface tension, (σ_S), predictions were obtained from reference [69]. Solid lines are equation 2.1, keeping K as a constant equal to 0.99 and allowing r to vary. Dashed lines are parameter free fits with equation 2.6, where C is from the regression curve from Figure 2.3. Shown in the subplot are data points with surface tension curves in the limited ranges up to the solubility limit for each species. Data references are summarized in Table 2.3.

with nitrates, followed by chlorides then sulfates. The regression in Figure 2.3 is C=$(2.878 * 10^4)e^{-14.0K_P}$. Combining equations 2.1 and 2.2 to eliminate r gives

$$\sigma = \sigma_W - (\sigma_S - \sigma_W)\frac{Ln\left(\frac{1-Ka_S}{1-Ka_S(1-C)}\right)}{Ln\left(\frac{1-K}{1-K(1-C)}\right)} \tag{2.6}$$

Equation 2.6 reduces to equation 2.5 for C=1. Using K=0.99 and the regression above for C as a function of K_p in equation 2.6 produces a parameter-free model

Solute	$n_m = 2$ (eq 2.1)			$n_m = 1$ (eq 2.1)		$n_m = 0$ (eq 2.6)
	r	K	$rmse$	r	$rmse$	$rmse$
$NaCl$	-4.78	0.99	1.59	-4.78	1.58	3.56
KCl	-4.77	0.99	0.594	-4.76	0.559	0.559
NH_4Cl	-3.64	0.99	0.834	-3.64	0.844	0.794
$CaCl_2$	-32.8	0.99	0.407	-	-	-
$RbCl$	-3.72	0.99	0.932	-3.72	0.926	-
$NaNO_3$	-5.52	0.99	0.493	-5.52	0.493	2.49
KNO_3	-3.84	0.99	0.120	-3.84	0.120	3.60
NH_4NO_3	-6.74	0.99	0.146	-6.82	0.146	1.03
K_2SO_4	-3.51	0.97	0.280	-3.88	0.285	0.436
$(NH_4)_2SO_4$	-4.04	0.99	0.999	-4.04	0.999	2.57

Table 2.2: Summary of model parameters resulting from electrolytes fits using equation 2.1 following parameter reduction for aqueous electrolyte solutions. For $n_m = 2$, an estimated value for σ_s from reference [63] was used to eliminate an adjustable parameter. For $n_m = 1$, the average value $K = 0.99$ was used for all electrolytes while r was allowed to vary. For $n_m = 0$, the model inputs are pure solute surface tension estimates and partition coefficients by Pegram and Record. [62] The activity sources are all from adsorption isotherms; [22–24] for the sulfates and $CaCl_2$, activity parameters are derived from a power law fit; for all other species, the energy of multilayer adsorption parameters are derived from Coulombic interactions. [28]

that is fully predictive. Results of reduction to double parameter (r and K), single parameter (r), and zero parameter versions of the model are summarized in Table 2.2.

Representative electrolyte results for surface tension predictions of ammonium aqueous solutions are found in Figure 2.4, using the full three parameter model (equation 2.1, $n_m = 3$), reduced model with pure electrolyte surface tension predictions from reference [69] (equation 2.1, $n_m = 2$), further reduced model with K as a constant (equation 2.1, $n_m = 1$), and finally a parameter free model based on calculated partitioning coefficients from reference [62] (equation 2.6, $n_m = 0$). Uncertainty of model parameters decreased through parameter reduction. For NH_4NO_3, standard errors

Solute	n_p	m_{max}	reference
$NaCl$	22^a	6.0	[69]
KCl	12	14	[69]
NH_4Cl	7	8.0	[69]
$CaCl_2$	10	7.0	[70]
$RbCl$	12	6.9	[71]
$NaNO_3$	15	14.0	[69]
KNO_3	7	3.6	[70]
NH_4NO_3	12	12.0	[69]
K_2SO_4	13	4.8	[69]
$(NH_4)_2SO_4$	7	14.0	[69]

Table 2.3: Summary of data references for aqueous electrolyte solutions. Number of data points, n_P, is given in the column labeled reference (ref.), with a maximum molality, m_{max} in kg/mol. ^{a}Data was taken from both reference [69] and by the author via Wilhemy plate method.

for r and K in the two parameter treatment are 0.621 and 0.138, respectively; for the single parameter fit in which K is held at 0.99, the standard error for r is 0.0557, a significant decrease from the 2 parameter fit. Similarly, for $(NH_4)_2SO_4$, standard errors for r and K are 1.68 and 0.428, and for just r, 0.267. For NH_4Cl, standard errors for r and K are 3.75 and 1.30, and for just r, 0.24. In general, the rmse values reported in Tables 2.1 and 2.2 are on the order of magnitude of 0.1 to 1.0 mN/m. The literature sources report errors no greater in magnitude than 0.1 mN/m. For example, Vasquez et al. [65] reports a maximum experimental error of $\pm$ 0.4% mN/m after averaging 5 to 10 measurements. Also, the International Critical Tables [69] typically report standard deviations of $\pm$ 0.1 mN/m.

Surface tension predictions of unparametrized electrolytes

Zero parameter model predictions are presented here for three electrolytes which were not used in the parameter reduction: NaI, NaBr, and KBr. Three parameters are needed to evaluate equation 2.6 (K, C, and σ_s). Pure electrolyte surface tension, σ_s, is calculated from Dutcher et al. 2010 [63] for each of the three compounds. Energy parameter C is found from the expression in Figure 2.3, since K_P values are available for each compound in Pegram and Record [62]. Finally, energy parameter K is a constant near unity, a global value among electrolytes. Figures 2.5 -2.7 show available data for each binary solution and parameter free model predictions. Plots showing a short ranges of data and model treatment are in Appendix B. Table 2.4 contains parameter values used for each case and error of fit.

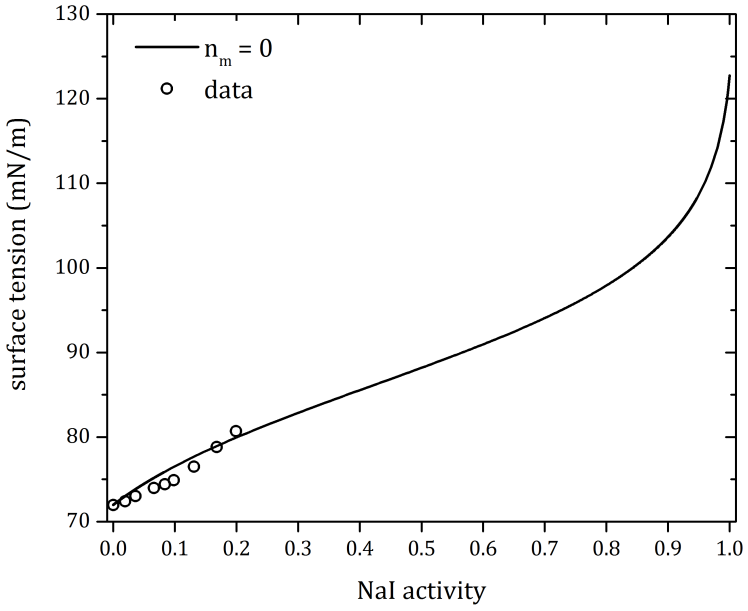

Figure 2.5: Surface tension of aqueous NaI versus solute activity. The cirlces are data and the solid line is parameter-free surface tension model predictions (equation 2.6), where n_m signifies the number of fit parameters. Parameter values and error of fit are in Table 2.4. Data source: Abramzon and Gaukhberg, 1993 [70].

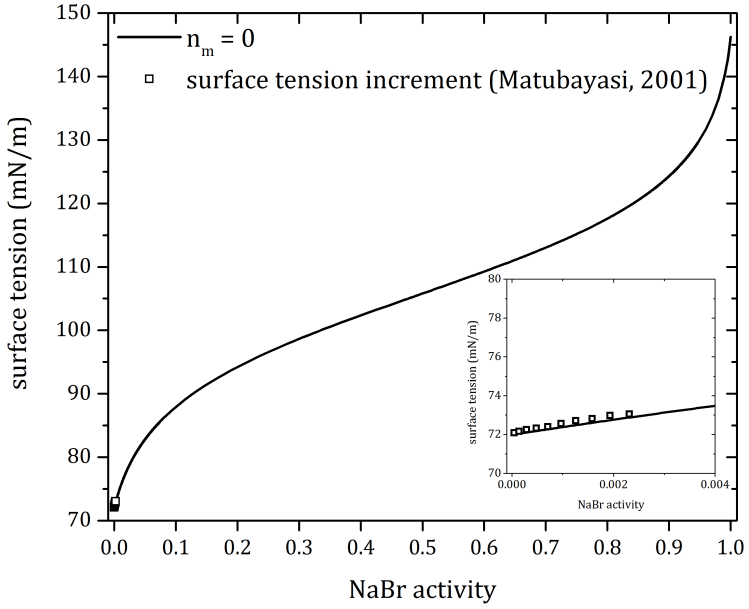

Figure 2.6: Surface tension of aqueous NaBr versus solute activity. Circles and squares are data and the solid line is parameter-free surface tension model predictions (equation 2.6), where n_m signifies the number of fit parameters. Parameter values and error of fit are in Table 2.4. Data sources: circles, surface tension data taken in optical tweezers from University of Bristol collaborators in the lab group of Professor Jonathan P. Reid (for more details on optical tweezers surface tension measurements, see Chapter 4); squares, dilute surface tension increment measurements from Matubayasi et al. 2001 [72]

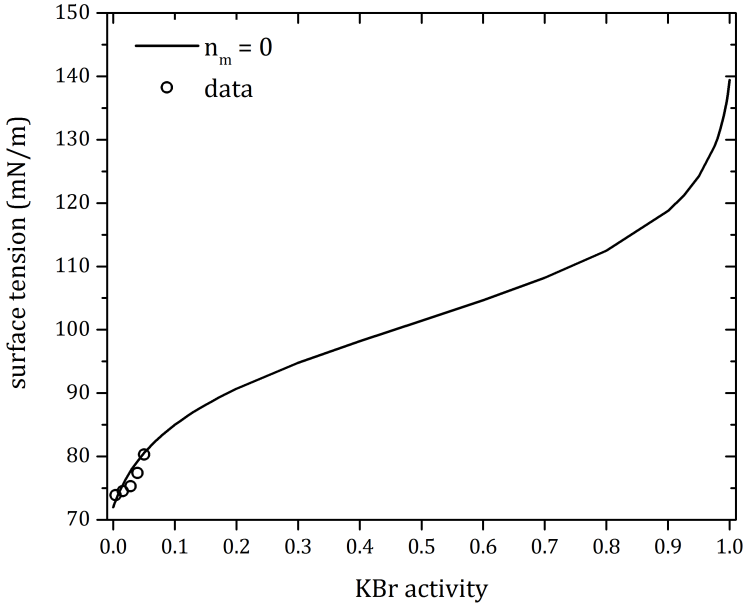

Figure 2.7: Surface tension of aqueous KBr versus solute activity. Circles are data and the solid line is parameter-free surface tension model predictions (equation 2.6), where n_m signifies the number of fit parameters. Parameter values and error of fit are in Table 2.4. Data source: Abramzon and Gaukhberg, 1993 [71].

electrolyte	r	K	C	σ_s (mN/m)	$K_P{}^a$	$rmse$
NaI	-3.78	0.99	7.34	122.75	0.591	1.078
$NaBr$	-4.84	0.99	46.59	146.23	0.459	0.195^b
KBr	-4.67	0.99	34.72	139.40	0.480	1.503

Table 2.4: Summary of parameter values and rmse of fit for sodium iodide, sodium bromide, and potassium bromide. ^{a}Partition coefficients for electrolytes from Pegram and Record, 2007 [62]. ^{b}Rmse value computed for Matubayasi [72] data only.

Summary

A model of surface tension as a function of solute activities was applied to electrolytes and organic aqueous solutions. Solute concentrations were converted from molalities to activities using the adsorption isotherm model of Dutcher et al. [22–24] Surface tension as a function of activity is given by equation 2.1 for both organic and electrolyte solutions, and requires 3 model parameters: r, K, and σ_S.

For the organics considered in this study, except glycerol and sucrose, a form of the Szyszkowski equation [64], equation 2.3, was used. The Szyszkowski equation, a limiting case of the full model where the solute primarily resides on the surface, requires only two free parameters, K' and σ_S. Since σ_S is known for many liquid organics, only a single model parameter, K', is needed for this limiting case. We showed that a simple relationship between the model parameter, K', and the molar volume, v, of the pure solute provides reasonably accurate estimates for surface tension as a function of solute activity, given in equation 2.5.

For binary electrolytes, the full model, equation 2.1 which requires three parameters, was applied to all electrolyte species represented in this work, including sulfates, nitrates, and chlorides. Additionally, bromides and an iodide were treated with no parametrization. Estimates of pure solute surface tension, σ_S, from Dutcher et al [63] at 298 K were used to replace that parameter. Next, evaluation of many electrolytes suggested that K could be considered a constant with a value of 0.99 reducing the number of model parameters to one. To obtain a parameter-free model for electrolytes, partitioning coefficients from Pegram and Record [62] were compared to our results for C, eliminating the final parameter. The reduced-parameter model for surface tension of binary electrolyte solutions is given in equation 2.6. The model of Wexler and

Dutcher was derived from fundamental statistical mechanics considerations and was shown in that work to accurately represent the surface tension-activity relationship over the full range of concentrations from pure solvent to pure solute. That model had two or three parameters, depending on the nature of the solute. In this work we related these parameters to properties of the solute in aqueous solution to increase the predictive capabilities of the model for compounds with insufficient data. The predictive surface tension models developed here will have important implications for fundamental thermodynamic studies of specific ion attraction or repulsion from the surface [73] and surface forces produced by image charges and ion hydration [74], as well as in crucial applications ranging from desalination of water [75] to atmospheric aerosol particle dynamics modeling [76, 77].

Appendices B and C provide details on model treatment of each electrolyte (Appendix B) and organic (Appendix C) in this chapter. The purpose of these appendices is to provide access to raw data and model parameters for data poor regimes of certain compounds or to extend the arbitrary model. Appendices E and F provide Matlab fitting routines for electrolytes (Appendix E) and organics (Appendix F).

In the next chapter, the surface tension model framework is reinstated for an important class of organic compounds that are abundant in the atmosphere: partially dissociating organic acids. Surface partition functions are derived for ternary aqueous solutions, where the acids are treated as two solutes (a neutral non-dissociated acid and an ionic dissociated acid) of equal size and opposite surface propensity.

Chapter 3

Statistical Thermodynamic Model for Surface Tension of Aqueous Organic Acids with Consideration of Partial Dissociation†

Strong evidence of organic solutes residing on the surface of aqueous solutions, particularly atmospheric aerosol droplets, is observed through surface tension depression with increasing amounts of organic solute. [77,78] In the atmosphere, the presence of organic compounds at liquid-vapor aerosol interfaces can significantly alter aqueous aerosol particle dynamics, including growth processes through the Kelvin effect [18,79] and their potential for acting as seed particles in the atmosphere, or cloud condensation nuclei (CCN), [12,13,80] which in turn affects supersaturation and cloud formation. To accurately describe processes leading to CCN activation, classical Köhler theory [17] requires water activity and surface tension, [16] otherwise the quantities

†Part of this chapter was published in Boyer, H.C. and Dutcher, C.S.; Statistical Thermodynamic Model for Surface Tension of Aqueous Organic Acids with Consideration of Partial Dissociation, *Journal of Physical Chemistry A*, **2016**, 4368-4375

are parameterized. [11] Surface tension is therefore an important property for determining interfacial processes of aqueous organics in the atmosphere.

Water soluble organic acids such as carboxylic and dicarboxylic acids are abundant in the troposphere, [81] spanning concentrated urban areas as well as vast open spaces over the Pacific Ocean and Antarctica. [82–89] For dicarboxylic acids, adsorption at the liquid-vapor interface and orientation of the neutral form of acid molecules have been verified experimentally using vibrational sum frequency spectroscopy (VSFS) and theoretically with molecular dynamics (MD) simulations. [90–92] In mixtures, there is recent evidence by Öhrwall and coworkers [93] of enhanced surface adsorption of the acid salt in the presence of electrolyte solutes, especially those commonly found in the atmosphere such as ammoniums. Additionally, it was shown by Lee and coworkers [94] that if the organic acid is a weak surfactant, like citric acid, halogen cations may be promoted to the surface instead of the organic molecules.

Several investigations into the structural properties and processes of surface adsorbed aqueous organic acids have been performed. While surface preference of organic acids has been shown to increase with number of carbons per molecule, there is also a possibility of solute expansion upon adsorption at the interface. [95] Additionally, their impacts on surface-based heterogeneous chemistry in the atmosphere have been observed through surficial reactions with the ambient gas phase, which have potential to release organic acids from the aerosol particle matrix into ambient surroundings through heterogeneous oxidation. [1, 96] Their potential to react with gas phase radicals in the atmosphere affects aerosol particle hygroscopicity, morphology and optical transmissivity. It is therefore critical to understand the effects of dicarboxylic acids, with consideration of their partial dissociation, on aqueous surfaces to

better predict their role in atmospheric interfacial processes.

Surface tension measurements of some aqueous organic acids are available in current literature. Hyvärinen et al. [97] provide tabulated surface tension data of oxalic, succinic, malic, malonic, maleic, and cis-pinonic acids, all measured with a thermally controlled Wilhemy plate apparatus. Found in Granados et al. [98] are data for aqueous formic, acetic, proprionic, and butyric acids by the pendant drop method. These datasets are limited to sub-saturated solutions, yet realistic atmospheric conditions create chemically complex systems in which one solute can be super-saturated with respect to other solutes, thus presenting a key challenge for obtaining atmospherically applicable thermodynamic data of aqueous solutions. One recent approach by Morris and coworkers [99] uses atomic force spectroscopy (AFM) to measure surface tension of deliquesced aqueous droplets with electrolyte and organic acid solutes, including NaCl, malonic and glutaric acids, at varying relative humidities. Fewer surface tension measurements are needed if predictive modeling is available. Wexler and Dutcher [21] recently developed a surface tension model of single solute aqueous solutions that extends across the full range of concentrations from pure water to pure solute. The model framework follows statistical mechanical methods of Dutcher et al. [22–24] and Ohm et al., [28] in which they used multilayer adsorption isotherms in solution and accounted for long- and short-range interactions between solute entities. Thermodynamic solution properties such as water activity, solute activity, and osmotic coefficient can be predicted using this isotherm approach. A key distinction between the solution and interface models is the assignment of sorbates and sorbents. In the solution model, the solvent (water) adsorbs to sites on the solute, while at the interface, solutes sorb to sites at the interface by displacing solvent molecules.

Applying the theoretical framework of multilayer adsorption to the interface results in a model that successfully predicts surface tension of binary aqueous solutions as a function of solute activity. [21, 25]

In this work, we apply the binary model to organic acid aqueous solutions for oxalic, malic, malonic, succinic, maleic, glutaric, citric, acetic, formic, propionic, and butyric acids. We consider the partial dissociation of these acids using dissociation constants K_1 (mol/kg) from literature sources, [100–102] thereby accounting for the concentration of both neutral and dissociated forms of the acid. To predict surface tension of these ternary systems, we extend the surface tension model to allow two separate solute species. Equilibrium of organic acid partial dissociation in water is represented by $HA \rightleftharpoons H^+ + A^-$ for species with one carboxylic group. In the case of di- and tricarboxylic acids, only the first dissociation is considered here, and the notation HA is used to symbolize organic acids with either one, two, or three functional groups.

Theory

Consider two types of solute species: a non-dissociating, neutral organic (HA) and a dissociating acid (H^+A^-). The maximum number of waters at the surface is $N_{s,w}$, which represents surface adsorption sites for the solutes. The surface partition function for the organic species is

$$\Omega_{s,HA} = \frac{N_{s,W}!_{\bar{r}}}{(N_{s,W} - \bar{r}N_{s,HA})!_{\bar{r}}(\bar{r}N_{s,HA})!_{\bar{r}}} \tag{3.1}$$

and for the acid species, the number of configurations remaining on the leftover adsorption sites is

$$\Omega_{s,H^+A^-} = \frac{(N_{s,W} - \bar{r}N_{s,HA})!_{\bar{r}}}{(N_{s,W} - \bar{r}N_{s,HA} - \bar{r}N_{s,H^+A^-})!_{\bar{r}}(\bar{r}N_{s,H^+A^-})!_{\bar{r}}} \tag{3.2}$$

where $N_{s,HA}$ and N_{s,H^+A^-} are the number of neutral organic and dissociated acid solute molecules displacing water molecules from the surface. In the single solute case from prior work, [21] r is a model parameter that represents the average number of water molecules displaced from the surface by a single solute molecule and therefore implies molecular size and surface density. Here, multifactorial skip $\bar{r}$ represents a collective effect of the two types of molecules, neutral and dissociated, together displacing $\bar{r}$ water molecules from the surface.

Multiplying equations 3.1 and 3.2, the surface partition function is

$$\Omega_{surface} = \frac{N_{s,W}!_{\bar{r}}}{(N_{s,W} - \bar{r}N_{s,HA} - \bar{r}N_{s,H^+A^-})!_{\bar{r}}(\bar{r}N_{s,HA})!_{\bar{r}}(\bar{r}N_{s,H^+A^-})!_{\bar{r}}} \tag{3.3}$$

A bulk partition function is defined to represent surface-bulk mixing of the neutral and dissociating species, resulting in

$$\begin{aligned} \Omega_{bulk} &= \frac{N_{HA}!}{N_{s,HA}!N_{b,HA}!}\frac{N_{H^+A^-}!}{N_{s,H^+A^-}!N_{b,H^+A^-}!} \\ &= \frac{N_{HA}!}{N_{s,HA}!(N_{HA} - N_{s,HA})!}\frac{N_{H^+A^-}!}{N_{s,H^+A^-}!(N_{H^+A^-} - N_{s,H^+A^-})!} \end{aligned} \tag{3.4}$$

where $N_{b,HA}$ and N_{b,H^+A^-} are the number of neutral organics and acids in the bulk and where N_{HA}=$N_{s,HA}$+$N_{b,HA}$ and $N_{H^+A^-}$=N_{s,H^+A^-}+N_{b,H^+A^-}. Configurational entropy is obtained from Boltzmann's formula, S=kLn($\Omega_{surface}\Omega_{bulk}$. Using Stirling's

approximation including skips $\mathrm{Ln}(\mathrm{N}!_{\bar{r}}) = \frac{N}{\bar{r}}\mathrm{Ln}\frac{N}{\bar{r}}\text{-}\frac{N}{\bar{r}}$,

$$
\begin{aligned}
&Ln(\Omega_{surface}\Omega_{bulk}) \\
&\qquad = N_{HA}Ln\frac{N_{HA}}{N_{HA}-N_{s,HA}} + N_{H^+A^-}Ln\frac{N_{H^+A^-}}{N_{H^+A^-}-N_{s,H^+A^-}} \\
&\qquad + \frac{N_{s,W}}{\bar{r}}Ln\frac{N_{s,W}}{N_{s,W}-\bar{r}N_{s,HA}-\bar{r}N_{s,H^+A^-}} \\
&\qquad + N_{s,HA}Ln\frac{(N_{s,W}-\bar{r}N_{s,HA}-\bar{r}N_{s,H^+A^-})(N_{HA}-N_{s,HA})}{\bar{r}N_{s,HA}^2} \\
&\qquad + N_{s,H^+A^-}Ln\frac{(N_{s,W}-\bar{r}N_{s,HA}-\bar{r}N_{s,H^+A^-})(N_{H^+A^-}-N_{s,H^+A^-})}{\bar{r}N_{s,H^+A^-}^2}
\end{aligned}
\tag{3.5}
$$

The system energy is the sum of all molecular energies,

$$
\begin{aligned}
E = &-N_{s,W}\varepsilon_{s,W} - N_{b,W}\varepsilon_{b,W} - N_{s,HA}\varepsilon_{s,HA} - N_{b,HA}\varepsilon_{b,HA} - N_{s,H^+A^-}\varepsilon_{s,H^+A^-} \\
&- N_{b,H^+A^-}\varepsilon_{b,H^+A^-}
\end{aligned}
\tag{3.6}
$$

which can be rearranged as

$$
\begin{aligned}
E = &-N_{s,W}\Delta\varepsilon_{s,W} - N_W\varepsilon_{b,W} - N_{s,HA}\Delta\varepsilon_{s,HA} - N_{HA}\varepsilon_{b,HA} - N_{s,H^+A^-}\Delta\varepsilon_{s,H^+A^-} \\
&- N_{H^+A^-}\varepsilon_{b,H^+A^-}
\end{aligned}
\tag{3.7}
$$

and represents waters on the surface ($\varepsilon_{s,W}$) and bulk ($\varepsilon_{b,W}$) and solutes on the surface (ε_{s,H^+A^-}) and $\varepsilon_{s,HA}$) and bulk (ε_{b,H^+A^-} and $\varepsilon_{b,HA}$),$\Delta\varepsilon_{s,HA}$=$\varepsilon_{s,HA}$-$\varepsilon_{b,HA}$ and $\Delta\varepsilon_{s,H^+A^-}$=$\varepsilon_{s,H^+A^-}$-$\varepsilon_{b,H^+A^-}$, and total system waters N_W=$\mathrm{N}_{s,W}$+$\mathrm{N}_{b,W}$. Assuming system pressure and volume changes to be negligible so that energy is approximately the

system enthalpy and combining equations 3.5 and 3.7, Gibbs free energy is

$$\frac{G}{kT} \approx \frac{E}{kT} - Ln(\Omega_{surface}\Omega_{bulk}) \tag{3.8}$$

The surface area is needed to calculate surface tension. Area is defined as

$$Area = \bar{r}S_W N)s, HA + \bar{r}S_W N_{s,H^+A^-} + S_W(N_{s,W} - \bar{r}N_{s,HA} - \bar{r}N_{s,H^+A^-}) = S_W N_{s,W} \tag{3.9}$$

where S_W is the occupied area of one water molecule (0.1 nm^2). Taking the derivative of equation 3.8 with respect to area results in

$$\sigma = \sigma_W + \frac{kT}{\bar{r}S_W} Ln\Big(\frac{N_{s,W} - \bar{r}N_{s,HA} - \bar{r}N_{s,H^+A^-}}{N_{s,W}}\Big) \tag{3.10}$$

where surface tension of the solution is $\sigma = \frac{1}{S_W}\frac{\partial G}{\partial N_{s,W}}$ and surface tension of pure water, $\sigma = -\frac{\Delta\varepsilon_{s,W}}{S_W}$, is 71.98 mN/m at 298 K. In the limit of zero solute, the right hand side of equation 3.10 correctly limits to σ_W.

Expressions for the activities of the neutral organic component (a_{HA}) and the dissociating acid component ($a_{H^+A^-}$) are obtained from taking the derivative of equation 3.8 with respect to N_{HA} and $N_{H^+A^-}$, respectively, resulting in

$$K_{HA}a_{HA} = 1 - \frac{N_{s,HA}}{N_{HA}} \tag{3.11}$$

$$K_{H^+A^-}a_{H^+A^-} = 1 - \frac{N_{s,H^+A^-}}{N_{H^+A^-}} \tag{3.12}$$

where K_{HA}=exp($\varepsilon_{b,HA}$/kT) and $K_{H^+A^-}$=exp(ε_{b,H^+A^-}/kT). The condition of equilibrium partitioning between the surface phase and bulk phase is imposed by minimizing

equation 3.8 with respect to $N_{s,HA}$ and N_{s,H^+A^-}, resulting in

$$C_{HA} = \frac{\bar{r}N_{s,HA}^2}{(N_{s,W} - \bar{r}N_{HA} - \bar{r}N_{H^+A^-})(N_{HA} - N_{s,HA})} \tag{3.13}$$

$$C_{H^+A^-} = \frac{\bar{r}N_{s,H^+A^-}^2}{(N_{s,W} - \bar{r}N_{s,HA} - \bar{r}N_{H^+A^-})(N_{H^+A-} - N_{s,H^+A-})} \tag{3.14}$$

where C_{HA}=exp($\Delta\varepsilon_{s,HA}$/kT) and $C_{H^+A^-}$=exp($\Delta\varepsilon_{s,H^+A^-}$/kT). Replacing all unknown N quantities in the expression for Gibbs free energy with K and C energy parameters, equations 3.11-3.14 are combined to yield surface tension as a function of solute activities:

$$\sigma = \sigma_W - \frac{kT}{\bar{r}S_W} Ln\Big(1 + \frac{C_{HA}K_{HA}a_{HA}}{(1 - K_{HA}a_{HA})} + \frac{C_{H^+A^-}K_{H^+A^-}a_{H^+A^-}}{(1 - K_{H^+A^-}a_{H^+A^-})}\Big) \tag{3.15}$$

In the next section, the model is recast to include the quantity σ_{acid}, which represents surface tension in the limit of pure solute. This provision allows the organic acids with known surface tension, for example acetic (σ_{acid} = 27.0 mN/m) and formic (σ_{acid} = 37.03 mN/m) acids, to reach an appropriate value of σ in equation 3.15 that must equal σ_{acid}. For organic acids which are solid at 298 K, σ_{acid} yields a hypothetical value for the liquid organic acid state.

Surface tension versus composition data of binary aqueous solutions with organic acids were found in literature sources such as Hyvärinen et al. [97] and Granados et al. [98] and also collected by the author with a Wilhemy plate system (Digital Tensiometer K10ST by Krüss, Table 3.1). Concentrations were converted to activities of the dissociating and non-dissociating species based on Raoult's Law, assuming ideal mixtures. The relative concentrations of the dissociating and non-dissociating

x	m (mol/kg)	$\rho\times 10^{-3}$ (kg/L)	σ (mN/m)	st. dev.[a]
		glutaric acid		
0.00316	0.176	1.000	68.6	0.1
0.00974	0.546	1.013	65.0	0.1
0.0167	0.941	1.028	62.4	0.3
0.0345	2.00	1.064	60.3	0.1
0.0600	3.54	1.069	57.9	0.1
0.0727	4.35	1.090	57.4	0.1
0.0862	5.23	1.112	56.9	0.1
0.121	7.63	1.132	54.6	0.2
		citric acid		
0.00528	0.295	1.013	71.5	0.1
0.00978	0.548	1.032	70.8	0.1
0.0219	1.24	1.080	69.7	0.0
0.0489	2.85	1.128	68.3	0.1
0.0573	3.37	1.140	68.3	0.1
0.0688	4.10	1.187	68.0	0.1
0.0846	5.11	1.207	68.0	0.0
0.116	7.28	1.281	67.8	0.1

Table 3.1: Mole fraction (x), density (ρ), and surface tension (σ) of dicarboxylic acid taken with a Wilhemy plate apparatus (Digital Tensiometer K10ST by Krüss) at T = 298 K. Standard deviations are based on 3 trials at each concentration. [a]Standard deviations are based on three trials at each concentration.

species can be found by using known dissociation constants, K_1, [100–102] given in Table 3.2 on a molality basis. The calculated molality of the non-dissociated acid and the acid salt can be converted to mole fractions, which are used to determine the mole-fraction based solute activities [103] used in the model equations in the following section. Concentrations were converted to activities of based on Raoult's Law, assuming ideal mixtures.

Methods

Nominally, equation 3.15 requires five parameters ($\bar{r}$, C_{HA}, K_{HA}, $C_{H^+A^-}$, $K_{H^+A^-}$). Since $K_{H^+A^-}$=exp(ε_{b,H^+A^-}/kT) in the model development by Wexler and Dutcher [21]

and ε_{b,H^+A^-} is defined to be negative, K_{HA} tends towards zero since the neutral organic form of the acid is known to be primarily surface active. Consequently, C_{HA} becomes very large so that organics adsorbed on the surface contribute to the change in surface tension. The second term in the logarithm in equation 3.15 can thus be rewritten as $C_{HA}K_{HA}a_{HA}$, or $K'_{HA}a_{HA}$. Note that the K'_{HA} here is used differently from equation 3.15 because it has absorbed C_{HA}. The model is reduced to

$$\sigma = \sigma_W - \frac{kT}{\bar{r}S_W} Ln\Big(1 + K'_{HA}a_{HA} + \frac{C_{H^+A^-}K_{H^+A^-}a_{H^+A^-}}{(1 - K_{H^+A^-}a_{H^+A^-})}\Big) \tag{3.16}$$

In the limit of pure solute, there are hypothetically dissociated and non-dissociated forms of the acid just as there are in aqueous solution, and thus the activities of each are equal to the pure solute mole fraction, denoted as x_{HA}* and $x_{H^+A^-}$* respectively. Solving for $C_{H^+A^-}$ under these conditions gives

$$C = \Big(\frac{1 + K_{H^+A^-}x^*_{H^+A^-}}{K_{H^+A^-}x^*_{H^+A^-}}\Big)\big\{exp\big((\sigma_W - \sigma_{acid})\bar{r}S_W/kT\big)K'_{HA}x^*_{HA} - 1\big\} \tag{3.17}$$

and substituting into equation 3.16, yields the full ternary model for surface tension,

$$\begin{aligned}\sigma = \sigma_W - \frac{kT}{\bar{r}S_W} Ln\Bigg(1 + K'_{HA}a_{HA} \\ + \frac{a_{H^+A^-}}{x^*_{H^+A^-}}\Big(\frac{1 + K_{H^+A^-}x^*_{H^+A^-}}{1 + K_{H^+A^-}a_{H^+A^-}}\Big)\Big\{exp\Big(\frac{\sigma_W - \sigma acid)\bar{r}S_W}{kT}\Big) - K'_{HA}x^*_{HA} - 1\Big\}\Bigg)\end{aligned} \tag{3.18}$$

In order to apply equation 3.18, predictions are needed for $\bar{r}$, σ_{acid}, K'_{HA}, and $K_{H^+A^-}$, detailed below.

Neglecting dissociation, equation 3.18 reduces to the binary model in the limiting

case for surface active organics:

$$\sigma = \sigma_W - \frac{kT}{\bar{r} S_W} Ln(1 + K'_{HA} a_{HA}) \tag{3.19}$$

which is the same form of the surface tension model derived by Wexler and Dutcher [21] and represents a form of the Szyszkowski equation. [64] Estimates for $\bar{r}$ and σ_{acid} can be directly obtained from equation 3.19 and applied to the full ternary model in equation 3.18 as these quantities do not change whether the system is treated as one solute or two solutes. In the limit of pure solute,

$$\bar{r} = \frac{S_W}{kT} Ln(1 + K'_{HA}) / (\sigma_W - \sigma_{acid}) \tag{3.20}$$

Equation 3.19 was fit to surface tension data from literature, allowing K'_{HA} and σ_{acid} to vary and calculating $\bar{r}$ from equation 3.20. Parameter K'_{HA} was found to have a strong correlation with molar volumes of the pure solutes, as shown in Figure 3.1, with an exponential trend for acids with one functional group and a linear trend for those with two or three. Replacing K'_{HA} with estimates from the volume relationships in Figure 3.1 leaves σ_{acid} as the single remaining parameter, producing a physico-chemically based estimate from the size of solute molecules and the number of functional groups.

For $K_{H^+A^-}$, in recent work by Boyer et al., [25] it was found that the K parameter for a binary aqueous solution could be approximated as a constant near unity for dissociating species ($K_{H^+A^-}$) in this work), such as electrolytes which tend to reside in the bulk. The surface tension model they used was similar in form to equation 3.16 if a_{HA} were taken to be zero, producing a binary model for fully dissociating solutes like electrolytes. Following the results of Boyer et al., [25] $K_{H^+A^-}$ is held as a

constant equal to unity for all organic acids.

Finally, for K'_{HA}, this last remaining parameter in the ternary model is eliminated by employing the volume relationship from the binary case. Equating the logarithm arguments of equations 3.18 and 3.19 results in

$$K'_{HA,ternary} = K'_{HA,binary}\left(\frac{a_{HA} + a_{H^+A^-} - \frac{a_{H^+A^-}}{x^*_{H^+A^-}}\left(\frac{1+K_{H^+A^-}x^*_{H^+A^-}}{1+K_{H^+A^-}a_{H^+A^-}}\right)}{a_{HA} - x^*_{HA}\frac{a_{HA}}{x^*_{HA}}\left(\frac{1+K_{H^+A^-}x^*_{H^+A^-}}{1+K_{H^+A^-}a_{H^+A^-}}\right)}\right) \tag{3.21}$$

where $K'_{HA,ternary}$ represents K'_{HA} in equation 3.18 and $K'_{HA,binary}$ represents the value found from the binary model (equation 3.19). The activities of the non-dissociated and dissociated species (a_{HA} and $a_{H^+A^-}$,) and pure solute mole fractions of each species (x_{HA}* and $x_{H^+A^-}$*) are calculated from dissociation constant K_1. Since all inputs (σ_{acid}, $\bar{r}$, K'_{HA}, and $K_{H^+A^-}$) are previously derived or estimated, the ternary model in equation 3.19 is fully predictive for all organic acids studied here.

Surface tension data measured with a Wilhemy plate (Digital Tensiometer K10ST by Krüss) for glutaric acid and citric acid aqueous solutions at varying concentrations are reported in Table 3.1. All organic acids in this study are listed in Table 3.2, including their chemical formulae and properties.

Results for dicarboxylic acids and citric acid.

Results of model application without dissociation, referred to as the binary model (equation 3.19), are shown in Figure 3.2a and 3.2b for dicarboxylic acids and Figure 3.3 for citric acid. Parameters and errors are reported in Table 3.3. Values of parameters K'_{HA} for all organic acids in this work were found to strongly correlate with pure solute molar, as shown in Figure 3.1. For dicarboxylic acids and citric acid, a linear regression curve $K'_{HA,binary}$=7.0812v-278.65 and R^2=0.907 was used to predict

K'_{HA} for those species. To ensure appropriate limiting behavior in the range of small molecular size, the regression includes data points for formic and acetic acids because of their lower molar volume.

As described in the next results section, the monocarboxylic acid group has a separate K'_{HA} correlation with molar volume because K'_{HA} is related to number of carboxyl functional groups in addition to size. The single remaining parameter for dicarboxylic acids (and citric acid) using the binary model is σ_{acid}, a quantity that is not known due to these species existing in crystalline form at room temperature. Surface tension predictions following the volume based parameter reduction of K'_{HA} are shown in Figure 3.2a and 3.2b.

acid	formula	v (cm^3/mol)	solubility[a]	K_1 (mol/kg)	σ data ref.	max. x
formic	$C_2H_2O_2$	37.73		1.80×10^{-4} [b]	[104]	1.0
acetic	$C_2H_4O_2$	57.24		1.75×10^{-5} [b]	[98]	1.0
propionic	$C_3H_6O_2$	74.98		1.38×10^{-5} [c]	[104]	1.0
butyric	$C_4H_8O_2$	92.50		1.48×10^{-4} [c]	[98]	1.0
malic	$C_4H_5O_5$	83.34	145	3.98×10^{-4} [d]	[97]	0.0087
malonic	$C_3H_4O_4$	64.30	161	1.42×10^{-4} [d]	[97]	0.158
succinic	$C_4H_6O_4$	75.70	8.80	6.17×10^{-4} [d]	[97]	0.0117
glutaric	$C_5H_8O_4$	100.4	116	4.57×10^{-4} [d]	[e]	0.121
citric	$C_6H_8O_7$	115.4	162	7.41×10^{-4} [b]	[e]	0.116
oxalic	$C_2H_2O_4$	66.32	12.0	5.29×10^{-4} [d]	[97]	0.0146
maleic	$C_4H_4O_4$	73.00	80.40	1.19×10^{-4} [d]	[97]	0.1083

Table 3.2: Properties of organic acids. [a](g of acid/100 g of water) at 25 °C , *CRC Handbook of Chemistry and Physics*. [102].[b]Perrin [101]. [c]Saxena et al. [105]. [d]Clegg and Seinfeld [100]. [e]Taken by author with Wilhelmy plate method (see Table 3.1 for data).

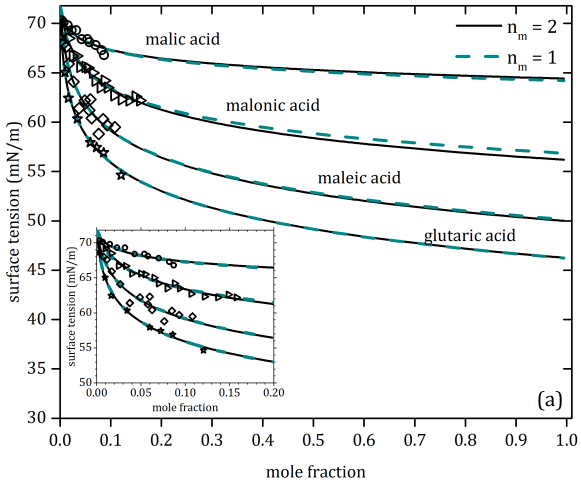

(a) Binary model for dicarboxylic acids of high solubility.

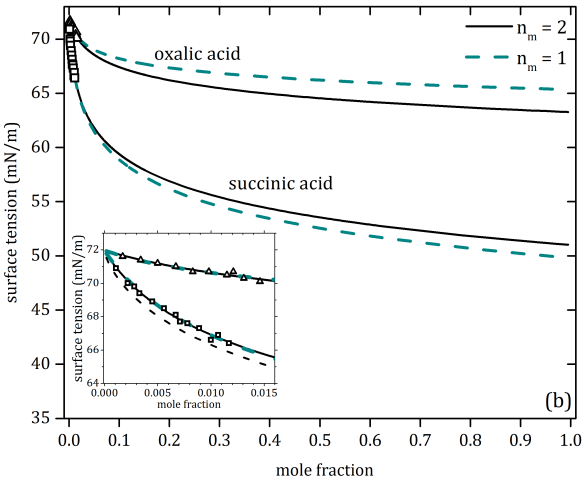

(b) Binary model for dicarboxylic acids of low solubility.

Figure 3.2: Surface tension versus mole fraction for dicarboxylic acids. The solid lines are from equation 3.19 with K'_{HA} and σ_{acid} as fit parameters and $\bar{r}$ is calculated from equation 3.20. See Table 3.4, column "binary, $n_m = 2$" for parameter values and rmse. The dashed lines are equation 3.19 with σ_{acid} as the only parameter. A predicted value of K'_{HA} is used from the regression curve in Figure 3.1 and is calculated from equation 3.20. See Table 3.4, column "binary, $n_m = 1$" for parameter values and rmse.

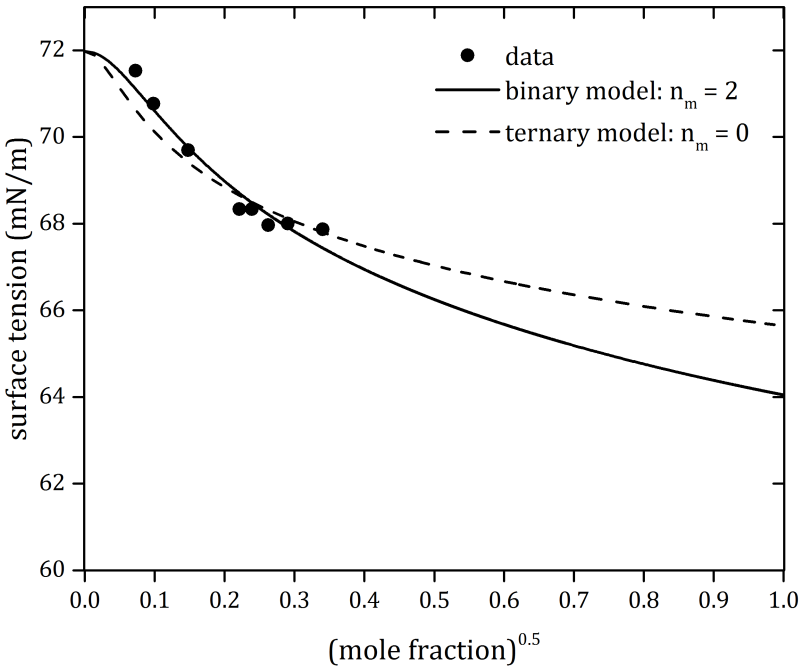

Figure 3.3: Surface tension versus square root of mole fraction for citric acid, where n_m signifies the number of model parameters for each curve. The solid line is equation 3.19, the binary model, using two fit parameters K'_{HA} and σ_{acid}. K'_{HA} can also be identified by the molar volume relationship in the caption of Figure 3.1, making σ_{acid} the single fit parameter. The dashed line is equation 3.18 using only the previously found binary parameters, since σ_{acid} should not vary and $K'_{HA,ternary}$ is computed from equation 3.21 and $K'_{H^+A^-}$, a constant equal to unity. See Table 3.3 for parameter values and error.

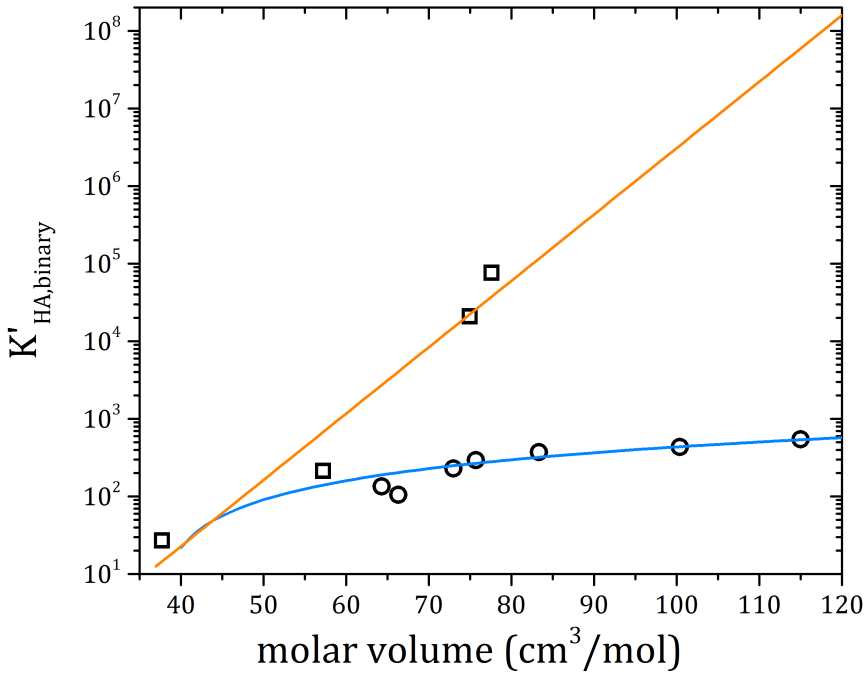

Figure 3.1: K'_{HA} obtained from fits using the binary model (equation 3.19) versus molar volume (cm^3/mol) for all organic acids in this study. Squares represent monocarboxylic acids (formic, acetic, propionic, and butyric) and circles represent dicarboxylic acids (glutaric, maleic, malic, malonic, oxalic, succinic) and a tricarboxylic acid (citric). The regression curve for carboxylic acids is $K'_{HA,binary}=0.0086e^{0.197}v$ and $R^2=0.947$. The regression curve for dicarboxylic acids is $K'_{HA,binary}=7.0812v-278.65$ and $R^2=0.907$, where v is molar volume. For corresponding molar volumes, refer to Table 3.2.

acid	σ_{acid}			$\bar{r}$		
	n_m=2	n_m = 1	n_m=0	n_m=2	n_m = 1	n_m=0
malic	64.39	64.17	64.17	32.08	30.26	30.26
malonic	56.12	56.78	56.78	12.75	14.03	14.03
succinic	50.93	49.72	49.72	11.12	10.27	10.27
glutaric	46.15	46.13	46.13	9.682	9.663	9.663
citric	64.05	65.64	65.64	25.48	40.82	40.82
oxalic	63.23	65.32	65.32	21.93	32.50	32.50
maleic	49.89	50.05	50.05	10.13	10.28	10.28
	K_{org}			rmse		
malic	371.38	311.50	311.71	0.392	0.394	0.394
malonic	135.05	176.67	176.80	0.359	0.380	0.380
succinic	294.28	257.40	257.54	0.128	0.133	0.150
glutaric	435.15	432.30	432.08	0.335	0.335	0.335
citric	134.90	535.79	536.07	0.277	0.441	0.461
oxalic	104.79	190.97	191.27	0.104	0.111	0.111
maleic	228.36	238.38	238.50	0.827	0.828	0.828

Table 3.3: Dicarboxylic acids parameter values and error. Columns labeled "$n_m = 2$" and "$n_m = 1$" use equation 3.19. The first has two parameters, σ_{acid} and K'_{HA}, and $\bar{r}$ is a function of K'_{HA} and σ_{acid} through equation 3.20. The second uses only σ_{acid} as a parameter, following estimation of K'_{HA} throug $K'_{HA,binary}$ = 7.0812v-278.65 from Figure 3.1. Columns labeled "$n_m = 0$" use equation 3.18, where input variables are the same as the previous column, except that K'_{HA} for the ternary case is calculated from equation 3.21. Not tabulated is $K_{H^+A^-}$, a constant equal to unity for all species. Citric acid contains three carboxyl groups and is therefore actually described as a tricarboxylic acid.

Results with consideration of partial dissociation, referred to as the ternary model (equation 3.18), are shown in Figure 3.4a and 3.4b for dicarboxylic acids and in Figure 3.3 for citric acid. Concentrations for a_{HA} and $a_{H^+A^-}$ were calculated using known dissociation constants K_1 (mol/kg) in Table 3.2, again using the ideal mixture approach. Surface tension predictions using the ternary model require zero adjustable parameters since, of the four initial parameters, σ_{acid} is predicted from the binary case, K'_{HA} is calculated from equation 3.21, $K_{H^+A^-}$ is unity, and $\bar{r}$ is calculated as a function of σ_{acid} and K'_{HA} using equation 3.20. Excellent agreement is found among the three treatments of dicarboxylic acids and citric acid shown in Figures 2.2 - 2.4, validating the ternary model developed here.

Surface tension depression for aqueous dicarboxylic acids, represented here as σ_W-σ_{acid}, is shown to relate to parameters $\bar{r}$, σ_{acid} and $K'_{HA}/\bar{r}$. In Figure 3.5, the distinct correlation between $K'_{HA}/\bar{r}$ and surface tension depression precipitates from the expression for surface concentration using Gibbs adsorption isotherm, Γ_{HA} = -1/kT$\partial\sigma/(\partial$Ln $a_{HA})$, resulting in $\Gamma_{HA} \propto K'_{HA}/\bar{r}$. Effects of odd acids C3 (malonic) and C5 (glutaric) are evident in their higher solubilities than even acids because of intermolecular torsion forces rotating molecules out of plane, thereby creating energetically unfavorable structures. [106] However, odd and even acids show no clear effects on surface tension depression.

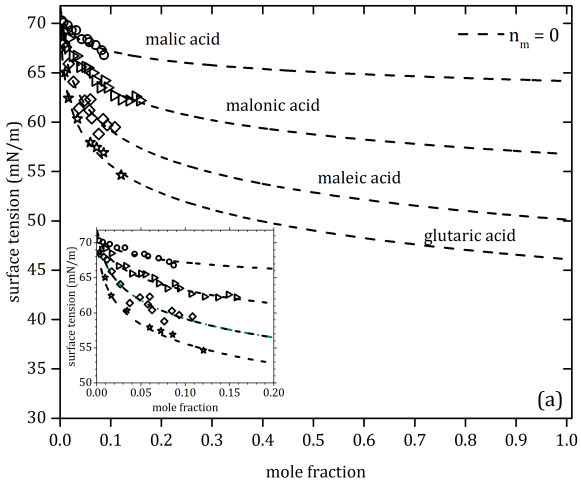

(a) Dissociation model for dicarboxylic acids of high solubility.

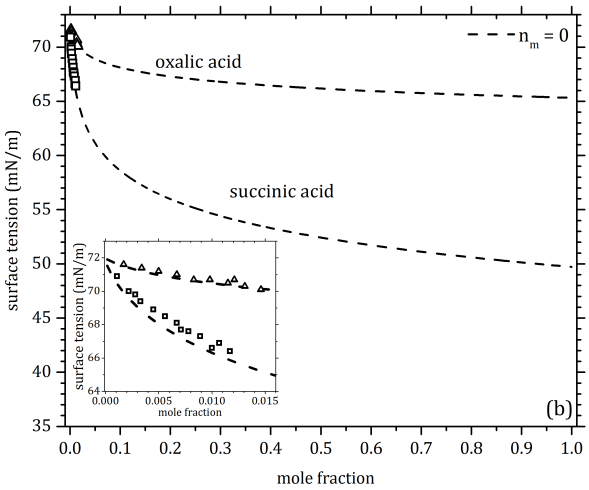

(b) Dissociation model for dicarboxylic acids of low solubility.

Figure 3.4: Surface tension versus mole fraction for dicarboxylic acids. The dashed lines are equation 3.18, using estimated values for variables σ_{acid}, K'_{HA}, and $\bar{r}$, requiring zero model parameters ($n_m = 0$). K'_{HA} is not the exact same value from the binary case; instead a predicted value is found from equation 3.21. $K_{H^+A^-}$ has a global value applied here, which is equal to one for dissociated electrolyte species. See Table 3.3, column $n_m = 0$ for parameter values and rmse.

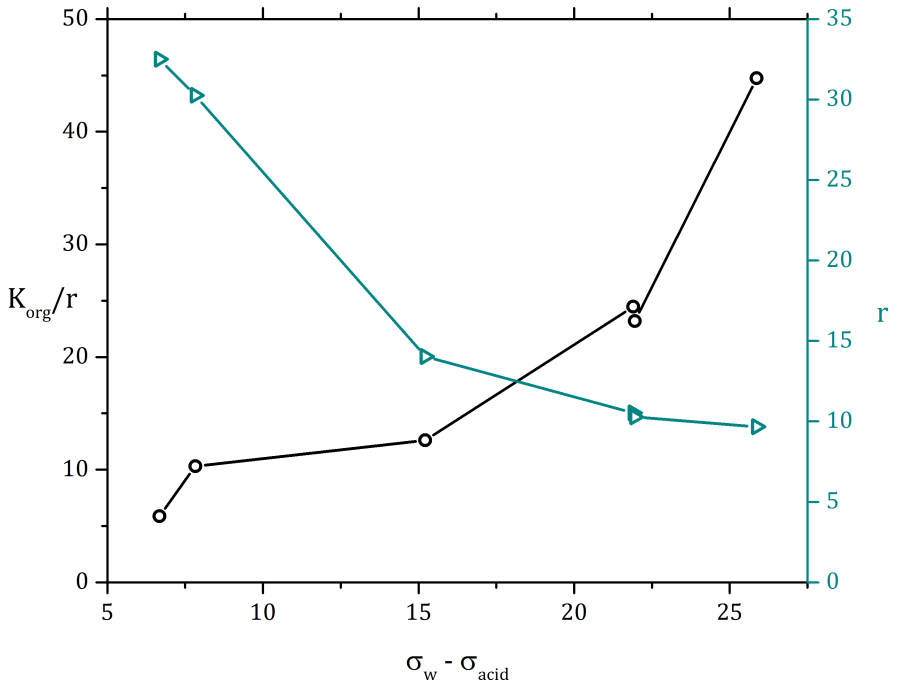

Figure 3.5: $\bar{r}$, σ_{acid} and $K'_{HA}/\bar{r}$ in order of increasing effect on surface tension depression,represented here as σ_W - σ_{acid}. The quantity $K'_{HA}/\bar{r}$ is related to surface excess Γ_{HA} through the Gibbs adsorption isotherm. Values for $\bar{r}$, σ_{acid}, and K'_{HA} are used from Table 3.3 under the columns labeled "ternary, $n_m = 0$".

Results for monocarboxylic acids

Results for the application of both the ternary (equation 3.18) and binary (equation 3.19) models for formic, acetic, and propionic acids are shown in Figure 3.6 and for butyric acid in Figure 3.7. Parameter values and errors are reported in Table 3.4. Surface tension versus mole fraction data for each species was fit with equation 3.19 using a single parameter, K'_{HA}, yielding a strong correlation with molar volume (Figure 3.1). Using the relationship between K'_{HA} and molar volume, K'_{HA} was estimated through the regression curve, $K'_{HA,binary}=0.0086e^{0.197v}$. For formic, propionic and butyric acid, $K'_{HA,binary}$ from this expression was used in equation 3.21 to find $K'_{HA,ternary}$ for the ternary model (equation 3.18).

Butyric acid surface tension depression is poorly captured using concentrations derived from the idealized Raoult's law, as shown by the green line in Figure 3.7. The initial surface adsorption and evident critical concentration beyond which the surface tension increment is small reflects strong deviations from ideal surface activity. The rmse for butyric acid is approximately 6.5, but error is much higher between dilute and moderate concentrations, where the surface tension depression is the steepest. To capture true effective concentrations, activity coefficients are found from the modeling work of Ohm et al., [28] a thermodynamic model of solution properties using methods of statistical mechanics of multilayer adsorption similar to those used to derive the current model at the interface.

Among the monocarboxylic acids, values for $K'_{HA}/\bar{r}$, an indicator of surface excess, were found to correlate strongly with oxygen to carbon ratio (O:C) and number of carbon atoms per molecule, as shown in Figure 3.8. Carbon content enhances hydrophobicity of the molecules, therefore driving them entropically to the aqueous

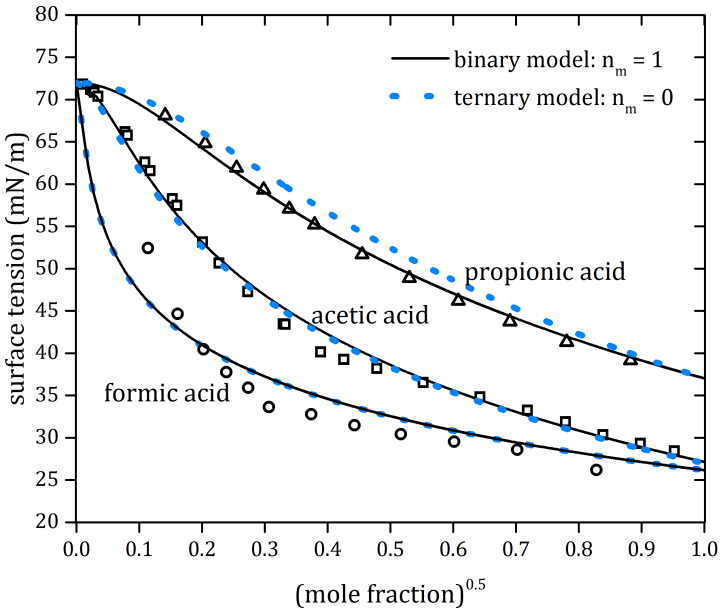

Figure 3.6: Surface tension versus mole fraction for formic (triangles), acetic (circles) and propionic (squares) acids, where n_m signifies the number of model parameters for each curve. For each acid, σ_{acid} is already known and $\bar{r}$ is obtained from equation 3.20. Solid lines are equation 3.19, the binary model, using one fit parameter K'_{HA}. Dashed lines are also equation 3.19, with K'_{HA} predicted the volume relationship in Figure 3.1, $K'_{HA,binary} = 0.0086e^{0.197v}$ and therefore zero parameters.

surface and making $K'_{HA}/\bar{r}$ higher. Also, carbon atoms give volume to the molecules and, since K'_{HA} is a function of volume (Figure 3.1), the trend is expectedly positive with number of carbons and negative with O:C. In complex aqueous aerosols, information on individual organic molecules is often difficult to obtain, so O:C is a simplified stand-in quantity for organic content.

acid	σ_{acid}			$\bar{r}$		
	n_m=2	n_m = 1	n_m=0	n_m=2	n_m = 1	n_m=0
acetic	27.0	27.0	27.0	4.910	5.966	4.910
butyric	26.1	26.1	26.1	12.75	10.08	9.450
formic	37.0	37.0	37.0	11.12	3.932	3.230
propionic	26.2	26.2	26.2	8.932	9.995	8.995
		K_{org}			rmse	
acetic	213.30	678.78	213.42	1.057	3.139	1.201
butyric	79,415	37,689	37,709	6.434	6.542	6.559
formic	27.216	14.539	14.547	0.538	1.904	1.882
propionic	20,847	22,361	22,361	2.603	2.604	2.610

Table 3.4: Monocarboxylic acids parameter values and error. Columns labeled "n_m = 1" and "n_m = 0" use equation 3.19. The first has a single parameter, K'_{HA}, and uses known values of σ_{acid}. $\bar{r}$ is a function of K'_{HA} and σ_{acid} through equation 3.20. The second requires zero parameters after estimating K'_{HA} through $K'_{HA,binary}$=$0.0086e^{0.197v}$ from Figure 3.1. Columns labeled "n_m = 0" use equation 3.18. Input variables are the same as the previous column, except that K'_{HA} for the ternary case is calculated from equation 3.21. Not tabulated is $K'_{H^+A^-}$, a constant equal to unity for all species. Butyric acid was also treated with the ternary model using estimated activity coefficients from reference [28] instead of Raoult's Law, using two parameters: $\bar{r}$ = 5.371, K'_{HA}= 489.01, rmse = 2.672.

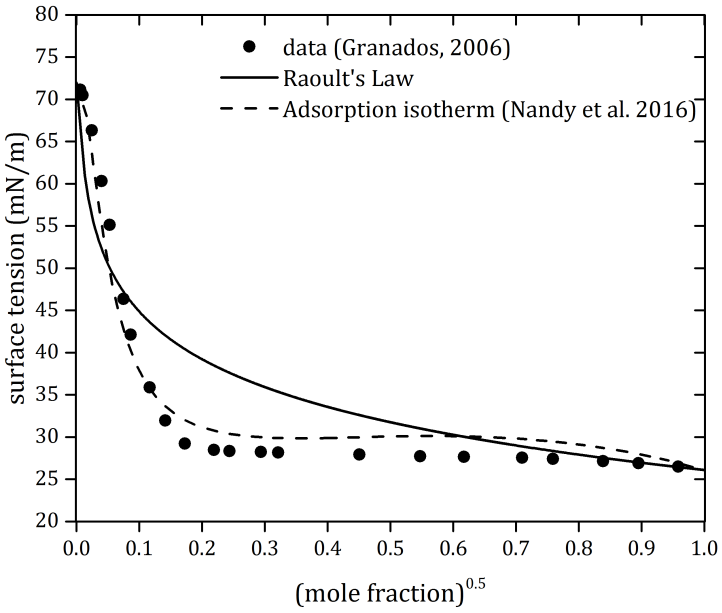

Figure 3.7: Surface tension versus square root of mole fraction for butyric acid, for which σ_{acid} is known. The solid line is equation 3.19, the ternary model. The solid line has zero parameters since $\bar{r}$ is calculated with equation 3.20, K'_{HA} is predicted from the volume relationship in Figure 3.1 and equation 3.21, and $K_{H^+A^-}$ is unity. See Table 3.4 for parameter values and rmse. For the ideal case, Raoult's Law was employed for concentration values and dissociation constants based on molality from literature sources [100, 101]. For the non-ideal case, activity coefficients were calculated from the modeling work of Ohm et al. [28] following a theoretical framework of multilayer adsorption in solution and assuming a fixed dissociation for neutral organic and dissociated forms of the acids to be 2:1 and a parameter related to radial distance between solute and solvent, ρ=0.08; energies of adsorption were unique for each layer (there are 3 multilayers for each solute): for the neutral organic "HA", [$C_{HA,1}$= 0.5488, $C_{HA,2}$ = 0.4229, $C_{HA,3}$=1.000] and deprotonated solute molecules "H+A-", [$C_{H^+A^-,1}$ = 0.0453, $C_{H^+A^-,2}$ = 3.223, $C_{H^+A^-,3}$= 1.000].

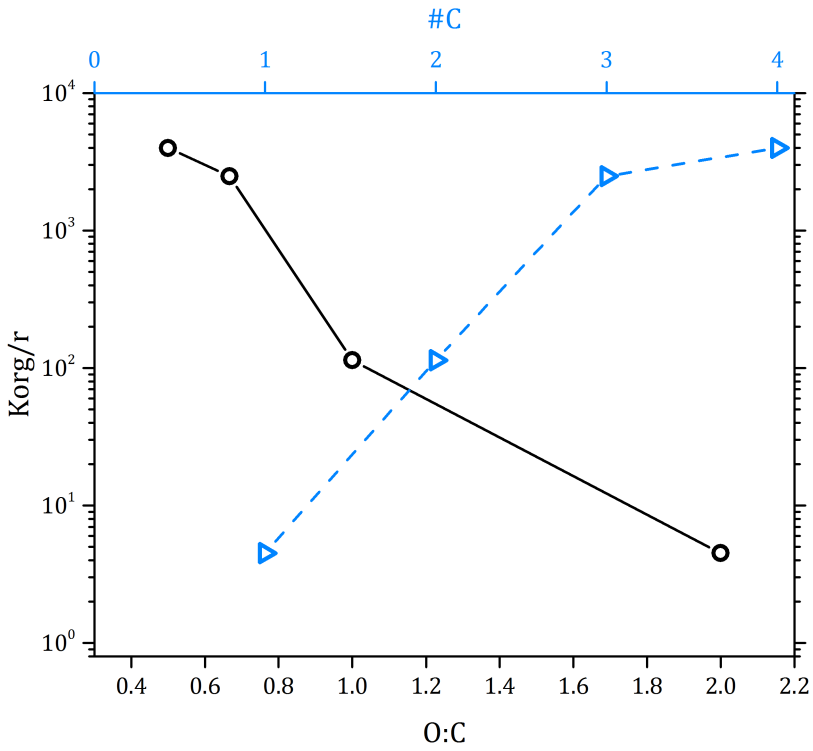

Figure 3.8: $K'_{HA}/\bar{r}$ versus oxygen to carbon ratio (O:C, circles) and number of carbon atoms per molecule (triangles) for the monocarboxylic acids in this study: formic (1C), acetic (2C), propionic (3C), and butyric (4C). For O:C for each species see Table 3.2 and $K'_{HA}/\bar{r}$ values for each species see Table 3.4.

Summary

A surface tension model previously developed for aqueous solutions containing either an electrolyte or non-electrolyte solute was applied to organic acids. Initially, aqueous organic acids were treated as binary (water + acid) systems. In the next step, a ternary model was developed, and tested using the known partial dissociation of the organic acids, in which acid molecules were either neutral or dissociating, referred to as ternary (water + neutral + dissociating) systems. Following statistical mechanics of multilayer adsorption at interfaces, [21] surface entropy and Gibbs free energy were defined for dissociating organic acid solutes in water. Surface tension was derived as a function of activities of the dissociating and non-dissociating forms of the acid. Physical interpretations of parameters are supported by their reflection of solute properties related to size and structure. The binary model recognized two independent unknowns σ_{acid} and K'_{HA}, where parameter K'_{HA} was found to correlate with pure component molar volume with trends diverging according to the number of functional groups. Incorporating the realistic picture of partial dissociation, the extended model creates an additional parameter, $K_{H^+A^-}$, related to the bulk energy for the ionized form of the acid molecules and set equal to unity. For eleven aqueous organic acids, the fully predictive surface tension modeling was demonstrated and a multi-component model was developed to advance predictive capabilities of the model for complex aqueous systems.

Appendix D provide details on model treatment of each organic acid in this chapter. The purpose of this appendix is to provide access to raw data and model parameters for data poor regimes of certain organic acids or to extend the arbitrary model.

In the next chapter, the model is again extended to treat ternary aqueous solutions, with the noted difference of a complete decoupling of model parameters. For the dissociation model, parameter r retained a collective meaning for the mixture, but now an r is assigned for each individual solute in the next version of the model.

Chapter 4

Statistical Thermodynamic Model for Surface Tension of Organic and Inorganic Aqueous Mixtures[†]

The surface tension of atmospheric aqueous aerosol particles is an essential factor in determining growth processes, heterogeneous chemistry, phase transitions, equilibrium morphology, and cloud activation. [16, 19] Chemical constituents known to be present in atmospheric aerosol are both organic (e.g. organic acids) and inorganic (e.g. ammonium salts). Most organic solutes lower the surface tension of pure water [77] by adsorbing at the surface. Inorganic electrolytes tend to remain in the solution interior to due attractive ion-water interactions, which results in a relative destabilizing of water interactions at the surface over in the bulk and an increase in surface tension with respect to pure water. In solutions containing mixtures, the effect of individual species on surfaces is convoluted.

[†]Part of this chapter was carried out in collaboration with University of Bristol researchers Professor Jonathan P. Reid and Dr. Bryan R. Bzdek and was published in Boyer, H.C.; Bzdek, B.R.; Reid, J.P.; and Dutcher, C.S., A Statistical Thermodynamic Model for Surface Tension of Organic and Inorganic Aqueous Mixtures, *Journal of Physical Chemistry A*, **2017**, 198-205

There are recent experimental and computational efforts to understand surface propensities of solutes in complex aqueous solutions. Öhrwall and coworkers [93] use synchrotron radiation spectroscopy to show that the addition of ammonium electrolytes enhances surface density of carboxylate ions in aqueous organic acid solutions. They propose that instead of a salting-out effect brought on by the salt, a surface bilayer of ammonium ions enhances deprotonation of the neutral species on the surface. Through molecular simulations of Venkateshwaran et al. [107], it was shown that ions at the surface of aqueous solutions exhibit unexpected behavior such as attraction between like charges in small ions when they are close to the vapor phase.

In the atmosphere, surface composition affects other surface-based properties and processes of aqueous aerosol. One effect of organic molecules residing on surfaces is that they can lower the critical supersaturation, [95] facilitating cloud droplet activation. [10] Organics can also enhance reaction rates between the liquid surface and ambient vapor, specifically with gaseous molecular chloride and bromide. [108] Recently, Reuhl et al. [19] and Noziere [109] highlighted the importance of accounting for surface tension depression by organic solutes on aqueous surfaces in predictions of cloud activation. In aqueous solutions of citric acid and sodium bromide, surface composition and resulting effects on uptake kinetics have been quantified using X-ray photoelectron spectroscopy (XPS). [94] Ammonium sulfate tends to depress the equilibrium vapor pressure of aqueous dicarboxylic acids, thus inhibiting partitioning into the gas phase. [110] Frosch et al. [11] have studied cloud activation as affected by solution properties (water activity) and surface properties (surface tension) in aqueous phases containing organic acids and inorganic electrolytes. The effects of solute mixtures on aqueous surfaces must be better understood to accurately predict the

fate of aerosol particles in the atmosphere.

There are a few existing surface tension models where the binary versions are successfully extended to mixtures (a solvent plus two or more solutes) with no additional parameters [63, 78, 111–114] that are constructed to treat each class of solute separately. Li et al. [111] developed a surface tension model using an adsorption isotherm similar to Langmuir that reaches solubility limits of many aqueous electrolytes with both single and multiple solutes as a function of osmotic coefficient. Extending the model to mixtures required no further parameterization. Solute activity was used to represent concentration, for which they used Pitzer's equation [115]. Li and Lu [112] also developed a multicomponent surface tension model, but instead covered only liquid organics solutes instead of electrolyte mixtures. They performed molecular simulations assuming Lennard-Jones liquids with the convenience of using surface tensions of pure liquids to determine parameters. Hu and Lee [113] demonstrate a simple thermodynamic model where surface tension is a function of water activities of the mixture and binary solutions of each solute at the same ionic strength. Finally, Lee and Hildeman [78,114] measured surface tension for aqueous solutions containing mixtures of dicarboxylic acids and fitted their results using the Szyzkowski equation [64] by extending the equation to ternary solutions. To our knowledge, there are currently no available models that sufficiently handle electrolyte and organic mixtures in the same solution without further parameterization and that can accurately extend to supersaturated concentrations. We present here a statistical thermodynamic model of surface tension for ternary systems using only optimized parameters from the binary cases [21, 25, 26] that is valid across the entire concentration range and accommodates organic and inorganic solutes in the same system.

In our prior work, a theoretical framework was developed in solution using adsorption isotherms, "hydrating" solutes with multi-layers with short-range energy parameters associated with each layer and long-range Coulombic interactions for charged solutes. [22–24,28,29] Using statistical mechanics, the model gave predictions of multicomponent solution properties, such as water activity, osmotic coefficient, and solute activity, as a function of solute molality. Next, the adsorption isotherm was applied to the surface of a single solute aqueous solution, [21] with the important distinction of solutes being the adsorbates, partitioning to the surface phase by displacing water molecules. Again using statistical mechanics, partition functions were written for the two regions: at the surface, representing the possible configurations of solvent and solute molecules that partition to the interface; and in the bulk, representing solute mixing between the surface and the bulk. While several multi-layers were necessary to predict water activity, the surface tension model was successful in using the surface as the monolayer, and the bulk as a single multi-layer. Using the same theoretical framework as the binary case, the statistical mechanical derivation for a multicomponent surface tension model and several applications are shown in the next section.

Excellent model agreement is shown with measurements from various sources. In particular, a novel approach to directly measure the surface tension of airborne picoliter droplets is used to compare to model results in the supersaturation regime. [116] This approach relies on the measurement of damped shape oscillations resulting from the coalescence of two airborne droplets. Building off of the parameterizations of the binary model, [21,25,26] predictions for ternary systems are demonstrated with absolutely no fitting. Model derivations for an arbitrary number of solutes are shown in the last section of this chapter so the model can be further extended.

Theory

Consider two solute species A and B in aqueous solution. The maximum number of waters at the surface is N_{WS}; each solute molecule displaces r_A and r_B waters from the surface. The partition function for the surface for solute A is

$$\Omega_{surface,A} = \frac{N_{WS}!_{r_A}}{(N_{WS} - r_A N_{AS})!_{r_A}(r_A N_{AS})!_{r_A}} \tag{4.1}$$

and for solute B, the number of configurations remaining on the leftover adsorption sites is

$$\Omega_{surface,B} = \frac{(N_{WS} - r_A N_{AS})!_{r_B}}{(N_{WS} - r_A N_{AS} - r_B N_{BS})!_{r_B}(r_B N_{BS})!_{r_B}} \tag{4.2}$$

where N_{AS} and N_{BS} are the numbers of molecules A and B displacing waters on the surface. In the single solute case, [21] r is a model parameter that represents the average number of water molecules displaced from the surface by a solute molecule and therefore is an indicator of size and surface density. In recent work, [26] $\bar{r}$ was used to represent a collective effect of two solutes in the development of a multicomponent model that did not distinguish between solute sizes. Here, r_A and r_B are used to treat individual size effects of each species. Multiplying equations 4.1 and 4.2 together, the surface partition function is

$$\Omega_{surface,AB} = \frac{N_{WS}!_{r_A}(N_{WS} - r_A N_{AS})!_{r_B}}{(N_{WS} - r_A N_{AS})!_{r_A}(r_A N_{AS})!_{r_A}(N_{WS} - r_A N_{AS} - r_B N_{BS})!_{r_B}(r_B N_{BS})!_{r_B}} \tag{4.3}$$

resulting in a partition function that gives solute A an arbitrary preference for surface adsorption sites over B. $\Omega_{surface,AB}$ must not change if alternatively written with

solute B in eq 4.1 and solute A in eq 4.2:

$$\Omega_{surface,BA} = \frac{N_{WS}!_{r_B}(N_{WS} - r_B N_{BS})!_{r_A}}{(N_{WS} - r_B N_{BS})!_{r_B}(r_B N_{BS})!_{r_B}(N_{WS} - r_B N_{BS} - r_A N_{AS})!_{r_A}(r_A N_{AS})!_{r_A}} \quad (4.4)$$

Therefore, to establish symmetry and therefore preserve equal probabilities of A and B surface adsorption, the surface partition function is written as

$$\Omega_{surface} = (\Omega_{surface,AB}\Omega_{surface,BA})^{1/2} \quad (4.5)$$

Next, the bulk partition functions represent mixing between surface and bulk phases. N_{AB} is the number of A molecules in the bulk and N_A=N_{AB}+N_{AS}, so the bulk partition function for A is

$$\Omega_{bulk,A} = \frac{N_A!}{N_{AS}!N_{AB}!} = \frac{N_A!}{N_{AS}!(N_A - N_{AS})!} \quad (4.6)$$

and for B,

$$\Omega_{bulk,B} = \frac{N_B!}{N_{BS}!N_{BB}!} = \frac{N_B!}{N_{BS}!(N_B - N_{BS})!} \quad (4.7)$$

where N_B=N_BB+N_{BS} and N_BB is the number of B molecules in the bulk. Letting χ = N_{WS} - $r_A N_{AS}$ - $r_B N_{BS}$, the full partition function is

$$\begin{aligned}\Omega = \Omega_{surface}\Omega_{bulk,A}\Omega_{bulk,B} &= \Omega_{surface}\Omega_{bulk} \\ &= \frac{N_A!N_B!}{(r_A N_{AS})!_{r_A}(r_B N_{BS})!_{r_B} N_{AS}!(N_A - N_{AS})!N_{BS}!(N_B - N_{BS})!} \\ &\quad \times \left(\frac{N_{WS}!_{r_A}(N_{WS} - r_A N_{AS})!_{r_B} N_{WS}!_{r_B}(N_{WS} - r_B N_{BS})!_{r_A}}{\chi!_{r_A}\chi!_{r_B}(N_{WS} - r_A N_{AS})!_{r_A}(N_{WS} - r_B N_{BS})!_{r_B}}\right)^{1/2}\end{aligned} \quad (4.8)$$

Configurational entropy is obtained from Boltzmann's formula, S=k ln($\Omega_{surface}$ Ω_{bulk}). Using Stirling's approximation including skips $\ln(N!_r) = \frac{N}{r}\ln(\frac{N}{r})$ -$\frac{N}{r}$,

$$\begin{aligned} ln\Omega = N_A ln\frac{N_A}{(N_A - N_{AS})} + N_B ln\frac{N_B}{(N_B - N_{BS})} \\ + \frac{N_{WS}}{2r_A} ln\frac{N_{WS}(N_{WS} - r_B N_{BS})}{\chi(N_{WS} - r_A N_{AS})} \\ + \frac{N_{WS}}{2r_B} ln\frac{N_{WS}(N_{WS} - r_A N_{AS})}{\chi(N_{WS} - r_B N_{BS})} + \frac{r_A N_{AS}}{2r_B} ln\frac{\chi}{(N_{WS} - r_A N_{AS})} \\ + \frac{r_B N_{BS}}{2r_A} ln\frac{\chi}{(N_{WS} - r_B N_{BS})} + \frac{N_{AS}}{2} \\ + ln\frac{\chi(N_{WS} - r_A N_{AS})(N_A - N_{AS})^2}{r_A^2 N_{AS}^4} \\ + \frac{N_{BS}}{2} ln\frac{\chi(N_{WS} - r_B N_{BS})(N_B - N_{BS})^2}{r_B^2 N_{BS}^4} \end{aligned} \quad (4.9)$$

The system energy is the sum of all molecular energies, represented by energies of waters on the surface (ε_{WS}) and in the bulk (ε_{WB}) and solute molecules on the surface and bulk (ε_{AS}, ε_{AB}, ε_{BS}, ε_{BB}).

$$E = -N_{WS}\varepsilon_{WS} - N_{WB}\varepsilon_{WB} - N_{AS}\varepsilon_{AS} - N_{AB}\varepsilon_{AB} - N_{BS}\varepsilon_{BS} - N_{BB}\varepsilon_{BB} \quad (4.10)$$

which can be rearranged as

$$E = -N_{WS}\Delta\varepsilon_{WS} - N_{W}\varepsilon_{WB} - N_{AS}\Delta\varepsilon_{AS} - N_{A}\varepsilon_{AB} - N_{BS}\Delta\varepsilon_{BS} - N_{B}\varepsilon_{BB} \quad (4.11)$$

where the total number of waters in the system is N_W =N_{WS}+N_{WB}. Assuming system energy is approximately the enthalpy due to negligible pressure and volume

changes and combining equations 4.9 and 4.11, Gibbs free energy is

$$G/kT \approx E/kT - ln\Omega \tag{4.12}$$

where S_W is the occupied area of one water molecule (0.1 nm^2). Taking the derivative of equation 4.12 with respect to area and letting σ represent solution surface tension and σ_W the surface tension of pure water (71.98 mN/m at 298 K) found in the limit of zero solute, then

$$\sigma = \sigma_W + \frac{kT}{2r_A S_W} ln\left(\frac{\chi(N_{WS} - r_A N_{AS})}{N_{WS}(N_{WS} - r_B N_{BS})}\right) + \frac{kT}{2r_B S_W} ln\left(\frac{\chi(N_{WS} - r_B N_{BS})}{N_{WS}(N_{WS} - r_A N_{AS})}\right) \tag{4.13}$$

Expressions for the activities of solute A (a_A) and solute B (a_B) are obtained from taking the derivative of equation 4.8 with respect to N_A and N_B, respectively, resulting in

$$K_A a_A = 1 - \frac{N_{AS}}{N_A} \tag{4.14}$$

$$K_B a_B = 1 - \frac{N_{BS}}{N_B} \tag{4.15}$$

where K_A=exp(-ε_{AB}/kT) and K_B=exp(-ε_{BB}/kT). The condition of equilibrium partitioning between the surface phase and bulk phase is imposed by minimizing equation 4.12 with respect to N_{AS} and N_{BS}, resulting in

$$C_A = exp\left(\frac{\Delta\varepsilon_{AS}}{kT}\right) = \left(\frac{\left(\frac{(N_{WS} - r_A N_{AS})}{\chi}\right)^{r_A/r_B}}{\chi(N_{WS} - r_A N_{AS})}\right)^{1/2} \frac{r_A N_{AS}^2}{N_A - N_{AS}} \tag{4.16}$$

$$C_B = exp\left(\frac{\Delta\varepsilon_{BS}}{kT}\right) = \left(\frac{\left(\frac{(N_{WS}-r_B N_{BS})}{\chi}\right)^{r_B/r_A}}{\chi(N_{WS}-r_B N_{BS})}\right)^{1/2} \frac{r_B N_{BS}^2}{N_B - N_{BS}} \tag{4.17}$$

In the case of a single solute A (N_{BS}=0), equations 4.14 and 4.16 are rearranged and substituted into equation 4.13, which results in

$$\sigma = \sigma_W + \frac{kT}{rS_W} ln\left(\frac{1 - K_A a_A}{1 - K_A a_A (1 - C_A)}\right) \tag{4.18}$$

which is the same form as the binary model from prior work by Wexler and Dutcher. [21] In the case of two solutes, if r_A and r_B are not treated separately, but instead as a unified quantity $\bar{r}$, equations 4.14 - 4.17 could be combined to give

$$\sigma = \sigma_W - \frac{kT}{\bar{r}S_W} ln\left(1 + \frac{C_A K_A a_A}{1 - K_A a_A} + \frac{C_B K_B a_B}{1 - K_B a_B}\right) \tag{4.19}$$

as shown by Boyer and Dutcher. [26] However, the multicomponent model for solutes of varied size, derived in this work, does not have a single analytic solution for surface tension of solution as a function of concentrations. The model is rather a system of nonlinear equations (4.13 - 4.17) that require numerical methods to solve, as detailed in the next section, to get predictions of surface tension, σ, as a function of activities a_A and a_B.

Computational Details

The set of equations 4.13 - 4.17 consist of model parameters (r_A, K_A, C_A, r_B, K_B, and C_A), quantities representing waters and solutes at the surface (N_{WS}, N_{AS}, N_{BS}, N_A, and N_B), solute activities (a_A and a_B) and solution surface tension (σ). In recent work by Boyer et al., [25] parameters r,K, and C for several electrolyte and organic binary aqueous solutions were determined with the surface tension model from Wexler

and Dutcher. [21] In the current work, those parameters identified for electrolytes and glycerol are applied as constants in the new model for ternary solutions. For organic solutes ethanol, glutaric acid, and succinic acid, new parameters were determined from the binary model shown in eq 4.18, since in prior work [25], [26] a modified form of the model was used for surface active species with a reduced number of parameters. All parameter values and data sources used in this work can be found in Table 4.1.

solute	r	K	C	σ_s	rmse	data ref.
ethanol	2.950	9.348×10^{-8}	3.743×10^{8}	22.20	1.425	[65]
NaCl	-19.89	0.9900	3.101×10^{4}	101.5	0.393	[69]
glutaric acid	9.663	9.700×10^{-3}	4.526×10^{4}	46.13	0.331	[26]
succinic acid	11.28	0.9579	312.4	39.62	0.128	[97]

Table 4.1: Parameters from binary modeling determined by equation 4.18.

For concentrations, activities for each solute a_A and a_B are calculated from the modeling work of Ohm et al.,27 a thermodynamic model of solution properties using methods of statistical mechanics of multilayer adsorption similar to those used to derive the current model at the interface. The remaining unknowns are the N quantities N_{WS}, N_{AS}, N_{BS}, N_A and N_B and surface tension σ. Since N_{WS} defines how many waters exist at the interface without solute adsorption, it is set at an arbitrary value. This leads to five unknowns are N_{AS}, N_{BS}, N_A, N_B and σ. Note that if there are zero solutes, the resulting value of σ will be σ_W no matter what value N_{WS} is used.

Equations 4.13 - 4.17 are a system of five nonlinear equations with five unknowns (N_{AS}, N_{BS}, N_A, N_B and σ). To simplify the system to two equations, equations 4.14 and 4.15 are substituted into 4.16 and 4.17, respectively, resulting in

$$C_A = exp\left(\frac{\Delta\varepsilon_{AS}}{kT}\right) = \left(\frac{\left(\frac{(N_{WS}-r_A N_{AS})}{\chi}\right)^{r_A/r_B}}{\chi(N_{WS}-r_A N_{AS})}\right)^{1/2} \frac{r_A N_{AS}(1-K_A a_A)}{K_A a_A} \tag{4.20}$$

$$C_B = exp\left(\frac{\Delta\varepsilon_{BS}}{kT}\right) = \left(\frac{\left(\frac{(N_{WS}-r_B N_{BS})}{\chi}\right)^{r_B/r_A}}{\chi(N_{WS}-r_B N_{BS})}\right)^{1/2} \frac{r_B N_{BS}(1-K_B a_B)}{K_B a_B} \tag{4.21}$$

Here, there are two equations (4.20 and 4.21) and two unknowns (N_{AS} and N_{BS}). Surface tension is found by substituting the solutions from equations 4.20 and 4.21 into equation 4.13, again noting that there are no ternary mixing parameters in the model.

Experimental Methods

For the binary NaCl-water and glutaric acid-water systems as well as for the ternary NaCl-glutaric acid-water system, model estimations were compared to surface tension measurements performed directly on 5-10 μm radius aerosol droplets using holographic aerosol optical tweezers. [116] Because the measurement is made on aerosol rather than bulk solutions, measurements on supersaturated solute states are accessible by this approach. The experimental apparatus has been described in detail previously. [116–119] In a typical experiment, two aqueous droplets were captured in two separate optical traps by nebulizing (Omron NE U22) a solution into a humidity-controlled trapping chamber. The two optical traps were created using a spatial light modulator (LCOS-SLM, Hamamatsu X10468) that dynamically shapes the phase front of a continuous wave 532 nm laser (Laser Quantum, Opus 3QW). The relative positions of these traps are controlled by a pre-calculated sequence of kinoforms, and the rate at which the kinoforms were changed was user-controlled. Once the trap separation was sufficiently small, the two droplets coalesced to one composite droplet. The capture and relative position of the droplets was monitored with a camera (Dalsa Genie HM 640, CMOS) utilizing widefield illumination with a high power LED (Thorlabs, 470 nm). Inelastic backscattered (Raman) laser light

was directed to a 0.5 m focal length spectrograph (Princeton Instruments, Action Spectra Prop SP-2500). The Raman spectrum from a spherical droplet consists of a broad underlying Stokes band with superimposed resonant structure at wavelengths commensurate with whispering gallery modes (WGMs; see Figure 4.1a), from which the radius, refractive index, and dispersion can be determined with accuracies better than 2 nm, 0.0005, and 3×10^{-8} cm respectively. [120] Elastic backscattered laser light (see Figure 4.1b) was collected using a silicon photodetector (Thorlabs, DET 110) and recorded using a low-load, 12 bit ADC resolution, 2.5 GS·s-1 sample rate oscilloscope (LeCroy, HDO 6034-MS).

The basic measurement involves monitoring the damped oscillations in droplet shape that occur upon the coalescence of two droplets with lower viscosity than 20 mPa-s. The time dependence of the changing shape of the composite droplet in the microseconds following coalescence is determined from highly time-resolved ($\sim$100 ns time resolution) measurements of the varying intensity of the elastic backscattered light, which corresponds to changes in droplet shape. [120] The frequency of these shape oscillations gives the surface tension of the composite droplet through equation 4.22. [121, 122]

$$\sigma = \frac{a^3 \rho \omega_l^2}{l(l-1)(l+2)} \tag{4.22}$$

where σ is the composite droplet surface tension, l is the mode order (a characteristic deformation in droplet shape), ω_l is the angular oscillation frequency of a given mode order, a is the droplet radius, and ρ is the droplet density. In general, surface tensions retrieved by this approach have an accuracy and precision better than ± 1 mN/m.

Figure 4.1 shows examples of experimental data for a sodium chloride droplet with high surface tension ($\sigma = 82$ mN/m, lower traces) and for a glutaric acid droplet with

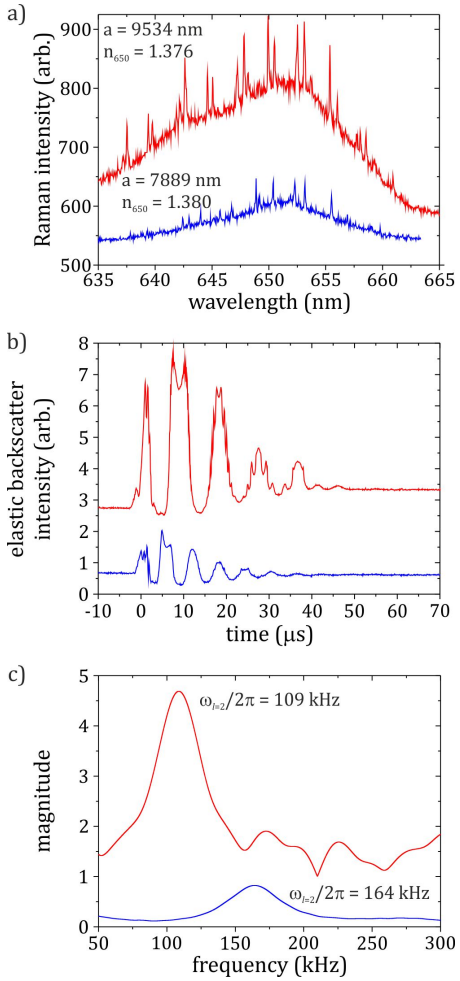

Figure 4.1: Holographic optical tweezers measurements require simultaneous acquisition of the Raman spectrum of a coalesced droplet and the elastic backscattered light from the coalescence event. Part (a) shows representative Raman spectra for a composite sodium chloride droplet (lower trace) and glutaric acid droplet (higher trace) immediately after the coalescence event. The best fit radius and refractive index are given for each droplet. The elastic backscatter intensity for both experiments are shown in part (b). Part (c) shows the Fast Fourier Transform of part (b) to determine the droplet shape oscillation frequency, which is reported in the figure.

low surface tension (σ = 57 mN/m, higher traces). In Figure 4.1a, a representative Raman spectrum is shown for the coalesced droplet in each experiment. The positions of the WGMs are used to extract the droplet radius and refractive index at 650 nm with high precision. From the measured refractive index, several droplet properties (solute concentration, density, and viscosity) are obtained through parametrizations of bulk data. [123] Figure 4.1b shows the elastic backscatter intensity during the coalescence event for both droplets. The difference in intensity results from the differing droplet sizes. The intensity maxima and minima correspond to the extremes in droplet shape distortion. [116], [124] It is clear from the elastic backscatter intensity that the oscillation frequency is higher for the NaCl droplet, which is a smaller droplet and has a higher surface tension. The Fast Fourier Transform is applied to the elastic backscatter intensity to give Figure 4.1c, which shows the droplet oscillation frequency for each droplet, with the frequency for the $l = 2$ mode most prominent as this is the mode that persists for the longest time during the shape relaxation. From the droplet oscillation frequency, radius, and refractive index, it is possible to quantify the droplet surface tension through equation 4.22.

Results and discussion

In Figure 4.2, surface tension measurements are compared to predictions for several binary and ternary aqueous solutions, demonstrating that the model was successfully applied to systems containing two electrolytes, two organics, or one organic and one electrolyte. Excellent agreement is found between predictions and measurements for the following systems: NaCl + KCl, NaCl + succinic acid, NaCl + glutaric acid, ethanol + glycerol, and NH_4NO_3 + $(NH_4)_2SO_4$. The rmse of fit, $rmse = \sqrt{\sum_{i=1}^{n_P}(\sigma_i^{data} - \sigma_i^{pred})^2/n_P}$, and data sources are in Table 4.2.

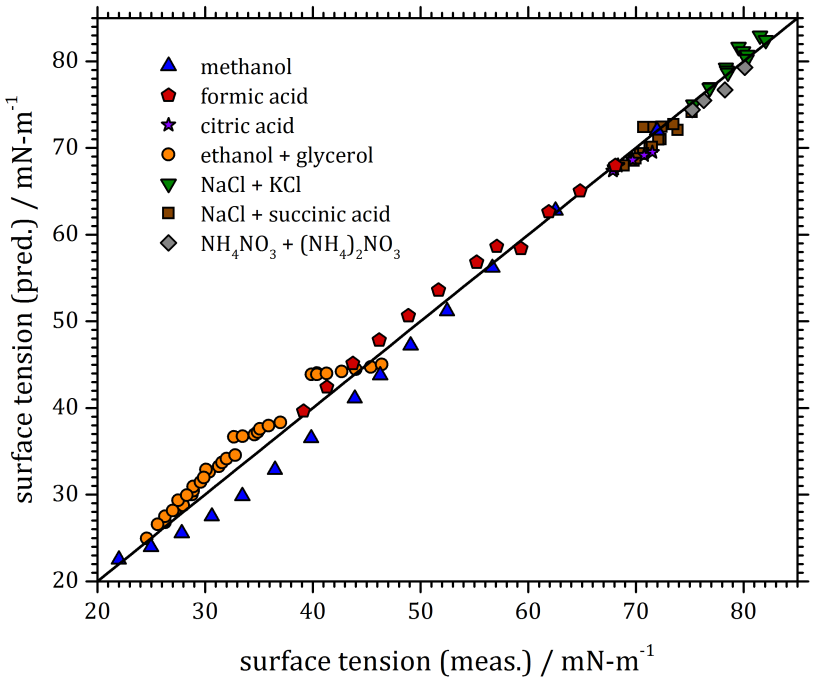

Figure 4.2: Surface tension model predictions (pred.) vs. surface tension data (meas.) for four ternary systems and three binary systems. For each point, a predicted value was found based on the concentrations of the two solutes in the corresponding measured point. Thus, any variation in the y-axis is purely from change in amount or type of solute. Data sources: methanol, citric acid, and NH_4NO_3 + $(NH_4)_2SO_4$ (taken by H.C.B with Wilhelmy plate, Digital Tensiometer K10ST by Krüss); formic acid (Alvarez et al., 1997 [104]); ethanol + glycerol (Ernst et al., 1936 [68]); NaCl + KCl, (Belton, 1935 [125]); NaCl + succinic acid (Vanhanen et al.l, 2008 [126]).

mixture	rmse[a]	n_p^b	data ref/meas.[c]
$ethanol + glycerol$	1.379	34	[68]
$NH_4NO_3 + (NH_4)_2SO_4$	0.424	4	[63]
$NaCl + succinic\ acid$	0.218	16	[125]
$NaCl + glutaric\ acid$	1.013	10	optical tweezers
$NaCl + KCl$	0.420	12	[125]

Table 4.2: Results for ternary aqueous mixtures. [a]Error from model fitting. [b]Number of data points. [c]Data references (measurements were taken by the authros for NH_4NO_3 - $(NH_4)_2SO_4$ and NaCl - glutaric acid.

Next, in Figures 4.3 - 4.5, a specific case for each type of system (electrolyte + organic, organic + organic, electrolyte + electrolyte) is examined to demonstrate that the surface tension is calculated as a function of activity of each solute and that reasonable predictions can be made in the absence of data. For all solutes except organic acids, solute activities in mixtures are found from the solution property modeling work using the adsorption isotherm of Dutcher et al. [22–24] and Ohm et al. [28] For organic acids, activities are found assuming ideal mixing with Raoult's Law, which was shown to work well for these systems when predicting surface tension. [26] Surface tension versus concentration curves in Figures 4.3 - 4.5 are predictions in which the system composition varies from zero solute (pure water) to zero water (pure solute), while the ratio of solutes is held constant as water content changes.

For several solute species (glycerol, ammonium nitrate, ammonium sulfate, potassium chloride), binary model parameters were determined in recent work in which parameters were reduced through correlations with physico-chemical properties, towards fully predictive surface tension modeling of binary solutions. [25] Binary predictions for the other solutes in this study (ethanol, NaCl, glutaric acid, succinic acid) are found by fitting equation 4.18 to bulk data and optimizing the three model

parameters r, K, and C (Table 4.1). The surface tension of pure solute, σ_s, can also be used as a parameter when equation 4.18 is evaluated in the limit of pure solute. If σ_s is a known quantity, as is the case for many liquid organics, then it can eliminate a parameter. Binary predictions for both solutes are found by fitting equation 4.18 to bulk data and optimizing the three model parameters r, K, and C. Model predictions for ternary solutions are found using methods detailed in the Computational Details section. As mole ratio increases to favor one solute, the curves progress towards the corresponding binary curve, and correctly limit to the binary case in the limit of one solute.

Electrolyte + organic + water. Model application to ternary aqueous mixtures containing an electrolyte (NaCl) and an organic (glutaric acid) are shown in Figure 4.3 as well as their respective binary curves. For the first time, we compare binary model predictions to surface tension measurements beyond the solubility limit. Ternary predictions are shown for a mass ratio of 1:1. Supporting data for binary NaCl, binary glutaric acid, and the mixture are provided by experiments using optical tweezers detailed in Experimental Methods. The optical tweezers data are also presented here for binary NaCl and glutaric acid aqueous solutions that extend into the supersaturated regime. As shown by the red and blue lines and full symbols in Figure 4.3, there is excellent agreement between model predictions and experiments. For organic and inorganic aqueous mixtures not discussed here, a "salting out" phenomenon may occur in which strongly dissolved salts force organic molecules out of solution, thereby driving them to the surface, and in turn lowering surface tension below that of the organic salt-free solution. The model successfully predicts surface tension of mixtures in Figure 4.3 by allowing organics and electrolytes to compete

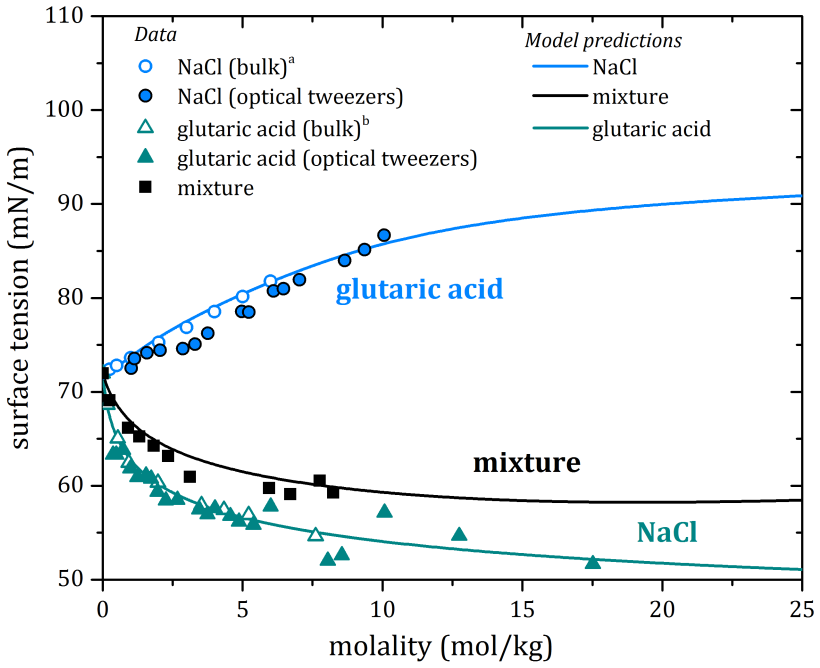

Figure 4.3: Surface tension model predictions and measurements versus molality. In the mixture, molality is the sum of the molalities of each solute. Model predictions for the binary systems are found through equation 4.18. For the mixture, which has a 1:1 composition by mass, there is no fitting to the data presented. Instead, the 6 total model parameters from the binary treatments are applied to equations 4.13, 4.20 and 4.21 to produce the curve. Data sources: [a]Washburn et al., 1928. [69]; [b]Boyer and Dutcher, 2016 [26].

for surface adsorption sites with equal probability. To capture salting out effects, a new parameter would be needed to account for solute-solute interactions, either in the surface tension model [21, 25, 26] or in the solution activity model. [22–24, 28, 29]

Organic + organic + water. In Figure 4.4, model prediction curves and data are shown at various constant mole ratios. Mixture data for equimolal solutions, or concentrations with mole ratio 1:1, are in close agreement with predictions. The additional curves shown in Figure 4.4 exhibit key capabilities of the model: sensitivity to mole ratio as well as specific effects of each compound. As the mole ratio changes, predictions tend toward the appropriate binary curve, while it is also clear that ethanol has a dominant effect at the surface.

Electrolyte + electrolyte + water. Model application to aqueous mixtures containing two electrolytes (ammonium nitrate and ammonium sulfate) are shown in Figure 4.5. Between the binary curves for each solute are model runs for different fixed mole ratios, accompanied by supporting data for the mole ratio 1:1 taken using a Wilhelmy plate (Digital Tensiometer K10ST by Krüss). Both binary fits use a single model parameter, r, where others have been eliminated through physical interpretation in recent work. [25] For ammonium sulfate, rmse for the single parameter fit was 0.999, and for ammonium nitrate, rmse was 0.146. When applied to the model presented here, the higher error for binary ammonium sulfate spreads into mixture predictions. Allowing three model parameters to vary instead of one decreases the error for ammonium sulfate to an rmse of 0.219.

Summary

Based on a previously derived surface tension model for binary aqueous solutions [21] that uses adsorption isotherms at the interface of solution, we have derived

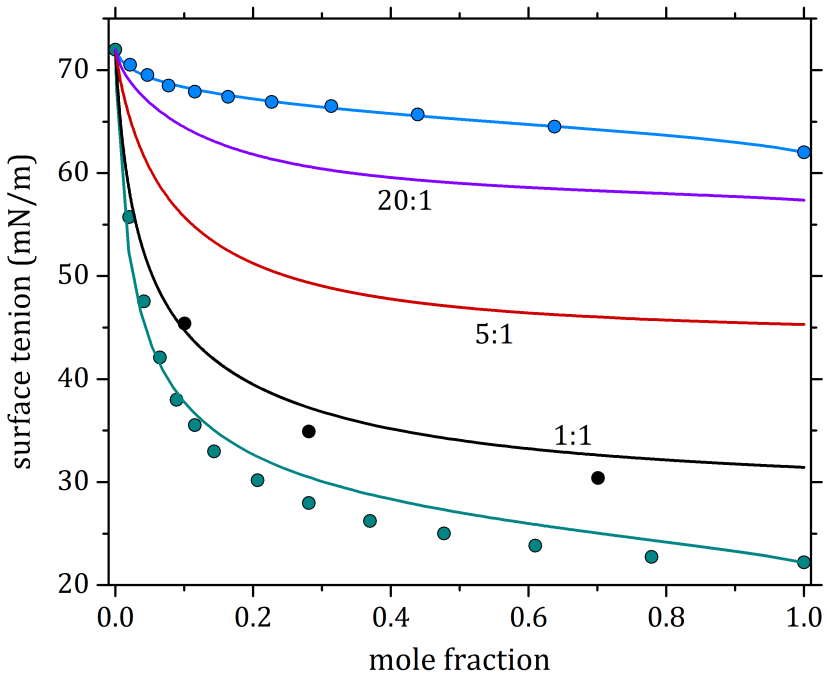

Figure 4.4: Surface tension versus mole fraction predictions for ethanol and glycerol aqueous solutions and mixtures (glycerol + ethanol + water) at different glycerol:ethanol (glyc:eth) mole ratios. Also shown are the curves of binary solutions with each solute and a sample of surface tension data for the 1:1 mixture that agree with predictions. Model predictions for the binary systems are found through equation 4.18. The mole fractions represent the fraction of total amount of solute. Data sources: Glycerol and mixture: Ernst et al., 1936 [68]; ethanol: Vazquez et al., 1995 [65].

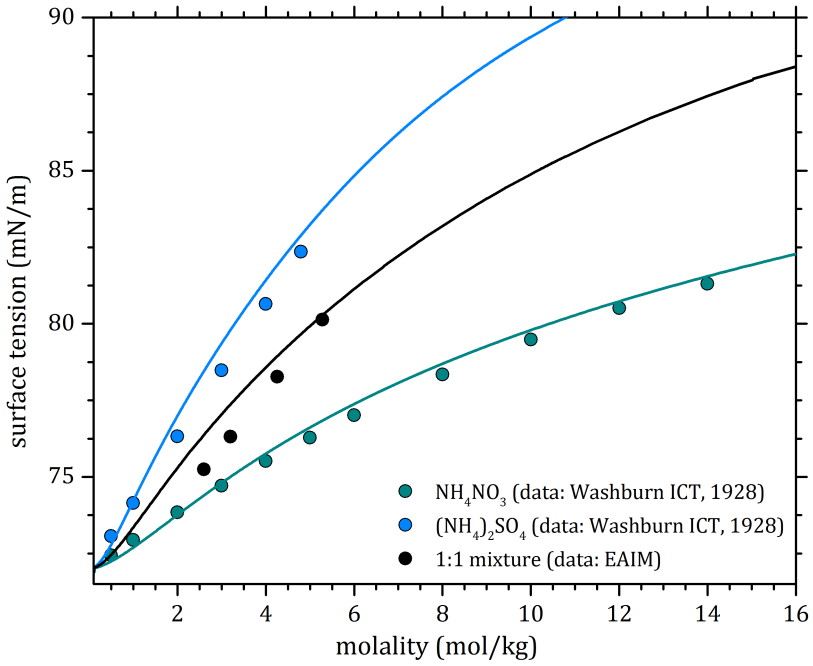

Figure 4.5: Surface tension model predictions and measurements versus molality for the ternary system consisting of NH_4NO_3 (AN) and $(NH_4)_2SO_4$ (AS) mixtures in aqueous solutions. In the mixture, molality is the sum of the molalities of each solute. Model predictions for the binary systems are found through equation 4.18.

a model that handles two separate solutes and is a function of solute concentration and solute ratio. The adsorption isotherm framework [22–24, 28] was developed beforehand to predict solution properties and subsequently applied to the interface. It was then demonstrated that the surface tension binary model works equally well for organic and electrolyte solutes, [21], [25] and can be extended to partially dissociating organic acids by decoupling a single model parameter. [26] Here, we present a multicomponent surface tension model for aqueous solutions containing two solutes and demonstrate its versatility by applying it to mixtures of water soluble organic and inorganic compounds. The efficacy of the model is shown by comparing predictions of ternary solutions to data. Although data for ternary solutions are scarce, there is remarkable agreement in cases where data are available for comparison with model predictions. Surface tension measurements for systems of aqueous NaCl, glutaric acid, and a mixture of the two are obtained using optical tweezers, which have the capability of measuring surface tension of picolitre droplets in supersaturated states. The overall excellent agreement between model predictions and data from bulk and optical tweezers measurements of ternary systems shows strong potential for adapting the model to solutions of increasing complexity.

The end of this chapter signifies the culmination of the thermodynamic modeling work in this thesis. As a final installment, the derivation for the surface tension model for an arbitrary number of solutes is presented in the next section. Then, the remaining chapters highlight experimental work using a microfluidics platform to study liquid-liquid interfaces.

Statistical mechanical derivation for an arbitrary number of solutes

For an arbitrary number of solutes, n, we define the number of possible configura-

tions of at the surface in equation 4.23, the surface partition function. Subscript j of the first multiplicative sum represents the solute that adsorbs at the surface (or bulk) first, where each solute in the system from A to Z has this position (n-1)! times. Solute k of the next multiplicative sum represents all solutes except for j, with the notation $k <$ j meaning the subsequent solutes that have the second spot in line (n-2)! times. The multiplicative sums are defined as needed for however many solutes are in the system. With this approach, there is a unique combination for each permutation of solute adsorption, making a total of n! possible surface partition functions. Therefore, the entire product is raised to the power 1/n!, resulting in

$$\Omega_{surface} = \left(\prod_{j}^{Z} \prod_{k<j} \prod_{l<k} \cdots \frac{\begin{array}{c} N_{WS}!_{r_j}^{(n-1)!} (N_{WS} - r_k N_{kS})!_{r_j}^{(n-2)!} \\ (N_{WS} - r_k N_{kS} - r_l N_{lS})!_{r_j}^{(n-3)!} \cdots \end{array}}{\begin{array}{c} \big(r_j N_{jS}\big)!_{r_j}^{n!} \big(N_{WS} - r_j N_{jS}\big)!_{r_j}^{(n-1)!} \\ \big(N_{WS} - r_j N_{jS} - r_k N_{kS}\big)!_{r_k}^{(n-2)!} \\ \big(N_{WS} - r_j N_{jS} - r_k N_{kS} - r_l N_{lS}\big)!_{r_l}^{(n-3)!} \cdots \end{array}} \right)^{1/n!} \tag{4.23}$$

The bulk partition function represents mixing between the surface and the bulk for each solute:

$$\Omega_{bulk} = \prod_{j=A}^{Z} \frac{N_j!}{N_{jS}!(N_j - N_{jS})!} \tag{4.24}$$

Gibbs free energy, G ≈ E - TS, must be found next. We obtain an expression for

entropy through Boltzmann's equation, $S = k_B \mathrm{Ln}\Omega_{bulk}\Omega_{surface}$, giving

$$\frac{S}{k_B} = \frac{1}{n!}\Bigg[\sum_{j=A}^{Z} N_j Ln\Big(\frac{N_j}{N_j - N_{jS}}\Big) + \sum_{k<j}\sum_{l<k}\ldots\frac{N_{WS}}{r_j}Ln\Bigg(\Big(\frac{N_{WS}}{N_{WS}-r_jN_{jS}}\Big)^{(n-1)!}\Big(\frac{r_k(N_{WS}-r_kN_{kS})}{r_j(N_{WS}-r_jN_{jS}-r_kN_{kS})}\Big)^{(n-2)!} \Big(\frac{r_l(N_{WS}-r_kN_{kS})-r_lN_{lS})}{r_j(N_{WS}-r_jN_{jS}-r_kN_{kS}-r_lN_{lS})}\Big)^{(n-3)!}\ldots\Bigg) + N_{jS}Ln\Bigg(\Big(\frac{N_j-N_{jS}}{N_{jS}^2}\Big)^{n!}\Big(\frac{N_{WS}-r_jN_{jS}}{r_j}\Big)^{(n-1)!}\Big(\frac{N_{WS}-r_jN_{jS}-r_kN_{kS}}{r_k}\Big)^{(n-2)!r_j/r_k} \Big(\frac{N_{WS}-r_jN_{jS}-r_kN_{kS}-r_lN_{lS}}{r_l}\Big)^{(n-3)!r_j/r_l}\ldots\Bigg) + N_{kS}Ln\Bigg(\Big(\frac{N_{WS}-r_jN_{jS}-r_kN_{kS}}{r_k}\Big)^{(n-2)!}\Big(\frac{r_j}{N_{WS}-r_kN_{kS}}\Big)^{(n-2)!r_k/r_j} \Big(\frac{N_{WS}-r_jN_{jS}-r_kN_{kS}-r_lN_{lS}}{r_l}\Big)^{(n-3)!r_k/r_l}\Big(\frac{r_j}{N_{WS}-r_kN_{kS}-r_lN_{lS}}^{(n-3)!r_k/r_j}\ldots\Big) + N_{lS}Ln\Bigg(\Big(\frac{N_{WS}-r_jN_{jS}-r_kN_{kS}-r_lN_{lS}}{r_l}\Big)^{(n-3)!} \Big(\frac{r_j}{N_{WS}-r_kN_{kS}-r_lN_{lS}}\Big)^{(n-3)!r_l/r_j}\ldots\Bigg)\ldots\Bigg] \quad (4.25)$$

The total energy is the sum of molecular energies of waters at the surface (ε_{WS}), waters in the bulk (ε_{WB}), solutes at the surface (ε_{jS}) and solutes in the bulk (ε_{jB}) multiplied by the number of each, giving

$$E = -N_{WS}\Delta\varepsilon_{WS} - N_W\varepsilon_{WB} - \sum_{j=A}^{Z}(N_{jS}\Delta\varepsilon_{jS} - N_j\varepsilon_{jB}) \quad (4.26)$$

Solute activity is the derivative of G with respect to number of solutes in the system, N_j, resulting in

$$K_j a_j = 1 - N_{jS}/N_j \quad (4.27)$$

where $K_j = \exp((-\varepsilon_{jB})/(k_B T))$. Equilibrium partitioning of a solute between the surface and bulk is imposed by taking the derivative of G with respect to number of solutes at the surface, N_{jS}, and setting it equal to zero, resulting in

$$
\begin{aligned}
C_j &= exp\Big(\frac{\Delta\varepsilon_{jS}}{k_B T}\Big) \\
&= \prod_{k<j}\prod_{l<k}\cdots\frac{N_{jS}^2}{N_j - N_{jS}}\Bigg[\left(\frac{r_j}{N_{WS} - r_j N_{jS}}\right)^{(n-1)!}\left(\frac{r_j}{N_{WS} - r_j N_{jS} - r_k N_{kS}}\right)^{(n-2)!} \\
&\quad\times\left(\frac{r_j}{N_{WS} - r_j N_{jS} - r_k N_{kS} - r_l N_{lS}}\right)^{(n-3)!} \\
&\quad\times\left(\frac{N_{WS} - r_j N_{jS}}{N_{WS} - r_j N_{jS} - r_k N_{kS}}\right)^{(n-2)!r_j/r_k} \\
&\quad\times\left(\frac{N_{WS} - r_j N_{jS} - r_k N_{kS}}{N_{WS} - r_j N_{jS} - r_k N_{kS} - r_l N_{lS}}\right)^{(n-3)!r_j)/r_l} \\
&\quad\times\left(\frac{N_{WS} - r_j N_{jS} - r_k N_{kS}}{r_k}\right)^{(n-3)!r_j/r_l} \\
&\quad\times\left(\frac{r_l}{N_{WS} - r_j N_{jS} - r_k N_{kS} - r_l N_{lS}}\right)^{(n-3)!r_j/r_l}\Bigg]^{\frac{1}{n!}}
\end{aligned}
\tag{4.28}
$$

Surface tension is obtained by taking the derivative of G with respect to area, approximated as the projected area of one water molecule, S_W, times the maximum number of waters at the surface, N_{WS}. There are also solutes at the surface, so area occupied by solutes is actually $r_j N_{jS} S_W$ and the area occupied by waters is S_W (N_{WS} - $r_j N_{jS}$),

making the total area S_W N_{WS}. The expression for surface tension is

$$\sigma = \sigma_w + \sum_{j=A}^{Z} \sum_{k<j} \sum_{l<k} \cdots \frac{k_B T}{r_j S_w} \frac{1}{n!} Ln \left[\left(\frac{N_{WS} - r_j N_{jS}}{N_{WS}} \right)^{(n-1)!} \times \left(\frac{r_j (N_{WS} - r_j N_{jS} - r_k N_{kS})}{(r_k (N_{WS} - r_k N_{kS})} \right)^{(n-2)!} \times \left(\frac{r_j (N_{WS} - r_j N_{jS} - r_k N_{kS} - r_l N_{lS})}{r_l (N_{WS} - r_k N_{kS} - r_l N_{lS})} \right)^{(n-3)!} \right] \quad (4.29)$$

Equations 4.25, 4.28, and 4.29 are evaluated for 4.23, 4.24, and 4.25 solute systems in Appendix A.

Chapter 5

Interfacial Tensions of Aged Organic Aerosol Particle Mimics Using a Biphasic Microfluidic Platform[†]

Introduction

The preceding chapters discussed advancements in surface tension model development, especially towards fully predictive modeling requiring no parameters for binary and multicomponent aqueous mixtures. Data are crucial for assessing the accuracy of the model, yet data are scarce for many atmospherically relevant systems. Model application to organic solutes that are abundant in the atmosphere is limited by a lack of data. Sample volumes of atmospheric aerosols are often too small to perform bulk measurements of surface tension. Microfluidic tensiometry is a highly advantageous technique for organic aerosol chemicals, as the samples themselves may be

[†]This work was carried out in collaboration with Dr. Andrew Metcalf and was published in Metcalf, A.; Boyer, H.C.; and Dutcher, C.S., Interfacial Tensions of Aged Organic Aerosol Particle Mimics Using a Biphasic Microfluidic Platform,*Environmental Science and Technology*, **2016**, 1251-1259

microfluids.

Secondary organic aerosol (SOA) particles are nearly ubiquitous in the atmosphere, [44, 46, 127] and yet there remains large uncertainties in their formation processes and ambient properties. [47, 128] These particles are complex microenvironments that can contain multiple interfaces due to internal liquid-liquid phase separation and to the external liquid-vapor surface. These aerosol interfaces can profoundly affect the fate of condensable organic compounds emitted into the atmosphere by altering the way in which organic vapors interact with the ambient aerosol. For example, organic thin films can shield the core of the aerosol from the ambient environment, which may disrupt equilibrium partitioning and mass transfer. To further understand SOA behavior in the atmosphere, it is necessary to investigate aerosol interfaces arising from liquid-liquid phase separation within aqueous aerosol. [129]

The presence of surface active constituents (i.e., organic acids, diacids, proteins, and humiclike substances) in atmospheric aerosol leads to the formation of surface films on aerosol particles due to hydrophobic groups preferentially protruding out of the particle into the surrounding gas phase. [130] Surface-active organics are known to reduce surface tension, [131,132] inhibit gas-phase uptake into [133–135] and evaporation from [136–138] the bulk of the aerosol, enhance ice [139] and cloud [140, 141] condensation nucleation, and modify heterogeneous chemistry [1, 142] and optical properties. [143] Some studies have shown that organic coatings actually do not have much effect on particles' ability to deliquesce or effloresce [144–146] or act as ice nuclei, [147] suggesting that particle morphology (i.e., incomplete coating of the organic) plays an important role in determining how particles behave in the atmosphere. However, the exact microphysical structure of ambient aerosol remains highly uncertain

and under-investigated. [47] Traditionally, ambient aerosol containing multiple condensed species has been modeled as well-mixed, homogeneous liquid droplets using volume- or mass-mixing rules for the different species (e.g., ref [148]). Many recent studies, though, have observed liquid-liquid phase separation in aerosol mimics in the laboratory, [2, 37, 38] leading to the identification of other aerosol morphologies, including thin-film (core-shell) structures, [137, 141, 149–152] partially engulfed lenses, [137, 153, 154] micelle-like aggregates, [155] solid inclusions, [156] liquid-liquid phase-separated islands (e.g., from spinodal decomposition), [157, 158] and other multiphase-separated structures. [51, 159] Predictions of ambient aerosol morphology are further complicated by the dependence of particle-phase chemical composition on environmental factors such as temperature and relative humidity.

Recently, a thermodynamic model of equilibrium morphology for an immiscible three-phase system of liquid drops in air based on spreading coefficients [160–162] was applied to mixed inorganic-organic aerosol. [37, 152, 153] The model assumes that the equilibrium configuration of a compound particle will have the lowest-total surface free energy

$$G_s = \Sigma \gamma_{ij} A_{ij} \tag{5.1}$$

where γ_{ij} is the interfacial tension (IFT) between phases i and j, and A_{ij} is the interfacial area between those respective phases. The spreading coefficient, S_i, is defined by

$$S_i = -\Delta G_s / A \tag{5.2}$$

where $\Delta \mathrm{G}_s$ is the free energy increase due to spreading of liquid i over another substrate (solid or liquid). [163] Thus, the spreading coefficient is the difference in

surface energy between a dry substrate, in which no spreading takes place, and that of a wet substrate over which liquid i has spread. If S_i is positive, then spreading takes place spontaneously and evenly over the substrate; otherwise, the liquid will form a partial droplet, or surface lens, on the substrate. [163, 164] Rewriting the spreading coefficient in terms of interfacial tension, equation 5.2 becomes

$$S_i = \gamma_{jk} - (\gamma_{ij} + \gamma_{ik}) \tag{5.3}$$

For phase-separated aerosol particles in air, the three-phase system is designated by the aqueous, organic, and gas phases labeled 1, 2, and 3, respectively. Thus, S_1 is the spreading of the aqueous phase over the organic phase and, due to interfacial tensions relevant to atmospheric aerosol, is assumed to always be negative, or to cost energy, and will not occur naturally in the atmosphere. [153] The spreading coefficient of the organic phase (S_2) and of air (S_3) can be positive or negative. Therefore, the possible particle configurations for an aerosol consisting of immiscible aqueous and organic phases are nonengulfing ($S_2 < 0$,$S_3 > 0$), where the two phases exist as side-by-side droplets with minimal contact; complete engulfing ($S_2 > 0$, $S_3 < 0$), where the organic phase completely surrounds the aqueous phase; and partially engulfing (S_2, $S_3 < 0$), the exact nature of which then depends on the volumes of each phase present in the whole particle. [37, 137, 153] By calculating the spreading coefficients for the relevant species in an aerosol particle, one can determine if the aerosol morphology is core-shell (i.e., completely engulfing) or partially engulfing. This spreading coefficient framework for predicting aerosol morphology has been validated for aerosols larger than ∼100 nm in diameter by comparison with molecular dynamics simulations [51] and experimental data. [37] Thus, knowledge of the interfacial tensions among the

chemical constituents relevant for ambient aerosol is important for predicting the morphology of liquid-liquid phase-separated aerosol.

One important constituent in ambient aerosol is methylglyoxal (MG, $C_3H_4O_2$), an oxidation product of many biogenic [165] and anthropogenic [166–170] volatile organic compounds (VOCs) and found in the gas phase at ppbv mixing ratios in urban atmospheres. [171–173] MG also partitions to the aqueous phase where it enhances cloud condensation nuclei (CCN) activity [174] and can be hydrated to form oligomers in solution. [175–177] MG has been detected in rain and cloud drops [87] and, with subsequent oligomerization, could result in organic material that remains in the particle phase after the evaporation of liquid droplets. [178]

Sareen et al. (2010) [179] studied the aqueous reactions of MG with ammonium salts and found that with reaction time (a proxy for aging of atmospheric aerosol), light-absorbing secondary products form in solution that additionally suppress the bulk surface tension of the mixture. The surface activity of species in these solutions is attributed to a methyl group, which adds hydrophobicity to MG and its oligomer products. [179] A detailed study [180] combining theory and measurements reveals that in a MG-water system, it is the singly hydrated methylglyoxal diol that populates the surface and is responsible for the surface-tension depression relative to pure water samples. The same singly hydrated MG was observed in a MG-ammonium sulfate (AS) system, [179] possibly explaining the surface tension depression observed for those systems as well.

Likewise, formaldehyde (F, CH_2O) is found at ppbv mixing ratios in urban atmospheres [181] and is both emitted directly and formed during atmospheric oxidation of some VOCs. [46, 182] Reactions of formaldehyde with amines and carbonyls

yield relatively nonvolatile and chemically stable organic salts, [183] which could explain the substantial amount of formaldehyde signal in the aerosol phase. [181] Aqueous formaldehyde can also form oligomers in solution, [182, 184, 185] similar to MG. Because of these oligomerization pathways, a combined MG-F-AS system was studied. [48] It was found that ternary mixtures of MG and either formaldehyde or acetaldehyde with AS exhibited surface tension behavior similar to binary mixtures with only MG with AS, indicating that MG is the dominant driver of surface activity in these solutions, likely due to the presence of the same singly hydrated MG molecule in solution.

The connection between surface-active organics and particle mixing state has not been well parameterized. [130] In this paper, we present an experimental framework to assess the interfacial activity of dissolved species in MG-F-AS aqueous systems. Specifically, we use biphasic microfluidics to measure the interfacial tension between an aqueous and an oil phase. These microfluidic experiments utilize high-speed imaging to monitor interfacial phenomena at the microscale. From these observations of interfacial tension of aerosol chemical mimics, the behavior and morphology of atmospheric aerosols due to interactions of liquid-liquid phase-separated interfaces within aerosol particles can be inferred.

Materials and Methods To measure interfacial tension, we fabricated a microfluidic device following the design of Hudson et al. (2005). [42] In the microfluidic device, a steady flow of immiscible drops ("dispersed phase") in a carrier fluid ("continuous phase") travels through a series of channel contractions and expansions. Each device is fabricated with multiple contractions and expansions to determine any dependence on interface age. The channel geometry sets up extensional flow

fields surrounding the droplets as they enter and exit narrow regions of the device. The droplets deform from an unperturbed, spherical shape to an elongated spheroidal shape due to the extensional stress on the droplet. Hydrodynamic forces are balanced by the interfacial tension at the boundary between the droplet and the surrounding carrier fluid.

The behavior of drop deformation in an extensional flow field is well-established, [40,41,186] and these results apply to the microscale. [187] The deformation, $D(x)$, is a scalar quantity describing the shape of the droplet as a function of spatial location, x, and is given by

$$D(x) = \frac{r_{major}(x) - r_{minor}(x)}{r_{major}(x) + r_{minor}(x)} \tag{5.4}$$

where x is the streamwise direction, r_{major}(x) is the major principal radius, and r_{minor}(x) is the minor principal radius of the droplet. The principal radii and deformation are functions of the x-direction because the droplets experience a changing extensional flow field as they travel through the device. For a Newtonian fluid, the material change of deformation of a spheroidal drop in steady, 1-D flow in the x-direction is given by [42, 187]

$$u(x)\frac{\partial D(x)}{\partial x} = \frac{5}{2\hat{\eta}+3}\dot{\varepsilon}(x) - \gamma\frac{D(x)}{\alpha\eta_c a_0} \tag{5.5}$$

where, $u(x)$ is droplet velocity, $\hat{\eta} = \eta_d/\eta_c$ is the relative viscosity between the drop (η_d) and surrounding fluid (η_c), $\dot{\varepsilon} = \partial u/\partial x$ is the surrounding fluid extension rate, γ is the interfacial tension, a_0 is the droplet equilibrium radius in the low-shear region

of the device, and α is a coefficient

$$\alpha = \frac{(2\hat{\eta}+3)(19\hat{\eta}+16)}{40(\hat{\eta}+1)} \tag{5.6}$$

which is a function of the relative viscosity. Rearranging 5.5 yields

$$\alpha\eta_c\left(\frac{5}{2\hat{\eta}+3}\dot{\varepsilon}(x) - u(x)\frac{\partial D(x)}{\partial x}\right) = \gamma\left(\frac{D(x)}{a_0}\right) \tag{5.7}$$

where every term is known (α, η_c, $\hat{\eta}$) or measured directly from video-microscopy image analysis ($u(x)$,$\dot{\varepsilon}$, $D(x)$, $\partial D/\partial x$, a_0), except interfacial tension, γ.

Droplet deformation is examined in the first contraction region, about 0.15 s after droplet formation, where the device geometry transitions from a wide (750 μm) to narrow (150 μm) channel width. For this study, we report measurements from the first contraction only, as we did not find any dependence on interface age between $\sim$0.15 and $\sim$0.71 s for the systems studied. These steady-state measurements imply that any depletion effects [188] that may be occurring inside each droplet are not affecting the equilibration time of the droplet interface in our system. Further effects of depletion on the absolute value of interfacial tension are not considered here, but it should be noted that similar effects are also expected in atmospheric aerosol of similar chemical composition to the mimic systems studied here.

Upstream of the deformation region, droplets are generated with a T-junction [189] or co-flow [190] geometry, both of which produce monodisperse droplets $\sim$40 - 150 μm in diameter at a rapid, steady rate. Each droplet is essentially a single-particle experiment that is rapidly repeated with each new droplet formed. In the current configuration, the droplet sizes are larger than the 2 - 20 μm diameter particles used in

other single particle techniques and are well above typical Kelvin diameters (<∼100 nm), [191] below which droplet curvature effects are important.

In the region of interest in the microfluidic device, a movie records droplets traveling into the contracting region at high frame rates (usually about 20000 frames per second) and captures droplet location and shape as it travels through the channel. Movies are typically less than one second in real time and contain ∼100 to 1000 individual droplets. Each frame of the movie is analyzed to determine droplet location (center of mass) and principal radii for all droplets in the frame. Analyzing each frame successively to follow individual droplets across the device determines droplet velocity and the change of these derived variables with location.

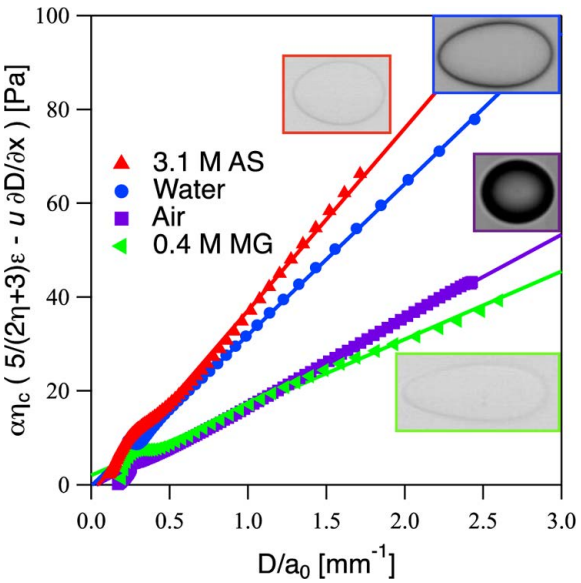

Figure 5.1: Taylor plot (from eq 7) for four individual droplets (3.1 M ammonium sulfate (AS), 0.4 M methylglyoxal (MG), and water) or bubble (air) in silicone oil. Each symbol is from a single frame of a movie tracking the individual droplets traveling through the microfluidic device. The solid lines are linear regressions to the data for each individual droplet, as described in the text. Bright-field raw images (not to scale) of the deformed droplets and bubble (equivalent diameters ∼40 - 105 μm) are shown to demonstrate the level of phase contrast for each type of dispersed phase.

The analysis follows previous work [42,187] with modifications in the mathematical treatment when poor phase contrast (e.g., see the images for 3.1 M AS and 0.4 M MG droplets in Figure 5.1) causes noise in the retrieved variables. After deformation and velocity are determined for a droplet's entire travel across the image, from the wide region of low extensional shear to the converging region of larger extensional shear, a polynomial of order 7 is fit to both $D(x)$ and $u(x)$ for all points where $D(x)$¡ 0.1 along the droplet's path. Derivatives of these polynomial fits yield $\partial D/\partial x$ and $\dot{\varepsilon}= \partial u/\partial x$ in 5.7. Interfacial tension is found by plotting the left-hand side of 5.7 versus $D(x)/\mathrm{a}_0$, as shown in Figure 5.1. On this "Taylor plot," [42] a line is fit over moderate deformations of $0.3 \leq D(x)/\mathrm{a}_0 \leq 2$, following criteria by Cabral and Hudson (2006). [187] The trend of the raw data at $D(x)/\mathrm{a}_0 \leq 0.3$ is dominated by the shapes of the polynomial fits and their derivatives at the edges of the limits used in the fit and thus do not represent physical phenomena in the drop deformation dynamics. The slope of the linear regression yields interfacial tension, γ, for each individual droplet, and there is negligible change in the linear fit whether it is forced through the origin or not. The range of deformation from 0.3 to 2 is large enough to be above any small oscillations in $D(x)$ and $u(x)$ values in 5.7 but small enough to avoid droplet rupture and breakup events. Note that despite the use of polynomial fits to smooth out noise, the final linear fit to the data is still susceptible to considerable variance when the image contrast is low. A sensitivity analysis reveals that the retrieved IFT is more sensitive to the droplet radii than to viscosity. For an uncertainty in the major or minor radii of 1%, which for these experiments is ∼2 pixels, the IFT can vary by as much as 15%. Fortunately, due to the large number of measurements performed in a single experiment, the median IFT value does not change significantly,

although the variance (error) for that median IFT value will increase as the radii uncertainty increases. Viscosity, however, has very little effect on the retrieved IFT. Even moderate uncertainties in viscosity of ∼30% yield a change in IFT of less than ∼0.1%. For a single experimental interfacial tension value, hundreds of individual droplets are analyzed. The distribution of single-droplet values are then compiled and a Gaussian function is fit to a histogram (see inset, Figure 5.2) of these values to yield the median interfacial tension with statistical uncertainty (the standard deviation of the Gaussian peak). A broader distribution of single-droplet values is typically observed for those samples with poor phase contrast or with few sample drops.

Details of the microfluidic device fabrication are as follows. From the device design criteria [42] mentioned earlier, a photolithography mask is drawn in DraftSight (Dassault Systems) and printed on a 20000 dpi high-resolution printer (CAD/Art Services, Inc.). A mold is prepared from this mask in a clean-room facility using standard photolithography techniques, [192–197] producing a silicon wafer that becomes a reusable master mold upon which the microfluidic devices are made. The microfluidic devices are constructed out of poly(dimethylsiloxane) (PDMS, Sylgard 184 Silicone Elastomer, Dow Corning Corporation), chosen for its ease in rapid prototyping [198] and successful applications in the microfluidic community. [42, 189, 194–196, 199–206] PDMS is cured over the master mold, and individual devices are cut from the wafer and sealed to a glass microscope slide coverslip. The microfluidic experiments are performed on an Olympus IX73 inverted microscope with phase contrast and bright-field imaging. Pressure-driven flow is generated by syringe pumps (Harvard Apparatus) with gas-tight syringes connected to PFA tubing and needles hermetically sealed to the PDMS device. Imaging is done with a Photron FASTCAM Mini UX100 high-

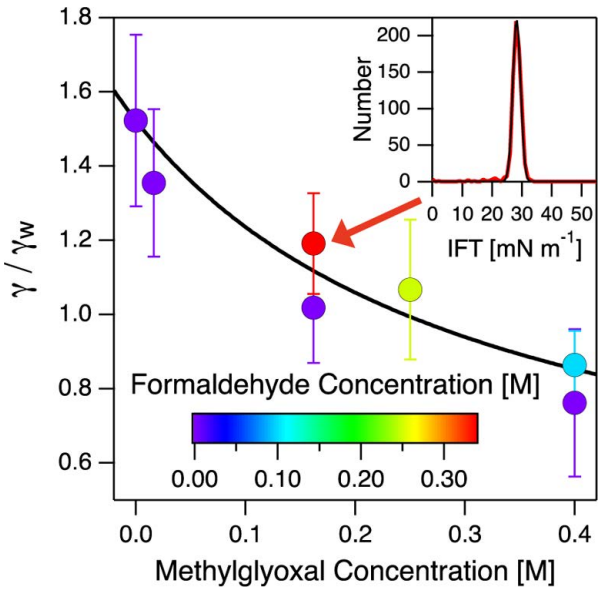

Figure 5.2: Relative interfacial tension at a reaction time of ∼24 h as a function of initial methylglyoxal (MG) content in 3.1 M ammonium sulfate (AS) solutions. The interfacial tension (IFT) is reported relative to that of water - silicone oil, γ_w. Marker colors indicate the amount of formaldehyde (F) in the solution. Error bars indicate statistical uncertainty of each measurement sample, given as the variance of the Gaussian probability distribution (inset) of measurements for hundreds of individual droplets at each concentration and time. The solid line is a Langmuir-like curve (eq 8) fit to the data, with parameters γ_0 = 1.52, S = 1.21, and b = 3.13. The inset graph shows a histogram (red) of droplet IFT values with a Gaussian fit (black), the median and variance of which is used to plot the experimental IFT for the solution of 0.162 M MG + 0.338 M F + 3.1 M AS (indicated with an arrow).

speed camera.

To properly quantify IFT, we independently measured the shear viscosity of the studied systems as a function of reaction time on an AR-G2 Rheometer from TA Instruments using a cup and bob geometry. A Mettler Toledo SevenExcellence multiparameter pH/conductivity meter was used to measure pH. Bulk-phase IFT measurements were performed on a Krüss Advanced Drop Shape Analysis Tensiometer using the pendant-drop method. Using this method, we measured the IFT between

water and silicone oil to be 24.27 ± 0.73 mN m-1, compared to 25.04 ± 2.31 mN m-1 with the microfluidic method. We also measured the IFT between 0.31 M ammonium sulfate solution and silicone oil to be 26.57 ± 2.32 mN m-1, compared to 25.46 ± 1.98 mN/m with the microfluidic method. These measurements are in agreement with prior validations of the microfluidic tensiometer method. [42]

In all experiments, the continuous-phase fluid is silicone oil (polydimethylsiloxane, Fisher Scientific, CAS 63148-62-9). In general, silicone oils consist of a linear chain of siloxane repeating units with various radical side groups, [207] resulting in a hydrophobic oil with a potentially high viscosity. In this study, silicone oil is used as a proxy for an immiscible organic phase that might be found attached to an aqueous phase in atmospheric aerosol. We measured a viscosity of 45.08 ± 0.63 mPa-s and a surface tension of 18.11 ± 1.28 mN/m for the specific silicone oil used here.

The dispersed phase fluid contains the solutions of interest. All water used in this study is HPLC-grade water (SigmaAldrich, CAS 7732-18-8). Stock solutions containing 3.1 M ammonium sulfate (AS, Avantor Performance Materials, CAS 7783-20-2) in HPLC water are mixed and used to make the organic solutions. Aqueous solutions up to 3.1 M AS are used to mimic ambient aerosol salt content. [76, 179, 208–210] Methylglyoxal solutions are prepared by adding the prescribed volume of a 40 wt% aqueous MG stock solution (Sigma-Aldrich, CAS 78-988) to the AS solutions. Solutions containing formaldehyde were added from a 37 wt% aqueous F stock solution (Sigma-Aldrich, CAS 50-00-0). All dispersed phase solutions in this study were stored in Pyrex jars with no special treatment to shield the jars from visible light, similar to previous studies. [179, 211] Results will be discussed in terms of reaction time, which is the time passed since adding the organic(s) to 3.1 M AS solution.

Results and Discussion Previous work has established that the addition of methylglyoxal to aqueous ammonium sulfate significantly suppresses the surface (aqueous-air) tension of the mixture. [179] Figure 5.2 shows normalized interfacial (aqueous-oil) tension as a function of MG content in 3.1 M AS solution, showing a similar trend as that of surface tension (cf. Figure 5.4, Sareen et al., 2010). [179] At low MG content, relative IFT is greater than 1 owing to the higher IFT for 3.1 M AS solution (38.13 ± 4.60 mN m-1) than for water (25.04 ± 2.31 mN m-1). As MG is increased, IFT decreases and approaches a minimum value. The dependence of IFT on MG content can be fit with a Langmuirlike curve, [30, 179]

$$\gamma = \gamma_0 - S\frac{bM_0}{1 + bM_0} \tag{5.8}$$

where γ_0 is the IFT with no MG, M0 is the MG concentration, and S and b are fit parameters. For the fit shown in Figure 5.2, γ_0, S, b = 1.52, 1.21, and 3.13, respectively. Over the range of MG concentration used, the trends of IFT suppression are the same as those previously reported for surface tension of this chemical system.

The IFT results in Figure 5.2 are measurements taken ∼24 h after the addition of the organic(s) to the AS solution. Over this reaction time, solutions containing MG become progressively darker (see pictures in Figure 5.3) due to the formation of lightabsorbing compounds in solution, resulting in a change in solution alkalinity (Figure 5.3, left). Recall that the fluid properties in 5.7 include solution viscosity as well as interfacial tension, so a change with time of the deformation behavior of the droplet could be due to a change in viscosity as the solution ages. However, within measurement uncertainty, the viscosity of the aqueous solutions containing varying amounts of MG and AS does not change with reaction time (Figure 5.3,

right). Because the bulk solution viscosity is constant in time, any differences in behavior of the droplet are explained through differences in the interfacial properties alone.

Previously, the surface tension of ternary mixtures of MG and F in 3.1 M AS solution have been shown to largely follow (within ∼10%) a single-component Szyszkowski-Langmuir curve. [48] Although the more-comprehensive Henning model [212] has been shown to describe well the behavior of surface tension for both nonreactive [212] and reactive [211] mixtures of organics, when accounting for the formaldehyde component in the Henning model, there is a larger deviation between measured and modeled values of surface tension. [48] These results indicate that for a MG-F-AS system, surface tension is largely governed by the amount of MG. As one might expect, the interfacial behavior of the same system here (Figure 5.2) behaves likewise, where the interfacial tension suppression is driven by MG, not F, content.

Results for interfacial tension measurements as a function of age are shown in Figure 5.4. Previous results for surface tension have indicated that after addition of MG to aqueous AS solutions, the measured surface tension will decrease over ∼24 h to a minimum value. [179] In contrast, it was found that IFT remained largely constant with reaction time for the MG + AS systems (Figure 5.4, top). MG has been shown to adsorb very slowly to the air-water interface in aqueous solutions; [180] thus, the rapid equilibration of IFT to oil could be the result of the microfluidic technique using a much smaller volume of solution than traditional bulk methods, where dissolved species need to travel far to find the interface. Even in pendant-drop experiments that can approach a similar droplet volume (∼2-16 mm3) [213] to those in this microfluidic study (∼3- 200 × 10-5 mm^3), suggesting that equilibration

time may be similar, the pendant-drop method is such that the droplet essentially has an infinite reservoir of surfactant available to the droplet interface, whereas the microfluidic droplets do not.

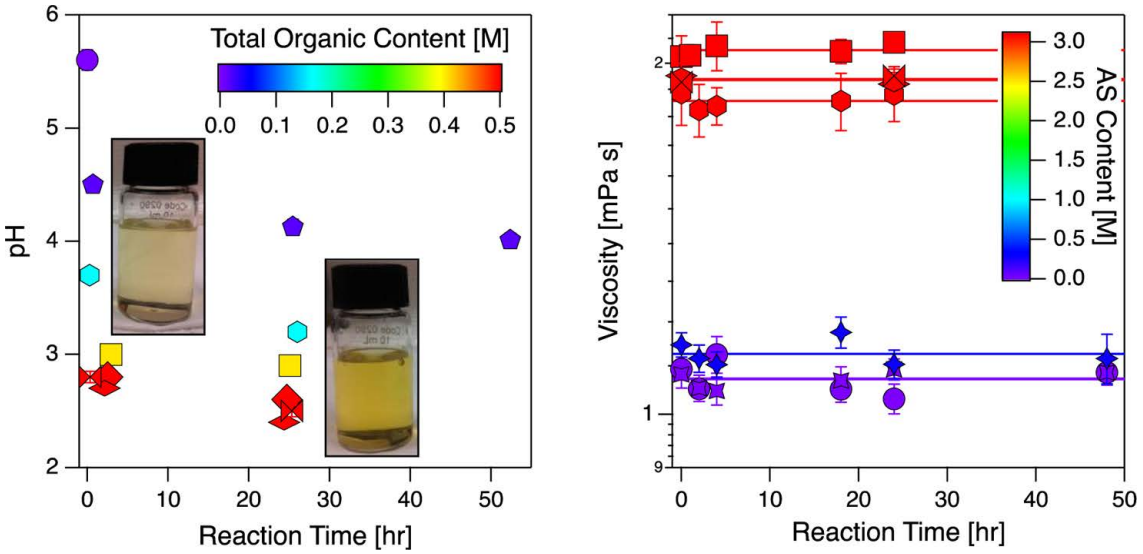

Figure 5.3: Solution pH (left) and viscosity (right) as a function of reaction time. Markers are colored by total organic content (left) and ammonium sulfate (AS) content (right) spanning the range of values used in this study. Error bars are one standard deviation; note that the error bars on the pH data are small enough to be hidden by the markers. Solid lines (right) are the average viscosities for each system. The images are vials of 0.162 M methylglyoxal in 3.1 M ammonium sulfate just after mixing (left) and after 24 h of reacting time (right).

To infer ambient aerosol morphology from these results, one can use the measured IFT values in 5.3 in combination with surface tensions previously reported. [179] For the MG-AS systems studied here, complete engulfing ($S_2 > 0$,$S_3 < 0$) is predicted for all concentrations of MG, and the change in surface tension with reaction time reported by Sareen et al. (2010) [179] is not a large enough change to cause a change in sign of either S_2 or S_3.

Surprisingly, in the presence of formaldehyde, aging effects on interfacial tension

become apparent (Figure 5.4, bottom). At the largest amount of MG content, the IFT remained constant with reaction time, behaving largely like the system with 0.4 M MG in 3.1 M AS displayed in the top of Figure 5.4. As the MG content decreases and F content increases, the IFT of the fresh mixture increases, and the change in IFT with age becomes more pronounced. For all three MG-F systems, the total organic content was fixed at 0.5 M and IFT suppression at ∼24 h reaction time for these systems is consistent with MG-only systems of similar MG content (Figure 5.2). The F dependence is a notable difference in these systems' IFT behavior with oil versus surface tension with air. Clearly, there is additional complexity to the chemical aging of these systems that is causing the surface activity to change with reaction time. To elucidate these differences, a future study on the detailed timedependent chemistry of this system should be performed, specifically to look for the behavior of surface-active species. As has been established for MG systems, the singly hydrated MG is a likely candidate as an important surface-active species. [180] Although this compound was observed in MG-F-AS systems, [48] it is unclear if this product might be consumed in later generations of reaction products, leading to an overall decrease in surface activity of the mixture.

The increase in IFT with chemical age for this system is consistent with an overall trend that lower-volatility oxidized (aged) organic aerosol shows a smaller departure from the surface tension of water than more hydrocarbon-like (fresh) organic aerosol (cf. Figure 6, McNeill et al., 2014). [77] Returning to 5.3 to infer ambient aerosol morphology of these systems, once again, complete engulfing is initially predicted for all ternary MG-F-AS systems studied here. However, in contrast to the binary MG-AS system, the large change in IFT with reaction time for the 0.25 M MG-0.25

M MG F system is large enough for S_2 to trend from a positive to negative value (within statistical uncertainty), meaning that this system is trending from complete engulfing toward a partial engulfing morphology.

This study has demonstrated the first use of a microfluidic experimental platform to investigate the interfacial properties of atmospheric aerosol mimics to assess the surface activity of dissolved constituents. In the current configuration, this platform allows rapid, repeatable measurements of interfacial tension between two immiscible liquids in a parameter space inaccessible to bulk measurements due to lengthy equilibration time scales of either the interface or the measurement itself.The results show that the interfacial tension of aqueous ammonium sulfate-methylglyoxal solutions to silicone oil have an interfacial tension depression similar to that of the solutions' surface tension depression. [179] However, unlike previous results for surface (aqueous-air) tension, the behavior of interfacial (aqueous-oil) tension of these solutions with the addition of formaldehyde exhibits a dependence on reaction time, indicating additional complexities as a result of species competition within the solution. Future work will assess a possible explanation for these complexities by considering the effect that depletion [188] might have on these chemical systems at the scale of atmospheric aerosol, by exploring alternate continuous phases for use in droplet microfluidic devices, and by performing bubble microfluidic tensiometry (for aqueous - air measurements).

In the next chapter, the techniques described in the current chapter are applied to organic acids and their ternary solutions with ammonium sulfate and real SOA samples. Interfacial tensions are measured for all these systems. Bulk surface tension measurements or model predictions are also presented for the organic acids. The

implications of our results on the spreading coefficients, and thus equilibrium morphology, are discussed.

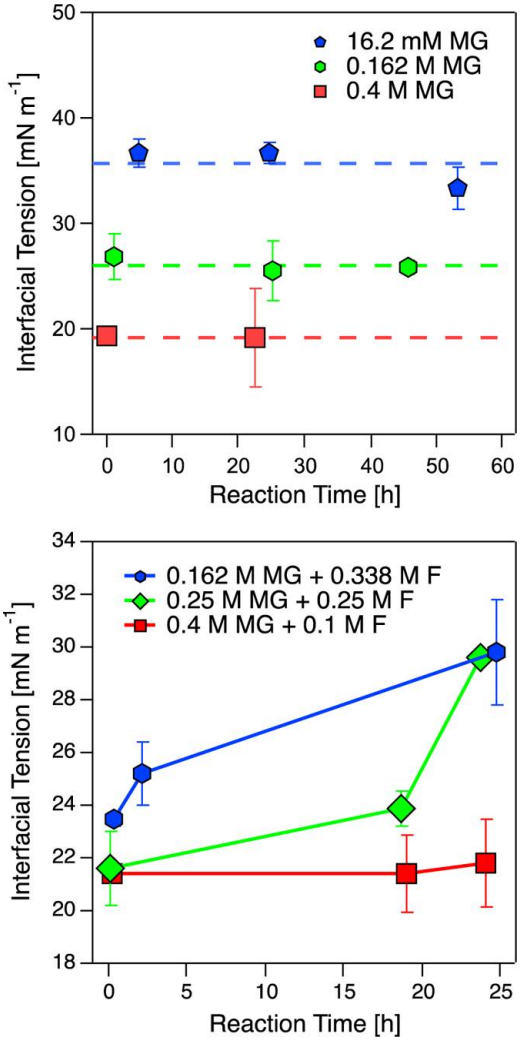

Figure 5.4: Interfacial tension as a function of reaction time for methylglyoxal (MG) + ammonium sulfate (AS) systems (top) and methylglyoxal + formaldehyde + ammonium sulfate systems (bottom). All solutions are in 3.1 M AS. Dashed lines (top) indicate average values for each system over all measurement times. Solid lines (bottom) connect the data points within each system as a guideline and do not indicate any functional dependence. Each data series is from a single solution allowed to react over the time displayed. Error bars on all data points show statistical uncertainty in the measurements.

Chapter 6

Interfacial Tensions of Secondary Organic Aerosol Containing Dicarboxylic Acids and Photo-oxidized Isoprene Samples[†]

Introduction

The methods described in the previous chapter for measuring interfacial tensions are applied here to organic aerosol chemical mimics and chamber samples. A certain class of organic acids, dicarboxylic acids, are studied here to complement the prior surface tension modeling work in Boyer and Dutcher, 2016 [26], as described in chapter 3. The chamber samples of secondary organic aerosol (SOA) material were derived from epoxides created by photooxidation of isoprene.

Recalling the discussion of organic acids in chapter 3, dicarboxylic acids span all major atmospheric systems, from urban to oceanic to arctic [82–89]. Dicarboxylic

[†]Part of this chapter was submitted recently in Boyer, H.C. and Dutcher, C.S. Atmospheric Aqueous Aerosol Surface Tensions: Isotherm-based Modeling and Biphasic Microfluidic Measurements,*Journal of Physical Chemistry A*, **2017**, Feature Article

acids are extremely relevant to aqueous atmospheric aerosols due to their abundance in the atmosphere coupled with their tendency to partition to solution surfaces [90–92]. Although organic acids are not considered to be strongly surface active, they cause non-negligable changes from the surface tension of pure water, where the surface tension decreases with increasing solute. By contrast, little is known of the surface propensities of isoprene photochemical reaction products.

Besides methane, isoprene (2-methyl-1,3-butadiene) is the most important and abundant volatile organic species (VOC) in the atmosphere. Biogenic in origin, roughly 600 Tg of isoprene are emitted into the atmosphere annually throughout the globe. [214] Isoprene is also highly reactive with oxidants, such as nitric oxides (NO_x), and leads to the formation of SOA. [47, 215–217]. In particular, epoxides derived from isoprene are known to be significant SOA precursors. [218–223] Reaction pathways from the gas phase photooxidation to SOA formation have been proposed for specific products, such as Lin and coworkers' study of methacrylic acid epoxide (MAE) [222]. Yet chemical partitioning to the particle phase mostly remains unclear. Since sample volume is quite small (<0.5 mL), bulk measurements are impossible; thus the microfluidic platform is highly advantageous for interfacial tension measurements. The outer phase is another liquid, rather than air, but the measurements can still inform chemical surface-bulk partitioning based on departure from the water/oil value.

Results for dicarboxylic acids

Interfacial tensions between aqueous dicarboxylic acids and an immiscible oil phase were measured for both binary solutions and ternary 3.1 M ammonium sulfate. In Figure 6.1, data are reported showing measurements for malonic acid (3C), succinic

acid (4C) and glutaric acid (5C) as 1.0 M pure solutions. Measurements for ternary solutions with ammonium sulfate are also reported in Figure 6.2 for two dilute organic concentrations. For the ternary solutions, the 4C organic acid is maleic acid instead of succinic acid. Succinic acid was available as a stock solution at a concentration of 1.0 M, and would therefore dilute the mixtures when added to them, hence the substitution of maleic acid for the ternary solutions. Data are reported in both plots where the surface is liquid - air (circles) and liquid - liquid (triangles). The circles are data taken with a pendant drop setup (Kruss Drop Shape Analysis 4) and the triangles are microfluidic measurements. Due to the lower relative values given by the liquid-liquid interfacial tensions, there could be a direct effect that the organic acids may have on the interface that is pronounced by the presence of the oil.

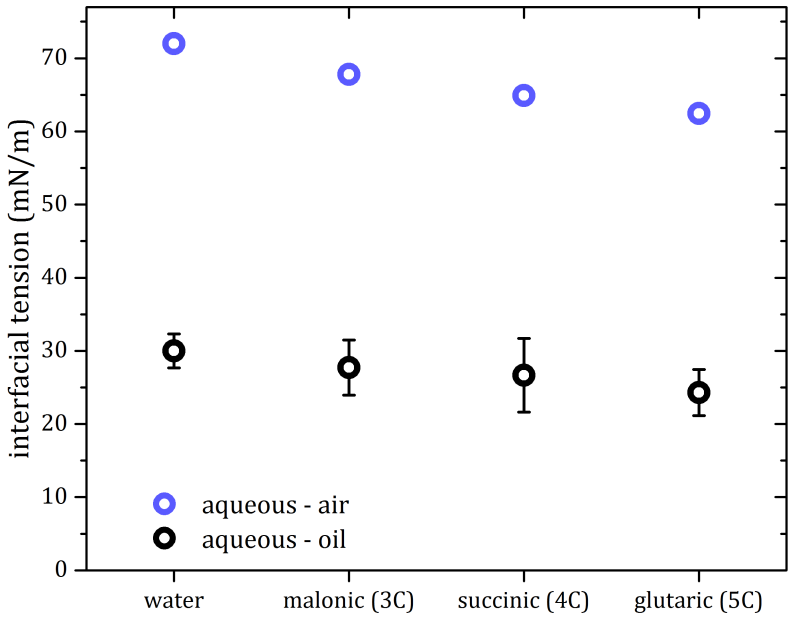

Figure 6.1: Interfacial tensions of aqueous solutions consisting of binary organic acids with respect to silicone oil (triangles) or air (circles).

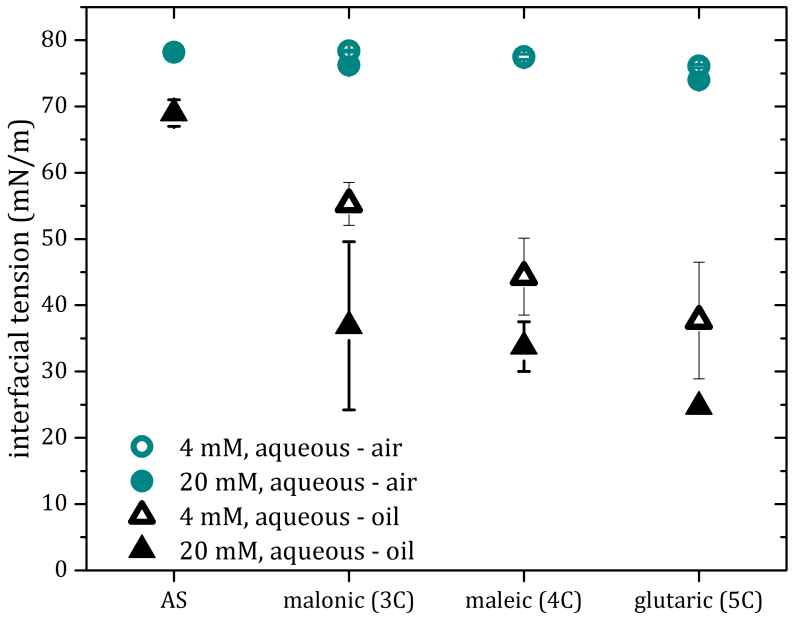

Figure 6.2: Interfacial tensions of ternary organic acids with 3.1 M ammonium sulfate (AS) with respect to silicone oil (triangles) or air (circles). Note the replacement of the 4C acid from Figure 6.1.

The organic acids may indirectly influence the shape of the particle by changing the liquid-air surface tension and the aqueous-organic interfacial tension. To measure the tendency of such systems to exist in certain morphologies, the spreading coefficient outlined in the previous chapter is calculated using equation 5.3. As a reminder, the spreading coefficient is a thermodynamic expression derived from minimizing free energy for multiple interfaces. Rewriting equation 5.3 gives

$$S_{oil} = \gamma_{aq,air} - (\gamma_{oil,air} + \gamma_{oil,aq}) \tag{6.1}$$

where the "aq" is the aqueous liquid, "oil" is the organic liquid, and "air" is the surrounding phase. Similarly,

$$S_{aq} = \gamma_{oil,air} - (\gamma_{aq,air} + \gamma_{oil,aq}) \tag{6.2}$$

Earlier work by Kwamena et al. [37] has demonstrated that spreading coefficients can predict non-spherical shapes when the values are negative for both organic (S_{oil}) and aqueous (S_{aq}) phases. S_{oil} is the level of spreading of the immiscible organic liquid over the aqueous phase, so a positive value indicates a core-shell morphology. S_{aq} is the level of adhesion between the two liquids, where a positive value indicates that the pure component surfaces are favorable to the shared surfaces. Thus, when $S_{oil} > 0$ and $S_{aq} < 0$, an organic shell with an aqueous core, or core-shell morphology, is predicted. When $S_{oil} < 0$, the aqueous core is partially engulfed by the organic liquid. Figure 6.3 shows the calculated spreading coefficients for aqueous dicarboxylic acids. Three solution concentrations are studied: 1.0 M (mol/L) binary, 4 mM (mmol/L) ternary, and 20 mM (mmol/L) ternary solutions. Binary solutions contain water and a single dicarboxylic acid (1 mol/L). Ternary solutions contain water, salt (3.1 M ammonium sulfate), and a dicarboxylic acid (4 or 20 mM).

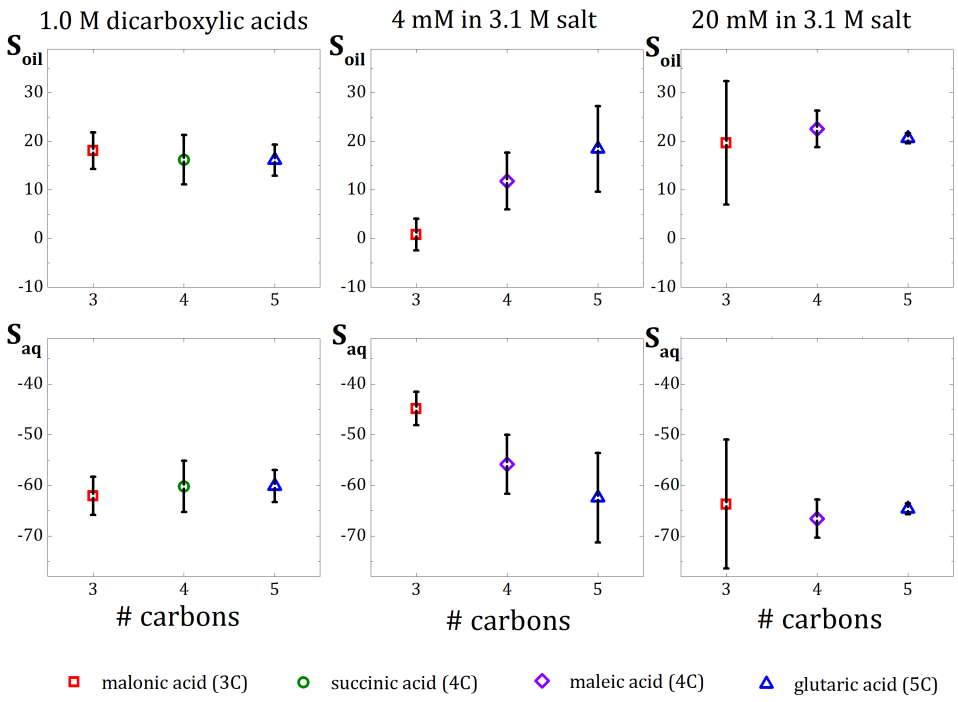

Figure 6.3: Spreading coefficent quantities S_{oil} and S_{aq} versus number of carbons of each compound studied for aqueous organic acids and their ternary solutions with 3.1 M ammonium sulfate.

Considering the variation in concentrations and the contrast of salty and non-salty solutions, noticeable changes in morphology could be expected. However, there are mostly small changes in S_{oil} and S_{aq} among the three concentrations. The exceptions are in the 4 mM plots, malonic and maleic acids show decreases in S_{oil} and increases in S_{aq}. The reason for this exception is perhaps the combination of low concentrations and the fact that these solutes are weak surfactants, thus driving the tendency of the aqueous phase towards an invidual surface, rather than a shared surface with the oil. For glutaric acid, all three solutions have remarkably similar spreading coefficients, possibly due to its relative propensity as a surfactant. The relative effects of this set

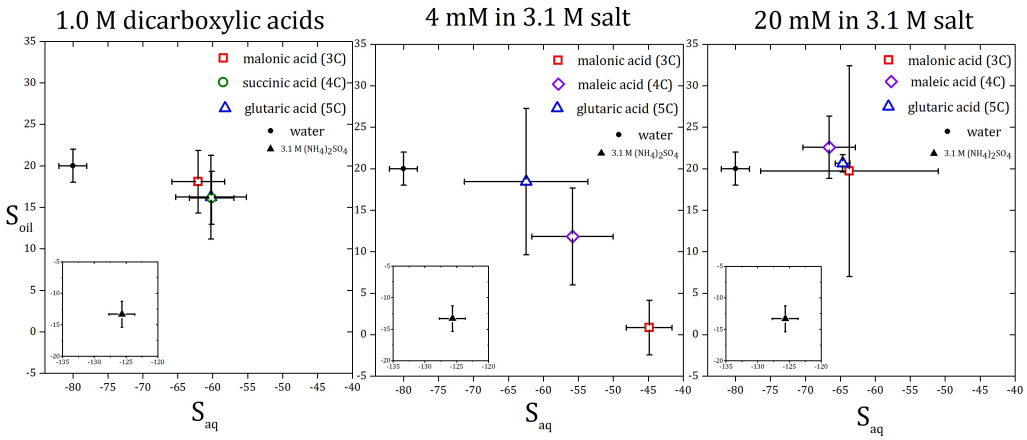

Figure 6.4: Spreading coefficients S_{oil} versus S_{aq} of aqueous organic acids, their ternary solutions with 3.1 M ammonium sulfate, and pure water (black circle). In the lower left corner of each panel, a subplot is shown with 3.1 M ammonium sulfate (black triangle).

of dicarboxylic acids on spreading coefficients are also shown by plotting S_{oil} versus S_{aq}, as in Figure 6.4.

Because of their high surface tensions, concentrated salty solutions tend to exhibit a partially engulfed morphology when in contact with an immiscible organic liquid. For example, the 3.1 M ammonium sulfate solution in Figure 6.4 is well into the lower left quadrant, indicating partial engulfing, while pure water and the organic solutions are all in the upper left quadrant, even though the ternary solutions contain dilute organics. In the very dilute solutions (middle plot), the effects of the number of carbons is pronounced, but at a slightly higher organic concentration (right plot) the core-shell structure becomes more stable, similar to that of pure water.

Results for SOA

We present interfacial tensions of select samples of SOA, which were available in limited quantities (0.5 mL each). The SOA are products of isoprene-derived epoxides and in liquid form because methanol/water solvent mixtures were used to extract

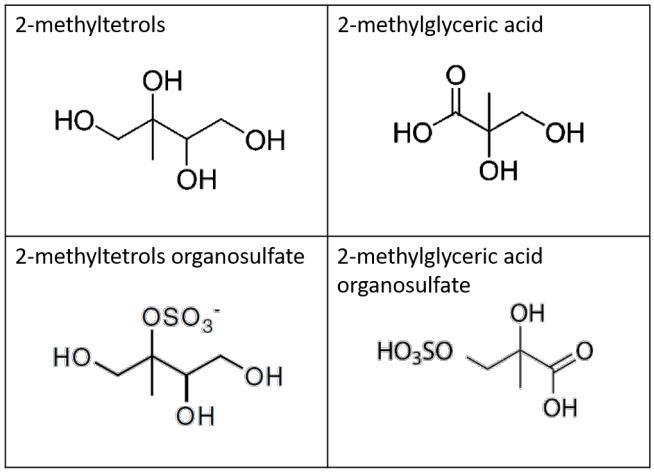

Figure 6.5: Chemical structures of photooxidized isoprene products.

them. The SOA samples contained 2-methylglyceric acid (2-MG) and 2-methyltetrol (tetrol) and their organosulfate derivatives (2-MG OS, tetrol OS). Chemical structures for the four samples are shown in Figure 6.5.

Initially, measurements were taken for solvents without SOA, particularly methanol and water mixtures at different volume fractions, as shown in Figure 6.6. Measurements agree well with data taken from the pendant drop method (Kruss Drop Shape Analyzer). Next, Figure 6.7 shows our preliminary data for SOA solutions and their respective pure solvents.

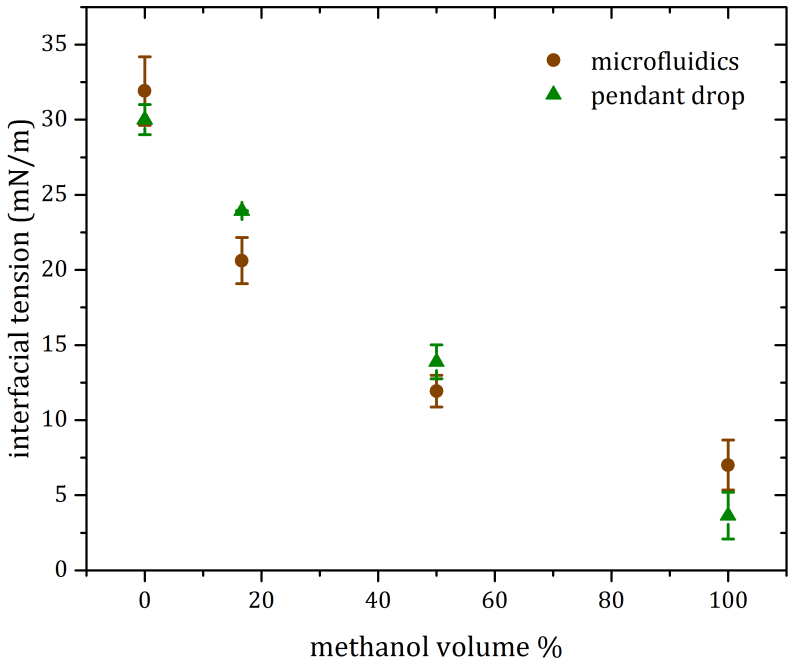

Figure 6.6: Interfacial tension measurements for pure methanol/water solvents as a function of methanol per cent. Measurements are taken using microfluidic tensiometry (brown circles) and pendant drop tensiometry (green triangles).

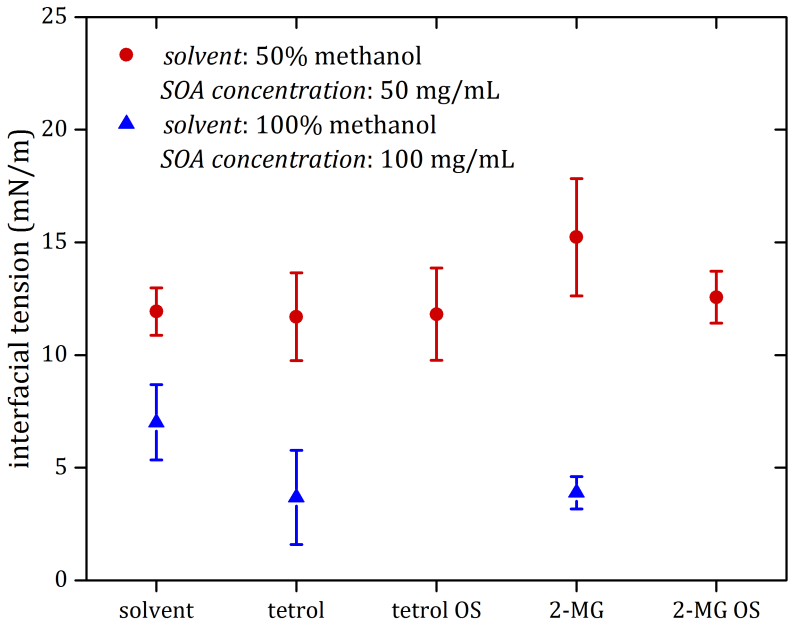

Figure 6.7: Interfacial tension measurements for the pure methanol/water solvents and solutions containing SOA, where the solvents are 50 % methanol by volume (red circles) and 100%methanol (blue triangles). The SOA material represented here are 2-methylglyceric acid (2-MG) and its organosulfate derivative (2-MG OS) and 2-methyltetrol (tetrol) and its organosulfate derivative (tetrol OS). The concentrations are 100 mg/mL of SOA in the 50 % methanol solvent and 50 mg/mL for the SOA in the 100 % methanol solvent, with units of mass of solute per volume of solution.

SOA	concentration (mg/mL)	solvent	IFT (mN/m)	std. dev.
2-MG	100	methanol	3.88	0.72
	50	50% methanol	15.23	2.60
tetrol	100	methanol	3.68	2.09
	50	50% methanol	11.70	1.95
2-MG-OS	10	50% methanol	12.57	1.15
tetrol OS	100	methanol	11.81	2.05

Table 6.1: Summary of microfluidic experiments for chamber samples of photo-oxidized organic aerosol material. Column labels are secondary organic aerosol (SOA), concentrations, solvent, interfacial tension measurements, and standard deviations.

The set of higher concentrated solutions tends to decrease the interfacial tension of the pure solvent, as evidenced by measurements for tetrol and 2-MG, each of which decreased the value by about 3 mN/m. For the lower concentrations, there are minimal differences in interfacial tensions of the solvent with and without SOA for tetrol, tetrol OS, and 2-MG OS at 50 mg/mL. For 2-MG, a slight increase with respect to the solvent interfacial tension contrasts with the decrease for the higher concentration. While 2-MG lowers the value for pure methanol, suggesting a surface propensity, the molecules could be hydrophilic enough to lose their surface active nature in the presence of water, which in that case would lead to an increase the interfacial tension. A summary of samples used so far in this study and results are found in Table 6.1.

Conclusions and future work

Throughout this thesis, discussions focused centrally on the surfaces relevant to atmospheric aqueous aerosols. Surfaces of atmospheric aerosol exhibit changes in their energies and compositions in response to molecular partitioning from the two bulk phases, which can be moderated by gas exchange or aqueous phase chemical reactions.

Since a significant portion of particle processing is surface-based, it is critical to understand particle surfaces as they are affected by varied chemical compositions in the bulk.

Advancements in modeling and measuring surface/interfacial tensions of liquid-liquid and liquid-vapor surfaces were presented in this thesis. The surface tension model was successful for a wide variety of solutes, including a host of inorganic electrolytes (chapter 2), alcohols and polyols (chapter 2), sugars (chapter 2), and partially dissociating organic acids (chapter 3). The model was rederived for multicomponent solutions (chapters 3 and 4), requiring no further fitting or parametrizing. The significance of the multicomponent model is that it accurately predicts surface tensions of mixtures containing more than one solute. Data were compared to model predictions for several combinations of solutes, including electrolytes and organics in the same solution, showing remarkable agreement for measurements on picolitre sized droplets.

The demonstrated efficacy of the multicomponent model is an important step towards handling chemically complex solutions applicable to the atmosphere. However, the model has not yet been applied to real aerosols. Measurements for the methylglyoxal, formaldehyde, and ammonium sulfate (chapter 5) and the current experiments with SOA could assist in further model development. There are two remaining compounds of SOA available to us: methylacrylic acid epoxide (MAE) and isoprene epoxydiol (IEPOX). Interfacial tension measurements for MAE have yet to be attempted; however, for IEPOX, upon flowing the sample into the microchannel, the sample did not disperse in the outer fluid, failing to form droplets.

Since the effects on interfacial tension in our results were minimal, the addition of a salt would potentially enhance the organics at the surface. We plan to mix our

remaining samples with concentrated aqueous ammonium sulfate and observe the effects on interfacial tensions of the samples. An indicator of "salting out" would be, for example, significant lowering of surface or interfacial tension upon addition of the salt to the aqueous organic solution. This information would be useful for both the dataset of interfacial properties of SOA material and for further developing the surface tension model to handle salting out effects.

Bibliography

[1] George, I. J.; Abbatt, J. P. D. Heterogeneous oxidation of atmospheric aerosol particles by gas-phase radicals. *Nat. Chem.* **2010**. 2 (9), 713–722. ISSN 1755-4330. doi:10.1038/nchem.806.

[2] You, Y.; Renbaum-Wolff, L.; Carreras-Sospedra, M.; Hanna, S. J.; Hiranuma, N.; Kamal, S.; Smith, M. L.; Zhang, X.; Weber, R. J.; Shilling, J. E.; Dabdub, D.; Martin, S. T.; Bertram, a. K. Images reveal that atmospheric particles can undergo liquid-liquid phase separations. *Proc. Natl. Acad. Sci.* **2012**. 109 (33), 13188–13193. ISSN 0027-8424. doi:10.1073/pnas.1206414109.

[3] IPCC, 2013: Climate Change 2013: The Physical Science Basis. Contribution of Working Group I to the Fifth Assessment Report of the Intergovernmental Panel on Climate Change. Technical report, IPCC, Cambridge, United Kingdom and New York, NY, USA **2013**.

[4] Twomey, S. Pollution and the Planetary Albedo. *Atmos. Environ.* **2007**. 41 (SUPPL.), 120–125. ISSN 13522310. doi:10.1016/j.atmosenv.2007.10.062.

[5] O'Dowd, C. D.; Facchini, M. C.; Cavalli, F.; Ceburnis, D.; Mircea, M.; Decesari, S.; Fuzzi, S.; Yoon, Y. J.; Putaud, J.-P. Biogenically driven organic contribution

to marine aerosol. *Nature* **2004**. 431 (7009), 676–680. ISSN 0028-0836. doi: 10.1038/nature02959.

[6] Meskhidze, N.; Nenes, A. Phytoplankton and Cloudiness in the Southern Ocean. *Science (80-.).* **2006**. 314 (December 2006), 1419–1423.

[7] Facchini, M. C.; Mircea, M.; Fuzzi, S.; Charlson, R. J. Cloud albedo enhancement by surface-active organic solutes in growing droplets. *Nature* **1999**. 401 (6750), 257–259. ISSN 0028-0836. doi:10.1038/45758.

[8] Booth, A. M.; Topping, D. O.; McFiggans, G. B.; Percival, C. J. Surface Tension of Mixed Inorganic and Dicarboxylic Acid Aqueous Solutions at 298.15 K and Their Importance for Cloud Activation Predictions. *Phys. Chem. Chem. Phys.* **2009**. 11 (36), 7759. ISSN 1463-9076. doi:10.1039/b916865f.

[9] Cruz, C. N.; Pandis, S. N. The effect of organic coatings on the cloud condensation nuclei activation of inorganic atmospheric aerosol. *J. Geophys. Res.* **1998**. 103 (D11), 13,111–113,123.

[10] Farmer, D. K.; Cappa, C. D.; Kreidenweis, S. M. Atmospheric Processes and Their Controlling Influence on Cloud Condensation Nuclei Activity. *Chem. Rev.* **2015**. 115 (10), 4199–4217. ISSN 15206890. doi:10.1021/cr5006292.

[11] Frosch, M.; Prisle, N. L.; Bilde, M.; Varga, Z.; Kiss, G. Joint effect of organic acids and inorganic salts on cloud droplet activation. *Atmos. Chem. Phys.* **2011**. 11 (8), 3895–3911. ISSN 1680-7324. doi:10.5194/acp-11-3895-2011.

[12] Novakov, T.; Penner, J. E. Large contribution of organic aerosols to cloud-condensation-nuclei concentrations. *Nature* **1993**. 365 (6449), 823–826. ISSN 0028-0836. doi:10.1038/365823a0.

[13] Shulman, M. L.; Jacobson, M. C.; Carlson, R. J.; Robert, E.; Young, T. E. Dissolution behavior and surface tension effects of organic compounds in nucleating cloud droplets. *Geophys. Res. Lett.* **1996**. 23 (3), 277–280. ISSN 00948276.

[14] Sun, J.; Ariya, P. Atmospheric organic and bio-aerosols as cloud condensation nuclei (CCN): A review. *Atmos. Environ.* **2006**. 40 (5), 795–820. ISSN 13522310. doi:10.1016/j.atmosenv.2005.05.052.

[15] Topping, D. O.; Mcfiggans, G. B.; Coe, H. A curved multi-component aerosol hygroscopicity model framework : Part 1 – Inorganic compounds. *Atmos. Chem. Phys.* **2005**. 1205–1222.

[16] Varga, Z.; Kiss, G.; Hansson, H.-C. Modelling the cloud condensation nucleus activity of organic acids on the basis of surface tension and osmolality measurements. *Atmos. Chem. Phys.* **2007**. 7 (17), 4601–4611. ISSN 16807324. doi:10.5194/acp-7-4601-2007.

[17] Köhler, H. The nucleus in and the growth of hygroscopic droplets. *Trans. Faraday Soc.* **1936**. 32 (1152), 1152. ISSN 0014-7672. doi:10.1039/tf9363201152.

[18] Thomson, S. W. On the equilibrium of vapour at a curved surface of liquid. *Philos. Mag.* **1871**. 4, 448–452.

[19] Ruehl, C. R.; Davies, J. F.; Wilson, K. An interfacial mechanism for cloud droplet formation on organic aerosols. *Science (80-.).* **2016**. 351 (6280), 1447–1450.

[20] Anttila, T.; Kerminen, V.-M. Influence of organic compounds on the cloud droplet activation: A model investigation considering the volatility, water solubility, and surface activity of organic matter. *J. Geophys. Res.* **2002**. 107 (D22), 1–13. ISSN 0148-0227. doi:10.1029/2001JD001482.

[21] Wexler, A. S.; Dutcher, C. S. Statistical mechanics of multilayer sorption: Surface tension. *J. Phys. Chem. Lett.* **2013**. 4 (10), 1723–1726. ISSN 19487185. doi:10.1021/jz400725p.

[22] Dutcher, C. S.; Ge, X.; Wexler, A. S.; Clegg, S. L. Statistical mechanics of multilayer sorption: Extension of the Brunauer-Emmett-Teller (BET) and Guggenheim-Anderson-de Boer (GAB) adsorption isotherms. *J. Phys. Chem. C* **2011**. 115 (33), 16474–16487. ISSN 19327447. doi:10.1021/jp203879d.

[23] Dutcher, C. S.; Ge, X.; Wexler, A. S.; Clegg, S. L. Statistical mechanics of multilayer sorption: 2. Systems containing multiple solutes. *J. Phys. Chem. C* **2012**. 116 (2), 1850–1864. ISSN 19327447. doi:10.1021/jp2084154.

[24] Dutcher, C. S.; Ge, X.; Wexler, A. S.; Clegg, S. L. An isotherm-based thermodynamic model of multicomponent aqueous solutions, applicable over the entire concentration range. *J. Phys. Chem. A* **2013**. 117 (15), 3198–3213. ISSN 10895639. doi:10.1021/jp310860p.

[25] Boyer, H.; Wexler, A.; Dutcher, C. S. Parameter Interpretation and Reduction for a Unified Statistical Mechanical Surface Tension Model. *J. Phys. Chem. Lett.* **2015**. 6 (17), 3384–3389. ISSN 1948-7185. doi:10.1021/acs.jpclett.5b01346.

[26] Boyer, H. C.; Dutcher, C. S. Statistical Thermodynamic Model for Surface Tension of Aqueous Organic Acids with Consideration of Partial Dissociation. *J. Phys. Chem. A* **2016**. 120 (25), 4368–4375. ISSN 15205215. doi:10.1021/acs.jpca.6b01469.

[27] Boyer, H. C.; Bzdek, B. R.; Reid, J. P.; Dutcher, C. S. A Statistical Thermodynamic Model for Surface Tension of Organic and Inorganic Aqueous Mixtures. *J. Phys. Chem. A* **2016**. acs.jpca.6b10057. ISSN 1089-5639. doi:10.1021/acs.jpca.6b10057.

[28] Ohm, P. B.; Asato, C.; Wexler, A. S.; Dutcher, C. S. Isotherm-Based Thermodynamic Model for Electrolyte and Nonelectrolyte Solutions Incorporating Long- and Short-Range Electrostatic Interactions. *J. Phys. Chem. A* **2015**. 119 (13), 3244–3252. ISSN 1089-5639. doi:10.1021/jp512646k.

[29] Nandy, L.; Ohm, P. B.; Dutcher, C. S. Isotherm-Based Thermodynamic Models for Solute Activities of Organic Acids with Consideration of Partial Dissociation. *J. Phys. Chem. A* **2016**. 120 (24), 4147–4154. ISSN 15205215. doi:10.1021/acs.jpca.6b01904.

[30] Langmuir, I. The Adsorption of Gases on Plane Surfaces of Glass, Mica and Platinum. *J. Am. Chem. Soc.* **1918**. 40 (9), 1361–1403. ISSN 00027863. doi:doi:10.1021/ja02242a004.

[31] Brunauer, S.; Emmett, P.; Teller, E. Adsorption of Gases in Multimolecular Layers **1938**. 60 (2), 309–319. ISSN 00027863. doi:citeulike-article-id:4074706$\backslash$backslash$rdoi:10.1021/ja01269a023.

[32] Stokes, R.; Robinson, R. Ionic hydration and activity in electrolyte solutions. *J. Am. Chem. Soc.* **1948**. 70 (5), 1870–1878. ISSN 0002-7863. doi:10.1021/ja01185a065.

[33] Ally, M. R.; Braunstein, J. Statistical mechanics of multilayer adsorption: electrolyte and water activities in concentrated solutions. *J. Chem. Thermodyn.* **1998**. 30 (1), 49–58. ISSN 00219614. doi:10.1006/jcht.1997.0278.

[34] Guggenheim, E. A. *Applications of Statistical Mechanics*. Clarendon Press:, Oxford, U.K. **1966**.

[35] Anderson, R. B. Modifications of the Brunauer, Emmett and Teller equation. *J. Am. Chem. Soc.* **1948**. 70 (5), 1727–1734. ISSN 0002-7863. doi:10.1021/ja01208a049.

[36] de Boer, J. H. *The Dynamical Character of Adsorption;*. Clarendon Press, Oxford, U.K. **1968**.

[37] Kwamena, N. O. a.; Buajarern, J.; Reid, J. P. Equilibrium morphology of mixed organic/Inorganic/Aqueous Aerosol droplets: Investigating the effect of relative humidity and surfactants. *J. Phys. Chem. A* **2010**. 114 (18), 5787–5795. ISSN 10895639. doi:10.1021/jp1003648.

[38] O'Brien, R. E.; Wang, B.; Kelly, S. T.; Lundt, N.; You, Y.; Bertram, A. K.; Leone, S. R.; Laskin, A.; Gilles, M. K. Liquid–Liquid Phase Separation in

Aerosol Particles: Imaging at the Nanometer Scale. *Environ. Sci. Technol.* **2015**. 49 (8), 4995–5002. ISSN 0013-936X. doi:10.1021/acs.est.5b00062.

[39] Metcalf, A. R.; Boyer, H. C.; Dutcher, C. S. Interfacial Tensions of Aged Organic Aerosol Particle Mimics Using a Biphasic Microfluidic Platform. *Environ. Sci. Technol.* **2016**. ISSN 0013-936X. doi:10.1021/acs.est.5b04880.

[40] Taylor, G. I. The Formation of Emulsions in Definable Fields of Flow. *Proc. R. Soc. A Math. Phys. Eng. Sci.* **1934**. 146 (858), 501–523. ISSN 1364-5021. doi:10.1098/rspa.1934.0169.

[41] Rallison, J. M. The Deformation of Small Viscous Drops and Bubbles in Shear Flows. *Annual* **1984**. (16), 45–66.

[42] Hudson, S. D.; Cabral, J. T.; Goodrum, W. J.; Beers, K. L.; Amis, E. J. Microfluidic interfacial tensiometry. *Appl. Phys. Lett.* **2005**. 87 (8), 8–10. ISSN 00036951. doi:10.1063/1.2034098.

[43] Cabral, J. T.; Hudson, S. D. Microfluidic approach for rapid multicomponent interfacial tensiometry. *Lab Chip* **2006**. 6, 427–436. ISSN 1473-0197. doi: 10.1039/b511976f.

[44] Zhang, Q.; Jimenez, J. L.; Canagaratna, M. R.; Allan, J. D.; Coe, H.; Ulbrich, I.; Alfarra, M. R.; Takami, a.; Middlebrook, a. M.; Sun, Y. L.; Dzepina, K.; Dunlea, E.; Docherty, K.; DeCarlo, P. F.; Salcedo, D.; Onasch, T.; Jayne, J. T.; Miyoshi, T.; Shimono, a.; Hatakeyama, S.; Takegawa, N.; Kondo, Y.; Schneider, J.; Drewnick, F.; Borrmann, S.; Weimer, S.; Demerjian, K.; Williams, P.; Bower, K.; Bahreini, R.; Cottrell, L.; Griffin, R. J.; Rautiainen, J.; Sun,

J. Y.; Zhang, Y. M.; Worsnop, D. R. Ubiquity and dominance of oxygenated species in organic aerosols in anthropogenically-influenced Northern Hemisphere midlatitudes. *Geophys. Res. Lett.* **2007**. 34 (13), 1–6. ISSN 00948276. doi: 10.1029/2007GL029979.

[45] Jimenez, A. J. L.; Canagaratna, M. R.; Donahue, N. M.; Prevot, a. S. H.; Zhang, Q.; Decarlo, P. F.; Allan, J. D.; Coe, H.; Ng, N. L.; Aiken, a. C.; Docherty, K. S.; Ulbrich, I. M.; Grieshop, P.; Robinson, a. L.; Duplissy, J.; Smith, J. D.; Wilson, K. R.; Lanz, V. a.; Hueglin, C.; Tian, J.; Laaksonen, a.; Raatikainen, T.; Rautiainen, J.; Vaattovaara, P.; Ehn, M.; Kulmala, M.; Tomlinson, M.; Collins, D. R.; Cubison, M. J.; Dunlea, E. J.; Prevot, a. S. H.; Zhang, Q.; Grieshop, a. P. Evolution of Organic Aerosols in the Atmosphere All use subject to JSTOR Terms and Conditions Evolution of Organic Aerosols in the Atmosphere **2015**.

[46] Seinfeld, J. H.; Pandis, S. N. *Atmospheric Chemistry and Physics: From Air Pollution to Climate Change*. John Wiley & Sons, Inc., New York, 2nd edition **2006**.

[47] Hallquist, M.; Wenger, J. C.; Baltensperger, U.; Rudich, Y.; Simpson, D.; Claeys, M.; Dommen, J.; Donahue, N. M.; George, C.; Goldstein, a. H.; Hamilton, J. F. The formation, properties and impact of secondary organic aerosol: current and emerging issues. *Atmos. Chem. Phys. Atmos. Chem. Phys.* **2009**. 9 (November 2008), 5155–5236. ISSN 1680-7324. doi:10.5194/acp-9-5155-2009.

[48] Li, Z.; Schwier, A. N.; Sareen, N.; McNeill, V. F. Reactive processing of formaldehyde and acetaldehyde in aqueous aerosol mimics: Surface tension de-

pression and secondary organic products. *Atmos. Chem. Phys.* **2011**. 11 (22), 11617–11629. ISSN 16807316. doi:10.5194/acp-11-11617-2011.

[49] Coury, C.; Dillner, A. M. A method to quantify organic functional groups and inorganic compounds in ambient aerosols using attenuated total reflectance FTIR spectroscopy and multivariate chemometric techniques. *Atmos. Environ.* **2008**. 42 (23), 5923–5932.

[50] Maria, S. F.; Russell, L. M.; Turpin, B. J.; Porcja, R. J. FTIR Measurements of Functional Groups and Organic Mass in Aerosol Samples Over the Caribbean. *Atmos. Environ.* **2002**. 36, 5185–5196.

[51] Maria, S. F. Organic Aerosol Growth Mechanisms and Their Climate-Forcing Implications. *Science (80-.).* **2004**. 306 (5703), 1921–1924. ISSN 0036-8075, 1095-9203. doi:10.1126/science.1103491.

[52] Allison C. Aiken, Peter F. DeCarlo, Jesse H. Kroll, Douglas R. Worsnop, J. Alex Huffman, Kenneth S. Docherty, Ingrid M. Ulbrich, Claudia Mohr, Joel R. Kimmel, Donna Sueper, Yele Sun, Qi Zhang, Achim Trimborn, Megan Northway, Paul J. Ziemann, Manjula R. Ca, U. B.; Jimenez, J. L. O/C and OM/OC Ratios of Primary, Secondary, and Ambient Organic Aerosols with High-Resolution Time-of-Flight Aerosol Mass Spectrometry. *Environ. Sci. Technol.* **2008**. 42 (12), 4478–4485.

[53] Saunders, S. M.; Jenkin, M. E.; Derwent, R. G.; Pilling, M. J. Tropospheric Degradation of Non-Aromatic Volatile Organic Compounds. *Atmos. Chem. Phys.* **2003**. 3, 161–180.

[54] Valorso, R.; Aumont, B.; Camredon, M.; Raventos-Duran, T.; Mouchel-Vallon, C.; Ng, N. L.; Seinfeld, J. H.; Lee-Taylor, J.; Madronich, S. Explicit Modelling of SOA Formation from α-pinene Photooxidation: Sensitivity to Vapour Pressure Estimation. *Atmos. Chem. Phys.* **2011**. 11 (14).

[55] Robinson, A. L.; Donahue, N. M.; Shrivastava, M. K.; Weitkamp, E. a.; Sage, A. M.; Grieshop, A. P.; Lane, T. E.; Pierce, J. R.; Pandis, S. N. Rethinking Organic Aerosols :. *Science (80-.).* **2007**. 315, 1259–1262. doi:10.1126/science.1133061.

[56] Cappa, C.; Wilson, K. Multi-Generation Gas-Phase Oxidation, Equilibrium Partitioning and the Formation and Evolution of Secondary Organic Aerosol. *Atmos. Chem. Phys.* **2012**. 12, 9505–9528.

[57] Hu, J.; Xiaoyi, Z.; Wang, Z. A Review on Progress in QSPR Studies for Surfactants. *Int. J. Mol. Sci.* **2010**. 11 (3), 1020–1047.

[58] Kier, L. B.; Hall, L. *Molecular Connectivity in Structure-Activity Analysis.* Letchworth: Research Studies Press **1986**.

[59] Stankevich, M.; Stenkevic, I.; Zefirov, N. Topological Indices in Organic Chemistry. *Russ. Chem. Rev.* **1988**. 57, 337–366.

[60] Stewart, J. MOPAC 6.0: A General Purpose Molecular Orbital Package **1989**.

[61] Wang, P.; Anderko, A.; Young, R. D. Modeling surface tension of concentrated and mixed-solvent electrolyte systems. *Ind. Eng. Chem. Res.* **2011**. 50 (7), 4086–4098. ISSN 03783812. doi:10.1016/j.fluid.2004.09.008.

[62] Pegram, L. M.; Record, M. T. Hofmeister salt effects on surface tension arise from partitioning of anions and cations between bulk water and the air-water interface. *J. Phys. Chem. B* **2007**. 111 (19), 5411–5417. ISSN 15206106. doi:10.1021/jp070245z.

[63] Dutcher, C. S.; Wexler, A. S.; Clegg, S. L. Surface tensions of inorganic multicomponent aqueous electrolyte solutions and melts. *J. Phys. Chem. A* **2010**. 114 (46), 12216–12230. ISSN 10895639. doi:10.1021/jp105191z.

[64] Szyszkowski, v. B. Experimentelle Studien uber kapillare Eigenschaften der wassrigen Losungen von Fettsauren. *Z. Phys. Chem.* **1908**. 64, 385.

[65] Vasquez, G.; Alvarez, E.; Navaza, J. M. Surface Tension of Alcohol + Water from 20 to 50 C. *J. Chem. Eng. Data* **1995**. 40 (3), 611–614. ISSN 0021-9568. doi:10.1021/je00019a016.

[66] Nakanishi, K.; Matsumoto, T.; Mitsuyoshi, H. Surface Tension of Aqueous Solutions of Some Glycols. *J. Chem. Eng. Data* **1971**. 16, 44–45.

[67] Yamada, M.; Fukusako, S.; Kawanami, T.; Sawada, I.; Horibe, A. Surface Tension of Aqueous Binary Solutions. *Int. J. Thermophys.* **1997**. 18, 1483–1493.

[68] Ernst, R. C.; Watkins, C. H.; Ruwe, H. H. The physical properties of the ternary system ethyl alcohol-glycerin-water. *J. Phys. Chem.* **1936**. 40 (5), 627. ISSN 0092-7325. doi:10.1021/j150374a008.

[69] Washburn, E.; West, C. J.; Hull, C. *International Critical Tables of Numerical Data, Physics, Chemistry, and Technology*, volume 4 **1928**.

[70] Abramzon, A.; Gaukhberg, R. Surface Tension of Salt Solutions (No. 8, Part 2). *Russ. J. Appl. Chem.* **1993**. 66, 1473–1479.

[71] Abramzon, A.; Gaukhberg, R. Surface Tension of Salt Solutions (No. 7, Part 2). *Russ. J. Appl. Chem.* **1993**. 66, 1473–1479.

[72] Matubayasi, N.; Tsunemtomo, K.; Sato, I.; Akizuki, I.; Morishita, T.; Matuzawa, A.; Natsukari, Y. Thermodynamic Quantities of Surface Formation of Aqueous Electrolyte Solutions. *J. Colloid Interface Sci.* **2001**. 243, 444–456. doi:10.1006/jcis.2001.7890.

[73] Drzymala, J.; Lyklema, J. Surface Tension of Aqueous Electrolyte Solutions. Thermodynamics. *116* **2012**. 6465–6472.

[74] Slavchov, R. I.; Novev, J. Surface Tension of Concentrated Electrolyte Solutions. *J. Colloid Interface Sci.* **2012**. 387, 234–243.

[75] Nayar, K.; Panchanathan, D.; McKinley, G.; Lienhard, J. Surface Tension of Seawater. *J. Phys. Chem. Ref. Data* **2014**. 43, 1–10.

[76] Schwier, A. N.; Viglione, G. A.; Li, Z.; Faye McNeill, V. Modeling the surface tension of complex, reactive organic-inorganic mixtures. *Atmos. Chem. Phys.* **2013**. 13 (21), 10721–10732. ISSN 16807316. doi:10.5194/acp-13-10721-2013.

[77] McNeill, V. F; Sareen, Neha; Schwier, A. N. Surface-Active Organics in Atmospheric Aerosols. *Top. Curr. Chem.* **2013**. 339 (4), 201–259. ISSN 1726670X. doi:10.1007/128.

[78] Lee, J. Y.; Hildemann, L. M. Surface tension of solutions containing dicarboxylic acids. *Atmos. Environ.* **2014**. 89, 260–267. ISSN 00218502. doi:10.1016/j.jaerosci.2013.06.004.

[79] Lewis, E. R. The effect of surface tension (Kelvin effect) on the equilibrium radius of a hygroscopic aqueous aerosol particle. *J. Aerosol Sci.* **2006**. 37 (11), 1605–1617. ISSN 00218502. doi:10.1016/j.jaerosci.2006.04.001.

[80] Asa-Awuku, a.; Nenes, a.; Sullivan, a. P.; Hennigan, C. J.; Weber, R. J. Investigation of molar volume and surfactant characteristics of water-soluble organic compounds in biomass burning aerosol. *Atmos. Chem. Phys. Discuss.* **2007**. 7, 3589–3627. ISSN 1680-7324. doi:10.5194/acpd-7-3589-2007.

[81] Chebbi, a.; Carlier, P. Carboxylic acids in the troposphere, occurrence, sources, and sinks: A review. *Atmos. Environ.* **1996**. 30 (24), 4233–4249. ISSN 13522310. doi:10.1016/1352-2310(96)00102-1.

[82] Bikkina, S.; Kawamura, K.; Imanishi, K.; Boreddy, S.; Nojiri, Y. Seasonal and Longitudinal Distributions of Atmospheric Water-Soluble Dicarboxylic Acids, Oxocarboxylic Acids, and α-dicarbonyls over the North Pacific. *J. Geophys. Res. Atmos.* **2015**. 120 (10), 5191–5213. ISSN 2169897X. doi:10.1002/2014JD022145.Received.

[83] Bikkina, S.; Kawamura, K.; Miyazaki, Y.; Fu, P. High abundances of oxalic, azelaic, and glyoxylic acids and methylglyoxal in the open ocean with high biological activity: Implication for secondary OA formation from isoprene. *Geophys. Res. Lett.* **2014**. 41 (10), 1419–1423. ISSN 19448007. doi:10.1002/2014GL059913.

[84] Fu, P.; Kawamura, K.; Usukura, K.; Miura, K. Dicarboxylic acids, ketocarboxylic acids and glyoxal in the marine aerosols collected during a round-the-world cruise. *Mar. Chem.* **2013**. 148, 22–32. ISSN 03044203. doi: 10.1016/j.marchem.2012.11.002.

[85] Kawamura, K.; Seméré, R.; Imai, Y.; Fujii, Y.; Hayashi, M. Water soluble dicarboxylic acids and related compounds in Antarctic aerosols. *J. Geophys. Res.* **1996**. 101 (D13), 18721. ISSN 0148-0227. doi:10.1029/96JD01541.

[86] Kawamura, K.; Yasui, O. Diurnal changes in the distribution of dicarboxylic acids, ketocarboxylic acids and dicarbonyls in the urban Tokyo atmosphere. *Atmos. Environ.* **2005**. 39 (10), 1945–1960. ISSN 13522310. doi:10.1016/j.atmosenv.2004.12.014.

[87] Sempere, R.; Kawamura, K. Comperative distribution of dicarboxylic acids and related polar compounds in snow, rain and aerosols from urban atmosphere. *Atmos. Environ.* **1994**. 28 (3), 449–459. ISSN 13522310. doi: 10.1016/1352-2310(94)90123-6.

[88] Sempéré, R.; Kawamura, K. Low molecular weight dicarboxylic acids and related polar compounds in the remote marine rain samples collected from western Pacific. *Atmos. Environ.* **1996**. 30 (10-11), 1609–1619. ISSN 13522310. doi:10.1016/1352-2310(95)00436-X.

[89] van Pinxteren, D.; Neusüß, C.; Herrmann, H. On the abundance and source contributions of dicarboxylic acids in size-resolved aerosol particles at continental sites in central Europe. *Atmos. Chem. Phys.* **2014**. 14 (8), 3913–3928. ISSN 1680-7324. doi:10.5194/acp-14-3913-2014.

[90] Blower, P. G.; Ota, S. T.; Valley, N. a.; Wood, S. R.; Richmond, G. L. Sink or surf: Atmospheric implications for succinic acid at aqueous surfaces. *J. Phys. Chem. A* **2013**. 117 (33), 7887–7903. ISSN 10895639. doi:10.1021/jp405067y.

[91] Blower, P. G.; Shamay, E.; Kringle, L.; Ota, S. T.; Richmond, G. L. Surface behavior of malonic acid adsorption at the air/water interface. *J. Phys. Chem. A* **2013**. 117 (12), 2529–2542. ISSN 10895639. doi:10.1021/jp310851j.

[92] Mahiuddin, S.; Minofar, B.; Borah, J. M.; Das, M. R.; Jungwirth, P. Propensities of oxalic, citric, succinic, and maleic acids for the aqueous solution/vapour interface: Surface tension measurements and molecular dynamics simulations. *Chem. Phys. Lett.* **2008**. 462 (4-6), 217–221. ISSN 00092614. doi: 10.1016/j.cplett.2008.07.085.

[93] Öhrwall, G.; Prisle, N. L.; Ottosson, N.; Werner, J.; Ekholm, V.; Walz, M.-M.; Björneholm, O. Acid–Base Speciation of Carboxylate Ions in the Surface Region of Aqueous Solutions in the Presence of Ammonium and Aminium Ions. *J. Phys. Chem. B* **2015**. 119 (10), 4033–4040. ISSN 1520-6106. doi:10.1021/jp509945g.

[94] Lee, M.-T.; Brown, M. a.; Kato, S.; Kleibert, A.; Türler, A.; Ammann, M. Competition between Organics and Bromide at the Aqueous Solution–Air Interface as Seen from Ozone Uptake Kinetics and X-ray Photoelectron Spectroscopy. *J. Phys. Chem. A* **2015**. 119, 4600–4608. ISSN 1089-5639. doi:10.1021/jp510707s.

[95] Aumann, E.; Hildemann, L. M.; Tabazadeh, a. Measuring and modeling the composition and temperature-dependence of surface tension for organic solutions. *Atmos. Environ.* **2010**. 44 (3), 329–337. ISSN 13522310. doi: 10.1016/j.atmosenv.2009.10.033.

[96] Enami, S.; Hoffmann, M. R.; Colussi, A. J. Stepwise Oxidation of Aqueous Dicarboxylic Acids by Gas-Phase OH Radicals. *J. Phys. Chem. Lett.* **2015**. doi:10.1021/jz502432j.

[97] Hyvärinen, A.; Lihavainen, H.; Gaman, A.; Vairila, L.; Ojala, H.; Kulmala, M.; Palme, E. Surface tensions and densities of oxalic, malonic, succinic, maleic, malic, and cis-pinonic acids. *J. Chem. Eng. Data* **2006**. 51 (1), 255–260.

[98] Granados, K.; Gracia-fadrique, J. Refractive Index , Surface Tension and Density of Aqueous Mixtures of Carboxylic Acids at 298 . 15 K . *J. Chem. Eng. Data* **2006**. 51, 1356–1360.

[99] Morris, H. S.; Grassian, V. H.; Tivanski, A. V. Humidity-dependent surface tension measurements of individual inorganic and organic submicrometre liquid particles. *Chem. Sci.* **2015**. 6, 3242–3247. ISSN 2041-6520. doi:10.1039/C4SC03716B.

[100] Clegg, S. L.; Seinfeld, J. H. Thermodynamic Models of Aqueous Solutions Containing Inorganic Electrolytes and Dicarboxylic Acids at 298.15 K. 2. Systems Including Dissociation Equilibria. *J. Phys. Chem. A* **2006**. 110 (17), 5718–5734. ISSN 1089-5639. doi:10.1021/jp056150j.

[101] Perrin, D. D. *Dissociation Constants of Organic Bases in Aqueous Solution*. Butterworths, London **1965**.

[102] Lide, D. R. *CRC Handbook of Chemistry and Physics, 2003-2004*, volume 53. 84th edition **2003**. ISBN 0849304849. doi:10.1136/oem.53.7.504.

[103] Robinson, E. S.; Saleh, R.; Donahue, N. M. Organic aerosol mixing observed by single-particle mass spectrometry. *J. Phys. Chem. A* **2013**. 117 (51), 13935–13945. ISSN 10895639. doi:10.1021/jp405789t.

[104] Alvarez, E. Surface Tension of Organic Acids + Water Binary Mixtures from 20 C to 50 C. *J. Chem. Eng. Data* **1997**. 42 (97), 957–960.

[105] Saxena, P.; Hildemann, L. M. Water-soluble organics in atmospheric particles: A critical review of the literature and application of thermodynamics to identify candidate compounds. *J. Atmos. Chem.* **1996**. 24 (1), 57–109. ISSN 0167-7764. doi:10.1007/BF00053823.

[106] Zhang, H.; Xie, C.; Liu, Z.; Gong, J. Identification and Molecular Understanding of the Odd–Even Effect of Dicarboxylic Acids Aqueous Solubility. *Ind. Eng. Chem. Res.* **2013**. 52 (51), 18458–18465. ISSN 0888-5885. doi: 10.1021/ie4030837.

[107] Venkateshwaran, V.; Vembanur, S.; Garde, S. Water-mediated ion-ion interactions are enhanced at the water vapor-liquid interface. *Proc. Natl. Acad. Sci. U. S. A.* **2014**. 111 (24), 8729–34. ISSN 1091-6490. doi:10.1073/pnas.1403294111.

[108] Faust, J. a.; Dempsey, L. P.; Nathanson, G. M. Surfactant-promoted reactions of Cl2 and Br2 with Br- in glycerol. *J. Phys. Chem. B* **2013**. 117 (41), 12602–12612. ISSN 15206106. doi:10.1021/jp4079037.

[109] Noziere, B. Dont' forget the surface. *Science (80-.).* **2016**. 351 (6280), 1396–1397.

[110] Yli-juuti, T.; Zardini, A. a.; Eriksson, A. C.; Hansen, A. M. K.; Pagels, J. H.; Swietlicki, E.; Svenningsson, B.; Glasius, M.; Worsnop, D. R.; Riipinen, I.; Bilde, M. Volatility of organic aerosol: evaporation of ammonium sulfate/ succinic acid aqueous solution droplets. *Environ. Sci. Technol.* **2013**. 47, 12123–12130.

[111] Li, Z.-B.; Li, Y.-G.; Lu, J.-F. Surface Tension Model for Concentrated Electrolyte Aqueous Solutions by the Pitzer Equation. *Ind. Eng. Chem. Res.* **1999**. 38, 1133–1139. ISSN 0888-5885. doi:10.1021/ie980465m.

[112] Li, Z.; Lu, B. C. On the Prediction of Surface Tension for Multicomponent Mixtures **2001**. 79, 402–411.

[113] Hu, Y. F.; Lee, H. Prediction of the surface tension of mixed electrolyte solutions based on the equation of Patwardhan and Kumar and the fundamental Butler equations. *J. Colloid Interface Sci.* **2004**. 269 (2), 442–448. ISSN 00219797. doi:10.1016/S0021-9797(03)00703-3.

[114] Lee, J. Y.; Hildemann, L. M. Surface tension of solutions containing dicarboxylic acids with ammonium sulfate, d-glucose, or humic acid. *J. Aerosol Sci.* **2013**. 64, 94–102. ISSN 00218502. doi:10.1016/j.jaerosci.2013.06.004.

[115] Pitzer, K. S. Thermodytriarnics of Electrolytes. I. Theoretical Basis and General Equations. *J. Phys. Chem.* **1973**. 77 (2), 268–277. ISSN 0022-3654. doi:10.1021/j100621a026.

[116] Bzdek, B. R.; Power, R. M.; Simpson, S. H.; Reid, J. P.; Royall, C. P. Precise, contactless measurements of the surface tension of picolitre aerosol droplets. *Chem. Sci.* **2016**. 7, 274–285. ISSN 2041-6520. doi:10.1039/C5SC03184B.

[117] Power, R. M.; Simpson, S. H.; Reid, J. P.; Hudson, a. J. The transition from liquid to solid-like behaviour in ultrahigh viscosity aerosol particles. *Chem. Sci.* **2013**. 4, 2597–2604. ISSN 2041-6520. doi:10.1039/c3sc50682g.

[118] Power, R. M.; Burnham, D. R.; Reid, J. P. Toward optical-tweezers-based force microscopy for airborne microparticles. *App. Opt.* **2014**. 53 (36), 8522–8534. ISSN 0003-6935. doi:10.1364/AO.53.008522.

[119] Power, R. M.; Reid, J. P. Probing the micro-rheological properties of aerosol particles using optical tweezers. *Rep. Prog. Phys.* **2014**. 77 (7), 074601. ISSN 1361-6633. doi:10.1088/0034-4885/77/7/074601.

[120] Preston, T. C.; Reid, J. P. Accurate and efficient determination of the radius, refractive index, and dispersion of weakly absorbing spherical particle using whispering gallery modes. *J. Opt. Soc. Am. B-Optical Phys.* **2013**. 30 (8), 2113–2122. ISSN 0740-3224. doi:10.1364/josab.30.002113.

[121] Rayleigh, L. On the capillary phenomena of jets. *Proc. R. Soc. London* **1879**. 29.

[122] Lamb, H. *Hydrodynamics*. Cambridge University Press, Cambridge, 6th edition **1932**.

[123] Cai, C.; Miles, R. E.; Cotterell, M. I.; Marsh, A.; Rovelli, G.; Rickards, A. M. J.; Zhang, Y.-H.; Reid, J. P. Comparison of methods for predicting the

composition dependence of the density and refractive index of organic-aqueous aerosols. *J. Phys. Chem. A* **2016**. 120, 6604–6617. ISSN 1089-5639. doi: 10.1021/acs.jpca.6b05986.

[124] Bzdek, B. R.; Collard, L.; Sprittles, J. E.; Hudson, A. J.; Reid, J. P. Dynamic measurements and simulations of airborne picolitre-droplet coalescence in holographic optical tweezers. *J. Chem. Phys.* **2016**. 145 (5), 054502. ISSN 0021-9606. doi:10.1063/1.4959901.

[125] Belton, J. The surface tensions of ternary solutions. Part III. *Trans. Faraday Soc.* **1935**. 31, 1648–1652. ISSN 00016160. doi:10.1016/0001-6160(56)90042-6.

[126] Vanhanen, J.; Hyvärinen, A.-P.; Anttila, T.; Raatikainen, T.; Viisanen, Y.; Lihavainen, H. Ternary solution of sodium chloride, succinic acid and water; surface tension and its influence on cloud droplet activation. *Atmos. Chem. Phys.* **2008**. 8, 4595–4604. ISSN 1680-7324. doi:10.5194/acp-8-4595-2008.

[127] Jimenez, J. L.; Canagaratna, M. R.; Donahue, N. M.; Prevot, A. S. H.; Zhang, Q.; Kroll, J. H.; DeCarol, P. F.; Allan, J. D.; Coe, H.; Ng, N. L.; Aiken, A. C.; Docherty, K. S. Evolution of Organic Aerosols in the Atmosphere. *Science (80-.).* **2009**. 326, 1525–1529.

[128] Goldstein, A. H.; Galbally, I. E. Known and unexplored organic constituents in the earth's atmosphere. *Environ. Sci. Technol.* **2007**. 41 (5), 1514–1521. ISSN 0013936X. doi:10.1021/es072476p.

[129] McNeill, V. F. Aqueous organic chemistry in the atmosphere: Sources and chemical processing of organic aerosols. *Environ. Sci. Technol.* **2015**. 49 (3), 1237–1244. ISSN 15205851. doi:10.1021/es5043707.

[130] Schwier, A. N.; Viglione, G. A.; Li, Z.; McNeill, V. F. Modeling the Surface Tension of Complex, Reactive Organic-Inorganic Mixtures. *Atmos. Chem. Phys.* **2013**. 13, 10721–10732.

[131] Facchini, M. C.; Decesari, S.; Mircea, M.; Fuzzi, S.; Loglio, G. Surface tension of atmospheric wet aerosol and cloud/fog droplets in relation to their organic carbon content and chemical composition. *Atmos. Environ.* **2000**. 34 (28), 4853–4857. ISSN 13522310. doi:10.1016/S1352-2310(00)00237-5.

[132] Taraniuk, I.; Graber, E. R.; Kostinski, A.; Rudich, Y. Surfactant properties of atmospheric and model humic-like substances (HULIS). *Geophys. Res. Lett.* **2007**. 34 (16), 1–5. ISSN 00948276. doi:10.1029/2007GL029576.

[133] Zuend, A.; Marcolli, C.; Peter, T.; Seinfeld, J. H. Computation of liquid-liquid equilibria and phase stabilities: Implications for RH-dependent gas/particle partitioning of organic-inorganic aerosols. *Atmos. Chem. Phys.* **2010**. 10 (16), 7795–7820. ISSN 16807316. doi:10.5194/acp-10-7795-2010.

[134] Ally, M. R.; Braunstein, J.; Shulman, M. L.; Charlson, R. J.; Davis, E. J.; O'Dowd, C. D.; de Leeuw, G.; Zuend, A.; Marcolli, C.; Peter, T.; Seinfeld, J. H.; McNeill, V. F.; Patterson, J.; Wolfe, G. M.; Thornton, J. A.; Lam, W.; Hakkinen, S. A. K.; McNeill, V. F.; Riipinen, I.; Folkers, M.; Mentel, T. F.; Wahner, A.; Buajarern, J.; Mitchem, L.; Reid, J. P. Computation of liquid-liquid equilibria and phase stabilities: Implications for RH-dependent

gas/particle partitioning of organic-inorganic aerosols. *J. Phys. Chem. A* **2007**. 30 (12), 7795–7820. ISSN 00948276. doi:10.1006/jcht.1997.0278.

[135] Folkers, M.; Mentel, T. F.; Wahner, A. Influence of an organic coating on the reactivity of aqueous aerosols probed by the heterogeneous hydrolysis of N2O5. *Geophys. Res. Lett.* **2003**. 30 (12), article number 1644. ISSN 00948276. doi: 10.1029/2003GL017168.

[136] Shulman, M. L.; Charlson, R. J.; Davis, E. J. The effects of atmospheric organics on aqueous droplet evaporation. *J. Aerosol Sci.* **1997**. 28 (5), 737–752. ISSN 00218502. doi:10.1016/S0021-8502(96)00469-7.

[137] Buajarern, J.; Mitchem, L.; Reid, J. P. Characterizing multiphase Organic Inorganic Aqueous aerosol droplets. *J. Phys. Chem. A* **2007**. 111, 9054–9061. ISSN 1089-5639. doi:10.1021/jp074366a.

[138] Davies, J. F.; Miles, R. E. H.; Haddrell, A. E.; Reid, J. P. Influence of organic films on the evaporation and condensation of water in aerosol. *Proc. Natl. Acad. Sci. U. S. A.* **2013**. 110 (22), 8807–12. ISSN 1091-6490. doi:10.1073/ pnas.1305277110.

[139] Baustian, K. J.; Cziczo, D. J.; Wise, M. E.; Pratt, K. A.; Kulkarni, G.; Hallar, A. G.; Tolbert, M. A. Importance of aerosol composition, mixing state, and morphology for heterogeneous ice nucleation: A combined field and laboratory approach. *J. Geophys. Res. Atmos.* **2012**. 117 (6), 1–13. ISSN 01480227. doi:10.1029/2011JD016784.

[140] Lance, S.; Nenes, A.; Rissman, T. A. Chemical and dynamical effects on cloud droplet number: Implications for estimates of the aerosol indirect effect. *J. Geophys. Res. D Atmos.* **2004**. 109 (22), 1–13. ISSN 01480227. doi:10.1029/2004JD004596.

[141] Ellison, G. B.; Tuck, A. F.; Vaida, V. Atmospheric processing of organic aerosols. *J. Geophys. Res.* **1999**. 104 (D9), 11633–11641. ISSN 0148-0227. doi:10.1029/1999JD900073.

[142] Bertram, A. K.; Ivanov, A. V.; Hunter, M.; Molina, L. T.; Molina, M. J. The reaction probability of OH on organic surfaces of tropospheric interest. *J. Phys. Chem. A* **2001**. 105 (41), 9415–9421. ISSN 10895639. doi:10.1021/jp0114034.

[143] Lang-Yona, N.; Abo-Riziq, A.; Erlick, C.; Segre, E.; Trainic, M.; Rudich, Y. Interaction of internally mixed aerosols with light. *Phys. Chem. Chem. Phys.* **2010**. 12 (1), 21–31. ISSN 1463-9084. doi:10.1039/b913176k.

[144] Wise, M. E.; Baustian, K. J.; Tolbert, M. a. Internally mixed sulfate and organic particles as potential ice nuclei in the tropical tropopause region. *Proc. Natl. Acad. Sci. U. S. A.* **2010**. 107 (15), 6693–8. ISSN 1091-6490. doi:10.1073/pnas.0913018107.

[145] Garland, R. M.; Wise, M. E.; Beaver, M. R.; DeWitt, H. L.; Aiken, a. C.; Jimenez, J. L.; Tolbert, M. a. Impact of palmitic acid coating on the water uptake and loss of ammonium sulfate particles. *Atmos. Chem. Phys. Discuss.* **2005**. 5 (2), 2047–2074. ISSN 1680-7324. doi:10.5194/acpd-5-2047-2005.

[146] Chan, M. N.; Chan, C. K. Mass transfer effects on the hygroscopic growth of ammonium sulfate particles with a water-insoluble coating. *Atmos. Environ.* **2007**. 41 (21), 4423–4433. ISSN 13522310. doi:10.1016/j.atmosenv.2007.01.047.

[147] Wise, M. E.; Garland, R. M.; Tolbert, M. A. Ice nucleation in internally mixed ammonium sulfate/dicarboxylic acid particles. *J. Geophys. Res. D Atmos.* **2004**. 109 (19), 1–14. ISSN 01480227. doi:10.1029/2003JD004313.

[148] Pankow, J. F. An absorption model of the gas/aerosol partitioning involved in the formation of secondary organic aerosol. *Atmos. Environ.* **1994**. 28 (2), 189–193. ISSN 13522310. doi:10.1016/j.atmosenv.2007.10.060.

[149] Gill, P. S.; Graedel, T. E.; Weschler, C. J. Organic films on atomspheric aerosol-particles, fog droplets, cloud droplets, raindrops, and snowflakes. *Rev. Geophys.* **1983**. 21 (4), 903–920.

[150] Freedman, M. A.; Baustian, K. J.; Wise, M. E.; Tolbert, M. A. Characterizing the morphology of organic aerosols at ambient temperature and pressure. *Anal. Chem.* **2010**. 82 (19), 7965–7972. ISSN 00032700. doi:10.1021/ac101437w.

[151] Bertram, A. K.; Martin, S. T.; Hanna, S. J.; Smith, M. L.; Bodsworth, A.; Chen, Q.; Kuwata, M.; Liu, A.; You, Y.; Zorn, S. R. Predicting the relative humidities of liquid-liquid phase separation, efflorescence, and deliquescence of mixed particles of ammonium sulfate, organic material, and water using the organic-to-sulfate mass ratio of the particle and the oxygen-to-carbon ele. *Atmos. Chem. Phys.* **2011**. 11 (21), 10995–11006. ISSN 16807316. doi:10.5194/acp-11-10995-2011.

[152] Song, M.; Marcolli, C.; Krieger, U. K.; Lienhard, D. M.; Peter, T. Morphologies of mixed organic/inorganic/aqueous aerosol droplets. *Faraday Discuss.* **2013**. 165, 289–316. ISSN 1359-6640. doi:10.1039/c3fd00049d.

[153] Reid, J. P.; Dennis-Smither, B. J.; Kwamena, N.-O. a.; Miles, R. E. H.; Hanford, K. L.; Homer, C. J. The morphology of aerosol particles consisting of hydrophobic and hydrophilic phases: hydrocarbons, alcohols and fatty acids as the hydrophobic component. *Phys. Chem. Chem. Phys.* **2011**. 13 (34), 15559–15572. ISSN 1463-9076. doi:10.1039/c1cp21510h.

[154] Assovskii, I. G.; Rashkovskii, S. A. Relaxation of drops of a mixture of two immiscible liquids to equilibrium shapes. *Dokl. Phys. Chem.* **2002**. 385 (1-3), 149–153. ISSN 00125016. doi:10.1023/A:1016547002153.

[155] Tabazadeh, A. Organic aggregate formation in aerosols and its impact on the physicochemical properties of atmospheric particles. *Atmos. Environ.* **2005**. 39 (30), 5472–5480. ISSN 13522310. doi:10.1016/j.atmosenv.2005.05.045.

[156] Freney, E. J.; Adachi, K.; Buseck, P. R. Internally mixed atmospheric aerosol particles: Hygroscopic growth and light scattering. *J. Geophys. Res. Atmos.* **2010**. 115 (19), 1–8. ISSN 01480227. doi:10.1029/2009JD013558.

[157] Ciobanu, V. G.; Marcolli, C.; Krieger, U. K.; Weers, U.; Peter, T. Liquid-liquid phase separation in mixed organic/inorganic aerosol particles. *J. Phys. Chem. A* **2009**. 113 (41), 10966–10978. ISSN 10895639. doi:10.1021/jp905054d.

[158] Song, M.; Marcolli, C.; Krieger, U. K.; Zuend, A.; Peter, T. Liquid-liquid phase separation and morphology of internally mixed dicarboxylic acids/ammonium

sulfate/water particles. *Atmos. Chem. Phys.* **2012**. 12 (5), 2691–2712. ISSN 16807316. doi:10.5194/acp-12-2691-2012.

[159] Cistola, D. P.; Hamilton, J. a.; Jackson, D.; Small, D. M. Ionization and phase behavior of fatty acids in water: application of the Gibbs phase rule. *Biochemistry* **1988**. 27 (6), 1881–1888. ISSN 0006-2960. doi:10.1021/bi00406a013.

[160] Torza, S.; Mason, S. G. Three-Phase Interactions In Shear and Electrical Fields ˜. *J. Colloid Interface Sci.* **1970**. 33 (2), 395–411.

[161] Harkins, W. D.; Feldman, A. Films. the Spreading of Liquids and the Spreading Coefficient. *J. Am. Chem. Soc.* **1922**. 44 (12), 2665–2685. ISSN 0002-7863. doi:10.1021/ja01433a001.

[162] Harkins, W. D. *The Physical Chemistry of Surface Films*. Reinhold Publishing Corporation, New York, NY **1952**.

[163] Shaw, D. J. *Introduction to Colloid and Surface Chemistry*. Butterworth-Heinemann Ltd, London, 4th edition **1992**.

[164] de Gennes, P. G.; Brochard-Wyart, F.; Quere, D. *Capillarity and Wetting Phenomena*. Springer Science & Business Media, New York, NY **2004**.

[165] Grosjean, D.; Williams, E. L.; Grosjean, E. Atmospheric chemistry of isoprene and of its carbonyl products. *Environ. Sci. Technol.* **1993**. 27 (5), 830–840. ISSN 0013-936X. doi:10.1021/es00042a004.

[166] Tuazon, E. C.; Atkinson, R.; MacLeod, H.; Biermann, H. W.; Winer, A. M.; Carter, W. P. L.; Pitts, Jr., J. N. Yields of Glyoxal and Methylglyoxal from

the NOx-Air Photooxidations of Toluene and m- and p-Xylene. *Environ. Sci. Technol.* **1984**. 18 (12), 981–984. ISSN 0013936X.

[167] Tuazon, E.; MacLeod, H.; Atkinson, R.; Carter, W. P. L. a-Dicarbonyl Yields from the NO,-Air Aromatic Hydrocarbons in Air Photooxidations of a Series. *Environ. Sci. Technol.* **1986**. 20 (4), 383–387.

[168] Smith, D. F.; Kleindienst, T.; McIver, C. Primary Product Distribution from the Reaction of OH with m-, p-Xylene, 1,2,4-and 1,3,5-Trimethylbenzene. *J. Atm. Chem.* **1999**. 34, 339–364.

[169] Paulsen, D.; Dommen, J.; Kalberer, M.; Prévôt, A. S. H.; Richter, R.; Sax, M.; Steinbacher, M.; Weingartner, E.; Baltensperger, U. Secondary organic aerosol formation by irradiation of 1,3,5-trimethylbenzene-NOx-H2O in a new reaction chamber for atmospheric chemistry and physics. *Environ. Sci. Technol.* **2005**. 39 (8), 2668–2678. ISSN 0013-936X. doi:10.1021/es0489137.

[170] Zhao, J.; Zhang, R.; Misawa, K.; Shibuya, K. Experimental product study of the OH-initiated oxidation of m-xylene. *J. Photochem. Photobiol. A Chem.* **2005**. 176 (1-3 SPEC. ISS.), 199–207. ISSN 10106030. doi:10.1016/j.jphotochem.2005.07.013.

[171] Grosjean, E.; Grosjean, D.; Fraser, M. P.; Cass, G. R. Air Quality Model Evaluation Data for Organics. 2. C1 - C14 Carbonyls in Los Angeles Air. *Environ. Res.* **1996**. 30 (9), 2687–2703. doi:10.1021/ES950758W.

[172] Grosjean, D.; Grosjean, E.; Moreira, L. F. R. Speciated ambient carbonyls in Rio de Janeiro, Brazil. *Environ. Sci. Technol.* **2002**. 36 (7), 1389–1395. ISSN 0013936X. doi:10.1021/es0111232.

[173] Fraser, M. P.; Kleeman, M. J.; Schauer, J. J.; Cass, G. R. Modeling the atmospheric concentrations of individual volatile organic compounds. *Environ. Sci. Technol.* **2000**. 34, 1302–1312. ISSN 13522310. doi:10.1016/1352-2310(94)00287-U.

[174] Sareen, N.; Schwier, A. N.; Lathem, T. L.; Nenes, A.; McNeill, V. F. Surfactants from the gas phase may promote cloud droplet formation. *Proc. Natl. Acad. Sci. U. S. A.* **2013**. 110 (8), 2723–8. ISSN 1091-6490. doi:10.1073/pnas.1204838110.

[175] Loeffler, K. W.; Koehler, C. A.; Paul, N. M.; De Haan, D. O. Oligomer formation in evaporating aqueous glyoxal and methyl glyoxal solutions. *Environ. Sci. Technol.* **2006**. 40 (20), 6318–6323. ISSN 0013936X. doi:10.1021/es060810w.

[176] Zhao, J.; Levitt, N. P.; Zhang, R. Y.; Chen, J. M. Heterogeneous reactions of methylglyoxal in acidic media: Implications for secondary organic aerosol formation. *Environ. Sci. Technol.* **2006**. 40 (24), 7682–7687. ISSN 0013-936X. doi:10.1021/es060610k.

[177] Barsanti, K. C.; Pankow, J. F. Thermodynamics of the formation of atmospheric organic particulate matter by accretion reactions - 2. Dialdehydes, methylglyoxal, and diketones. *Atmos. Environ.* **2005**. 39 (35), 6597–6607. ISSN 13522310. doi:10.1016/j.atmosenv.2005.07.056.

[178] Blando, J. D.; Turpin, B. J. Secondary organic aerosol formation in cloud and fog droplets: A literature evaluation of plausibility. *Atmos. Environ.* **2000**. 34 (10), 1623–1632. ISSN 13522310. doi:10.1016/S1352-2310(99)00392-1.

[179] Sareen, N., Schwier, A. N., Shapiro, E. L., Mitroo, D., and McNeill, V. F. Secondary organic material formed by methylglyoxal in aqueous aerosol mimics. *Atmos. Chem. Phys.* **2010**. 10 (3), 997–1016.

[180] Wren, S. N.; Gordon, B. P.; Valley, N. A.; McWilliams, L. E.; Richmond, G. L. Hydration, Orientation, and Conformation of Methylglyoxal at the Air-Water Interface. *J. Phys. Chem. A* **2015**. 119 (24), 6391–6403. ISSN 15205215. doi:10.1021/acs.jpca.5b03555.

[181] Grutter, M.; Flores, E.; Andraca-Ayala, G.; Báez, A. Formaldehyde levels in downtown Mexico City during 2003. *Atmos. Environ.* **2005**. 39 (6), 1027–1034. ISSN 13522310. doi:10.1016/j.atmosenv.2004.10.031.

[182] Finlayson-Pitts, B. J.; Pitts, J. N., J. *Chemistry of the Upper and Lower Atmosphere: Theory, Experiments, and Applications.* Elsevier Science, Amsterdam, The Netherlands **2000**.

[183] Wang, X.; Gao, S.; Yang, X.; Chen, H.; Chen, J.; Zhuang, G.; Surratt, J. D.; Chan, M. N.; Seinfeld, J. H. Evidence for high molecular weight nitrogen-containing organic salts in urban aerosols. *Environ. Sci. Technol.* **2010**. 44 (12), 4441–4446. ISSN 0013936X. doi:10.1021/es1001117.

[184] Balashov, A. L.; Krasnov, V. L.; Danov, S. M.; Chernov, A. Y.; Sulimov, A. V. Formation of cyclic oligomers in concentrated aqueous solutions of

formaldehyde. *J. Struct. Chem.* **2001**. 42 (3), 398–403. ISSN 00224766. doi: 10.1023/A:1012408904389.

[185] Toda, K.; Yunoki, S.; Yanaga, A.; Takeuchi, M.; Ohira, S. I.; Dasgupta, P. K. Formaldehyde content of atmospheric aerosol. *Environ. Sci. Technol.* **2014**. 48 (12), 6636–6643. ISSN 15205851. doi:10.1021/es500590e.

[186] Taylor, G. I. Viscosity of a Fluid Containing Small Drops of Another Fluid. *Proc. R. Soc. A Math. Phys. Eng. Sci.* **1932**. 138 (834), 41–48. ISSN 1364-5021. doi:10.1098/rspa.1983.0054.

[187] Cabral, J. T.; Hudson, S. D. Microfluidic approach for rapid multicomponent interfacial tensiometry. *Lab Chip* **2006**. 6, 427–436. ISSN 1473-0197. doi: 10.1039/b511976f.

[188] Alvarez, N. J.; Vogus, D. R.; Walker, L. M.; Anna, S. L. Using bulk convection in a microtensiometer to approach kinetic-limited surfactant dynamics at fluid-fluid interfaces. *J. Colloid Interface Sci.* **2012**. 372 (1), 183–191. ISSN 00219797. doi:10.1016/j.jcis.2011.12.034.

[189] Christopher, G. F.; Noharuddin, N. N.; Taylor, J. a.; Anna, S. L. Experimental observations of the squeezing-to-dripping transition in T-shaped microfluidic junctions. *Phys. Rev. E - Stat. Nonlinear, Soft Matter Phys.* **2008**. 78 (3), 1–12. ISSN 15393755. doi:10.1103/PhysRevE.78.036317.

[190] Anna, S. L.; Bontoux, N.; Stone, H. a. Formation of dispersions using "flow focusing" in microchannels. *Appl. Phys. Lett.* **2003**. 82 (3), 364–366. ISSN 00036951. doi:10.1063/1.1537519.

[191] Bilde, M.; Barsanti, K.; Booth, M.; Cappa, C. D.; Donahue, N. M.; Emanuelsson, E. U.; McFiggans, G.; Krieger, U. K.; Marcolli, C.; Topping, D.; Ziemann, P.; Barley, M.; Clegg, S.; Dennis-Smither, B.; Hallquist, M.; Hallquist, s. M.; Khlystov, A.; Kulmala, M.; Mogensen, D.; Percival, C. J.; Pope, F.; Reid, J. P.; Ribeiro Da Silva, M. A. V.; Rosenoern, T.; Salo, K.; Soonsin, V. P.; Yli-Juuti, T.; Prisle, N. L.; Pagels, J.; Rarey, J.; Zardini, A. A.; Riipinen, I. Saturation Vapor Pressures and Transition Enthalpies of Low-Volatility Organic Molecules of Atmospheric Relevance: From Dicarboxylic Acids to Complex Mixtures. *Chem. Rev.* **2015**. 115 (10), 4115–4156. ISSN 15206890. doi:10.1021/cr5005502.

[192] Duffy, D. C.; Schueller, O. J. a.; Brittain, S. T.; Whitesides, G. M. Rapid prototyping of microfluidic switches in poly(dimethyl siloxane) and their actuation by electro-osmotic flow. *J. Micromechanics Microengineering* **1999**. 9 (3), 211–217. ISSN 0960-1317. doi:10.1088/0960-1317/9/3/301.

[193] Effenhauser, C. S.; Bruin, G. J. M.; Paulus, A.; Ehrat, M. Integrated Capillary Electrophoresis on Flexible Silicone Microdevices: Analysis of DNA Restriction Fragments and Detection of Single DNA Molecules on Microchips. *Anal. Chem.* **1997**. 69 (17), 3451–3457. ISSN 0003-2700. doi:10.1021/ac9703919.

[194] Schueller, O. J. A.; Duffy, D. C.; Rogers, J. A.; Brittain, S. T.; Whitesides, G. M. Reconfigurable diffraction gratings based on elastomeric microfluidic devices. *Sensors Actuators, A Phys.* **1999**. 78 (2), 149–159. ISSN 09244247. doi:10.1016/S0924-4247(98)00242-8.

[195] Jackman, R. J.; Duffy, D. C.; Ostuni, E.; Willmore, N. D.; Whitesides, G. M. Fabricating large arrays of microwells with arbitrary dimensions and filling them

using discontinuous dewetting. *Anal. Chem.* **1998**. 70 (11), 2280–2287. ISSN 0003-2700. doi:10.1021/ac971295a.

[196] Mcdonald, J. C.; Duffy, D. C.; Anderson, J. R.; Chiu, D. T. Review General Fabrication of microfluidic systems in poly (dimethylsiloxane) **2000**.

[197] Xia, Y. N.; Whitesides, G. M. Soft lithography. *Annu. Rev. Mater. Sci.* **1998**. 37 (5), 551–575. ISSN 0084-6600. doi:10.1146/annurev.matsci.28.1.153.

[198] Duffy, D. C.; McDonald, J. C.; Schueller, O. J. A.; Whitesides, G. M. Rapid prototyping of microfluidic systems in poly(dimethylsiloxane). *Anal. Chem.* **1998**. 70 (23), 4974–4984. ISSN 00032700. doi:10.1021/ac980656z.

[199] Delamarche, E.; Bernard, a.; Schmid, H.; Michel, B.; Biebuyck, H. Patterned delivery of immunoglobulins to surfaces using microfluidic networks. *Science* **1997**. 276 (5313), 779–781. ISSN 00368075. doi:10.1126/science.276.5313.779.

[200] Delamarche, E.; Schmid, H.; Bietsch, A.; Michel, B.; Biebuyck, H. Microfluidic Networks for Chemical Patterning of Substrates **1998**. 120 (3), 500–508.

[201] Qin, Dong; Xia, Younan; Whitesides, G. Rapid Prototyping of Complex Structures with Feature Sizes Larger Than 20 microns. *Adv. Mater.* **1996**. 8 (11), 917–919.

[202] Tran, T. M.; Lan, F.; Thompson, C. S.; Abate, a. R. From tubes to drops: droplet-based microfluidics for ultrahigh-throughput biology. *J. Phys. D. Appl. Phys.* **2013**. 46 (11), 114004. ISSN 0022-3727. doi:10.1088/0022-3727/46/11/114004.

[203] Seemann, R.; Brinkmann, M.; Pfohl, T.; Herminghaus, S. Droplet based microfluidics. *Rep. Prog. Phys. Rep. Prog. Phys* **2012**. 75 (75), 16601–41. ISSN 1361-6633. doi:10.1088/0034-4885/75/1/016601.

[204] Tanyeri, M.; Schroeder, C. M. Manipulation and confinement of single particles using fluid flow. *Nano Lett.* **2013**. 13 (6), 2357–2364. ISSN 15306984. doi: 10.1021/nl4008437.

[205] Tanyeri, M.; Ranka, M.; Sittipolkul, N.; Schroeder, C. M. A microfluidic-based hydrodynamic trap: design and implementation. *Lab Chip* **2011**. 11 (10), 1786. ISSN 1473-0197. doi:10.1039/c0lc00709a.

[206] Alvarez, N. J.; Walker, L. M.; Anna, S. L. A microtensiometer to probe the effect of radius of curvature on surfactant transport to a spherical interface. *Langmuir* **2010**. 26 (16), 13310–13319. ISSN 07437463. doi:10.1021/la101870m.

[207] Barca, F.; Caporossi, T.; Rizzo, S. Silicone oil: Different physical proprieties and clinical applications. *Biomed Res. Int.* **2014**. 2014. ISSN 23146141. doi: 10.1155/2014/502143.

[208] Shapiro, E. L.; Szprengiel, J.; Sareen, N.; Jen, C. N.; Giordano, M. R.; McNeill, V. F. Light-absorbing secondary organic material formed by glyoxal in aqueous aerosol mimics. *Atmos. Chem. Phys. Discuss.* **2009**. 9 (1), 59–80. ISSN 1680-7324. doi:10.5194/acpd-9-59-2009.

[209] Tang, I. N.; Tridico, A. C.; Fung, K. H. Thermodynamic and optical properties of sea salt aerosols. *J. Geophys. Res. Atmos.* **1997**. 102 (D19), 23269–23275. ISSN 01480227. doi:10.1029/97JD01806.

[210] Tang, I. N.; Munkelwitz, H. R. Water Activitities, Densities, and Refractive Indices of Aqueous Sulfates and Sodium Nitrate Droplets of Atmospheric Importance. *J. Geophys. Res.* **1994**. 99 (D9), 18801–18808.

[211] Schwier, A. N.; Sareen, N.; Mitroo, D.; Shapiro, E. L.; McNeill, V. F. Glyoxal-methylglyoxal cross-reactions in secondary organic aerosol formation. *Environ. Sci. Technol.* **2010**. 44 (16), 6174–82. ISSN 1520-5851. doi:10.1021/es101225q.

[212] Henning, S.; Rosenørn, T.; D'Anna, B.; Gola, a. a.; Svenningsson, B.; Bilde, M. Cloud droplet activation and surface tension of mixtures of slightly soluble organics and inorganic salt. *Atmos. Chem. Phys. Discuss.* **2004**. 4, 7463–7485. ISSN 16807324. doi:10.5194/acpd-4-7463-2004.

[213] Morita, A. T.; Carastan, D. J.; Demarquette, N. R. Influence of drop volume on surface tension evaluated using the pendant drop method. *Colloid Polym. Sci.* **2002**. 280 (9), 857–864. ISSN 0303402X. doi:10.1007/s00396-002-0694-z.

[214] Guenther, A.; Karl, T.; Harley, P.; Wiedinmyer, C.; Palmer, P. I.; Geron, C. and Physics Estimates of global terrestrial isoprene emissions using MEGAN (Model of Emissions of Gases and Aerosols from Nature) **2006**. 3181–3210.

[215] Kroll, J. H.; Ng, N. L.; Murphy, S. M.; Flagan, R. C.; Seinfeld, J. H. Secondary organic aerosol formation from isoprene photooxidation under high-NOx conditions. *Geophys. Res. Lett.* **2005**. 32 (18), 1–4. ISSN 00948276. doi:10.1029/2005GL023637.

[216] Surratt, J. D.; Murphy, S. M.; Kroll, J. H.; Ng, N. L.; Hildebrandt, L.; Sorooshian, A.; Vermeylen, R.; Maenhaut, W.; Claeys, M.; Flagan, R. C.;

Seinfeld, J. H.; Szmigielski, R. Chemical Composition of Secondary Organic Aerosol Formed from the Photooxidation of Isoprene Chemical Composition of Secondary Organic Aerosol Formed from the Photooxidation of Isoprene. *Society* **2006**. 110 (31), 9665–9690. doi:10.1021/jp061734m.

[217] Carlton, A. G.; Wiedinmyer, C.; Kroll, J. H. and Physics A review of Secondary Organic Aerosol (SOA) formation from isoprene **2009**. 4987–5005.

[218] Budisulistiorini, S. H.; Li, X.; Bairai, S. T.; Renfro, J.; Liu, Y.; Liu, Y. J.; McKinney, K. a.; Martin, S. T.; McNeill, V. F.; Pye, H. O. T.; Nenes, a.; Neff, M. E.; Stone, E. a.; Mueller, S.; Knote, C.; Shaw, S. L.; Zhang, Z.; Gold, a.; Surratt, J. D. Examining the effects of anthropogenic emissions on isoprene-derived secondary organic aerosol formation during the 2013 Southern Oxidant and Aerosol Study (SOAS) at the Look Rock, Tennessee ground site. *Atmos. Chem. Phys.* **2015**. 15 (15), 8871–8888. ISSN 16807324. doi:10.5194/acp-15-8871-2015.

[219] Kramer, A. J.; Rattanavaraha, W.; Zhang, Z.; Gold, A.; Surratt, J. D.; Lin, Y. H. Assessing the oxidative potential of isoprene-derived epoxides and secondary organic aerosol. *Atmos. Environ.* **2016**. 130, 211–218. ISSN 18732844. doi:10.1016/j.atmosenv.2015.10.018.

[220] Lin, Y.-H. Y.; Zhang, H.; Pye, H. H. O. T.; Zhang, Z.; Marth, W. J.; Park, S.; Arashiro, M.; Cui, T.; Budisulistiorini, S. H.; Sexton, K. G.; Vizuete, W.; Xie, Y.; Luecken, D. J.; Piletic, I. R.; Edney, E. O.; Bartolotti, L. J.; Gold, A.; Surratt, J. D. Epoxide as a precursor to secondary organic aerosol formation from isoprene photooxidation in the presence of nitrogen oxides. *Proc. ...*

2013. 110 (17), 6718–23. ISSN 1091-6490. doi:10.1073/pnas.1221150110/-/DCSupplemental.www.pnas.org/cgi/doi/10.1073/pnas.1221150110.

[221] Lin, Y. H.; Budisulistiorini, S. H.; Chu, K.; Siejack, R. a.; Zhang, H.; Riva, M.; Zhang, Z.; Gold, A.; Kautzman, K. E.; Surratt, J. D. Light-absorbing oligomer formation in secondary organic aerosol from reactive uptake of isoprene epoxydiols. *Environ. Sci. Technol.* **2014**. 48 (20), 12012–12021. ISSN 15205851. doi:10.1021/es503142b.

[222] Lin, Y. H.; Zhang, Z.; Docherty, K. S.; Zhang, H.; Budisulistiorini, S. H.; Rubitschun, C. L.; Shaw, S. L.; Knipping, E. M.; Edgerton, E. S.; Kleindienst, T. E.; Gold, A.; Surratt, J. D. Isoprene epoxydiols as precursors to secondary organic aerosol formation: Acid-catalyzed reactive uptake studies with authentic compounds. *Environ. Sci. Technol.* **2012**. 46 (1), 250–258. ISSN 0013936X. doi:10.1021/es202554c.

[223] Zhang, Z.; Lin, Y. H.; Zhang, H.; Surratt, J. D.; Ball, L. M.; Gold, a. Technical Note: Synthesis of isoprene atmospheric oxidation products: Isomeric epoxydiols and the rearrangement products cis-and trans-3-methyl-3,4- dihydroxytetrahydrofuran. *Atmos. Chem. Phys.* **2012**. 12 (18), 8529–8535. ISSN 16807316. doi:10.5194/acp-12-8529-2012.

Appendix A

Generalized Multicomponent Model Evaluated for 1, 2, and 3 Solutes

This appendix contains expressions derived in Chapter 4 (Entropy: equation 4.25; C_j: equation 4.28; and σ: equation 4.29). Each equation is evaluated for 1, 2, and 3 solutes and can be further extended as needed to an infinite number of solutes. Let $\chi_{AB} = N_{WS} - r_A N_{AS} - r_B N_{BS}$, $\chi_{AC} = N_{WS} - r_A N_{AS} - r_C N_{CS}$, $\chi_{ABC} = N_{WS} - r_A N_{AS} - r_B N_{BS} - r_C N_{CS}$, and so forth.

n	Entropy (S/k_B)
1	$N_A Ln\left(\frac{N_A}{N_A-N_{AS}}\right)+\frac{N_{WS}}{r_A}\left(\frac{N_{WS}}{N_{WS}-r_A N_{AS}}\right)+\frac{(N_{WS}-r_A N_{AS})(N_A-N_{AS})}{r_A N_{AS}^2}$
2	$N_A Ln\frac{N_A}{(N_A-N_{AS})}+N_B Ln\frac{N_B}{(N_B-N_{BS})}+\frac{N_{WS}}{2r_A}Ln\frac{N_{WS}(N_{WS}-r_B N_{BS})}{\chi_{AB}(N_{WS}-r_A N_{AS})}$ $+\frac{N_{WS}}{2r_B}Ln\frac{N_{WS}(N_{WS}-r_A N_{AS})}{\chi_{AB}(N_{WS}-r_B N_{BS})}+\frac{r_A N_{AS}}{2r_B}Ln\frac{\chi_{AB}}{(N_{WS}-r_A N_{AS})}$ $+\frac{r_B N_{BS}}{2r_A}Ln\frac{\chi_{AB}}{(N_{WS}-r_B N_{BS})}+\frac{N_{AS}}{2}Ln\frac{\chi_{AB}(N_{WS}-r_A N_{AS})(N_A-N_{AS})^2}{r_A^2 N_{AS}^4}$ $+\frac{N_{BS}}{2}Ln\frac{\chi_{AB}(N_{WS}-r_B N_{BS})(N_B-N_{BS})^2}{r_B^2 N_{BS}^4}$
3	$N_A Ln\frac{N_A}{(N_A-N_{AS})}+N_B Ln\frac{N_B}{(N_B-N_{BS})}+N_C Ln\frac{N_C}{(N_C-N_{CS})}$ $+\frac{N_{AS}}{6}Ln\left(\frac{(N_A-N_{AS})^6\chi_{AB}\chi_{AC}\chi_A^2\chi_{ABC}^2}{(r_A N_{AS}^{12})}\right)+\frac{N_{BS}}{6}Ln\left(\frac{(N_B-N_{BS})^6\chi_{AB}\chi_{BC}\chi_B^2\chi_{ABC}^2}{r_B N_{BS}^{12}}\right)$ $+\frac{N_{CS}}{6}Ln\left(\frac{(N_C-N_{CS})^6\chi_{AC}\chi_{BC}\chi_C^2\chi_{ABC}^2}{r_C N_{CS}^{12}}\right)+\frac{N_{WS}}{6r_A}Ln\frac{N_{WS}^2\chi_B\chi_C\chi_{BC}^2}{\chi_{AC}\chi_{AB}\chi_A^2\chi_{ABC}^2}$ $+\frac{N_{WS}}{6r_B}Ln\frac{N_{WS}^2\chi_A\chi_C\chi_{AC}^2}{\chi_{BC}\chi_{AB}\chi_B^2\chi_{ABC}^2}+\frac{N_{WS}}{6r_C}Ln\frac{N_{WS}^2\chi_A\chi_B\chi_{AB}^2}{\chi_{AC}\chi_{BC}\chi_C^2\chi_{ABC}^2}+\frac{r_A N_{AS}}{6r_B}Ln\frac{\chi_{AB}\chi_{ABC}^2}{\chi_A\chi_{AC}^2}$ $+\frac{r_A N_{AS}}{6r_C}Ln\frac{\chi_{AC}\chi_{ABC}^2}{\chi_A\chi_{AB}^2}+\frac{r_B N_{BS}}{6r_C}Ln\frac{\chi_{BC}\chi_{ABC}^2}{\chi_B\chi_{AB}^2}+\frac{r_B N_{BS}}{6r_A}Ln\frac{\chi_{AB}\chi_{ABC}^2}{(\chi_B\chi_{BC}^2}$ $+\frac{r_C N_{CS}}{6r_B}Ln\frac{\chi_{BC}\chi_{ABC}^2}{\chi_C\chi_{AC}^2}+\frac{r_C N_{CS}}{6r_A}Ln\frac{\chi_{AC}\chi_{ABC}^2}{\chi_C\chi_{BC}^2}$

Table A.1: Entropy (equation 4.25) evaluated for n solutes.

n	C_j
1	$C_A = \frac{r_A N_{AS}^2}{(N_A - N_{AS})(N_{WS} - r_A N_{AS})}$
2	$C_A = \frac{r_A N_{AS}^2}{N_A - N_{AS}} \left(\frac{\left(\frac{N_{WS} - r_A N_{AS}}{\chi_{AB}}\right)^{r_A/r_B}}{(N_{WS} - r_A N_{AS})\chi_{AB}} \right)^{1/2}$
3	$C_A = \frac{r_A N_{AS}^2}{N_A - N_{AS}} \left(\frac{\left(\frac{(N_{WS} - r_A N_{AS})\chi_{AC}^2}{\chi_{AB}\chi_{ABC}^2}\right)^{r_A/r_B} \left(\frac{(N_{WS} - r_A N_{AS})\chi_{AB}^2}{\chi_{AC}\chi_{ABC}^2}\right)^{r_A/r_C}}{\chi_{AB}\chi_{AC}(N_{WS} - r_A N_{AS})^2 \chi_{ABC}^2} \right)^{1/6}$

Table A.2: C_j (equation 4.28) evaluated for n solutes.

n	surface tension (σ)
1	$\sigma = \sigma_W + \frac{k_B T}{r_A S_W} Ln\left(\frac{N_{WS} - r_A N_{AS}}{N_{WS}}\right)$
2	$\sigma = \sigma_W + \frac{k_B T}{2 r_A S_W} Ln\left(\frac{\chi_{AB}(N_{WS} - r_A N_{AS})}{N_{WS}(N_{WS} - r_B N_{BS})}\right) + \frac{k_B T}{2 r_B S_W} Ln\left(\frac{\chi_{AB}(N_{WS} - r_B N_{BS})}{N_{WS}(N_{WS} - r_A N_{AS})}\right)$
3	$\sigma = \sigma_W + \frac{k_B T}{6 r_A S_W} Ln\left(\frac{\chi_{AB}\chi_{AC}\chi_{ABC}^2 (N_{WS} - r_A N_{AS})^2}{N_{WS}^2 \chi_{BC}^2 (N_{WS} - r_B N_{BS})(N_{WS} - r_C N_{CS})}\right)$ $+ \frac{k_B T}{6 r_B S_W} Ln\left(\frac{\chi_{AB}\chi_{BC}\chi_{ABC}^2 (N_{WS} - r_B N_{BS})^2}{N_{WS}^2 \chi_{AC}^2 (N_{WS} - r_A N_{AS})(N_{WS} - r_C N_{CS})}\right)$ $+ \frac{k_B T}{6 r_C S_W} Ln\left(\frac{\chi_{AC}\chi_{BC}\chi_{ABC}^2 (N_{WS} - r_C N_{CS})^2}{N_{WS}^2 \chi_{AB}^2 (N_{WS} - r_A N_{AS})(N_{WS} - r_B N_{BS})}\right)$

Table A.3: Surface tension, σ (equation 4.29), evaluated for n solutes.

Appendix B

Binary Solution Treatments: Electrolytes

This appendix contains surface tension versus activity plots with surface tension data and model predictions for binary aqueous solutions of the following electrolytes: NaCl, KCl, NH_4Cl, NH_4NO_3, KNO_3, $NaNO_3$, K_2SO_4, $(NH_4)_2SO_4$.

Model predictions are presented using three parameters ($n_m = 3$), two parameters ($n_m = 2$), or zero parameters ($n_m = 0$). Single parameter treatments are left out because they agree perfectly with the two parameter fits. The use of K as a parameter is included in the two parameter model and as a constant near unity in the single parameter model.

The equation used for the $n_m = 3$ and $n_m = 2$ curves is equation 2.1:

$$\sigma = \sigma_w + \frac{kT}{rS_w} Ln\left(\frac{1 - Ka_s}{1 - Ka_s(1 - C)}\right) \tag{B.1}$$

The equation used for the $n_m = 0$ curves is equation 2.6:

$$\sigma = \sigma_W - (\sigma_S - \sigma_W)\frac{Ln\left(\frac{1-Ka_S}{1-Ka_S(1-C)}\right)}{Ln\left(\frac{1-K}{1-K(1-C)}\right)} \tag{B.2}$$

NaCl

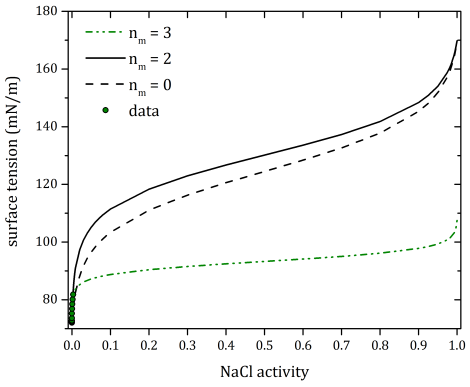

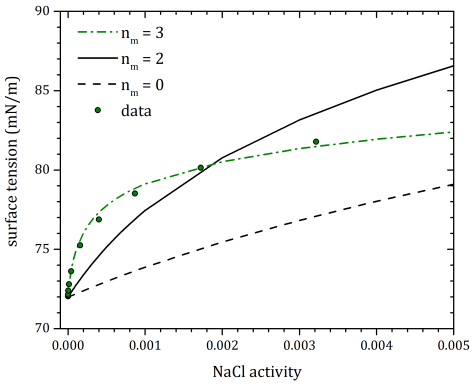

solute activity	surface tension (mN/m)	molality (mol/kg)	Data ref.
5.78E-08	72.03	0.03	Washburn, ICT
2.06E-07	72.07	0.05	
7.12E-07	72.15	0.10	
3.52E-06	72.40	0.25	
1.17E-05	72.80	0.50	
4.02E-05	73.62	1.00	
1.58E-04	75.26	2.00	
4.01E-04	76.88	3.00	
8.68E-04	78.52	4.00	
1.72E-03	80.15	5.00	
3.21E-03	81.78	6.00	

n_m	r	K	C	σ_s	rmse
3	-19.8935	0.99	31011	102.77	0.393
2	-4.78	0.99	899.8736	169.74	1.59
1	-4.78	0.99	899.8736	169.74	1.59
0	-4.78	0.99	28780	169.74	3.56

KCl

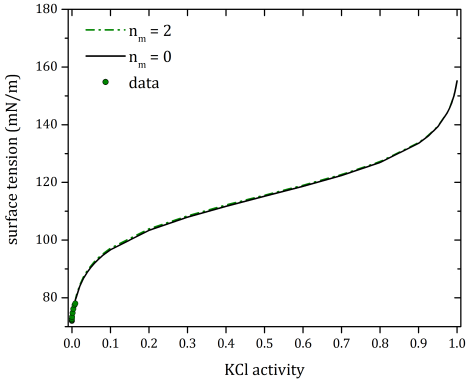

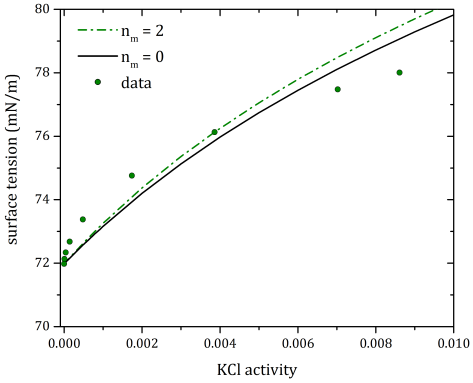

solute activity	surface tension (mN/m)	molality (mol/kg)	Data ref.
8.06E-06	72.131	0.1	Washburn, ICT
4.11E-05	72.336	0.25	
0.00014	72.676	0.5	
0.00048	73.376	1	
0.001738	74.756	2	
0.003865	76.126	3	
0.007022	77.476	4	
0.008609	78.006	4.4	

n_m	r	K	C	σ_s	rmse
2	-4.77	0.99	161.86	155.2	0.594
1	-4.77	0.99	161.86	155.2	0.594
0	-4.77	0.99	146.85	155.2	0.559

NH_4Cl

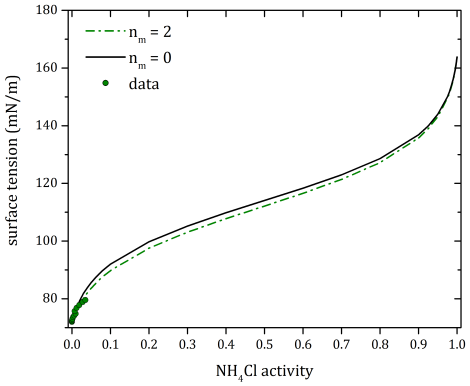

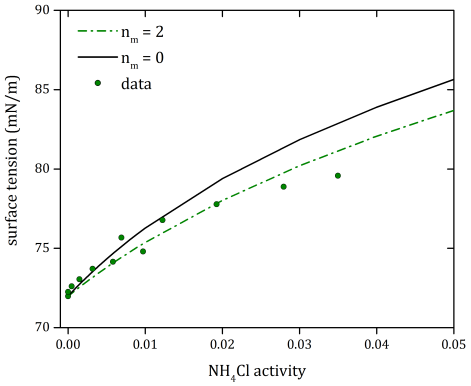

solute activity	surface tension (mN/m)	molality (mol/kg)	Data ref.
0.00	72.25	0.1355	Washburn, ICT
4.73E-04	72.6	0.706	
0.001479	73.05	1.3266	
0.003187	73.7	2.0043	
0.005831	74.15	2.7474	
0.009738	74.8	3.5656	
0.006923	75.676	3	
0.012257	76.776	4	
0.019262	77.776	5	
0.027945	78.876	6	
0.034983	79.576	6.7	

n_m	r	K	C	σ_s	rmse
2	-3.64	0.99	35.13	163.83	0.834
1	-3.64	0.99	35.13	163.83	0.834
0	-3.64	0.99	48.59	163.83	0.794

NH_4NO_3

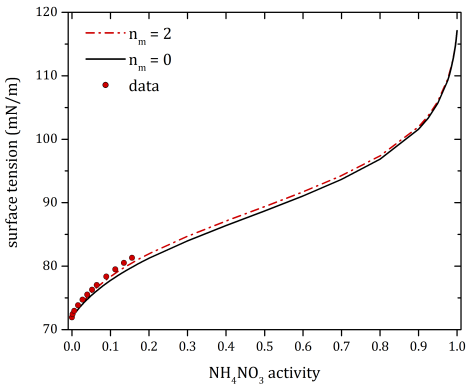

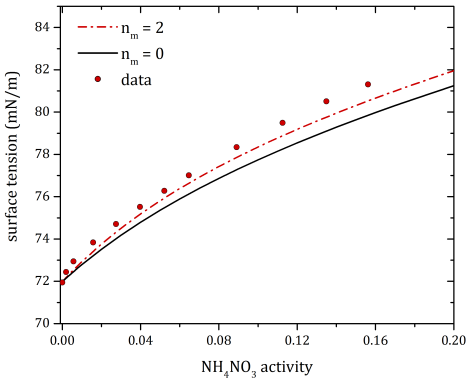

solute activity	surface tension (mN/m)	molality (mol/kg)	Data ref.
0.001994	73.23984	0.5	Washburn, ICT
0.005779	73.73984	1	
0.015821	74.63984	2	
0.027444	75.50984	3	
0.039715	76.31984	4	
0.052192	77.07984	5	
0.064649	77.80984	6	
0.089064	79.13984	8	
0.112514	80.28984	10	
0.134895	81.30984	12	
0.156223	82.10984	14	

n_m	r	K	C	σ_s	rmse
2	-3.64	0.99	35.13	117.11	0.594
1	-3.64	0.99	35.13	117.11	0.594
0	-3.64	0.99	48.59	117.11	0.559

KNO_3

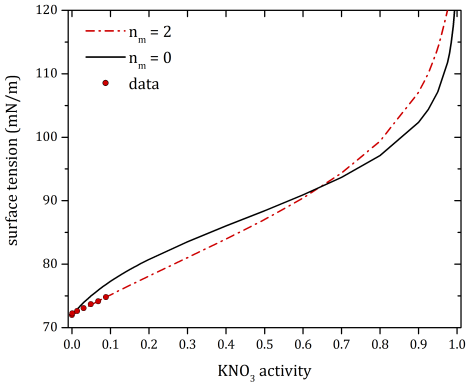

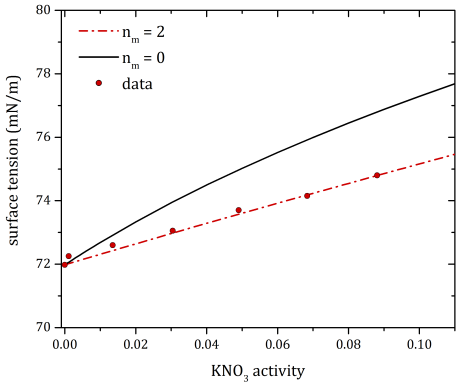

solute activity	surface tension (mN/m)	molality (mol/kg)	Data ref.
0.001096	72.25	0.1355	Abramzon and Gaukhberg, vol. 66, No. 8 part 2
0.013494	72.6	0.706	
0.030438	73.05	1.3266	
0.049041	73.7	2.0043	
0.068384	74.15	2.7474	
0.088084	74.8	3.5656	

n_m	r	K	C	σ_s	rmse
2	-3.84	0.99	3.16	133.35	0.12
1	-3.84	0.99	3.16	133.35	0.12
0	-3.84	0.99	11.17	133.35	3.6

$NaNO_3$

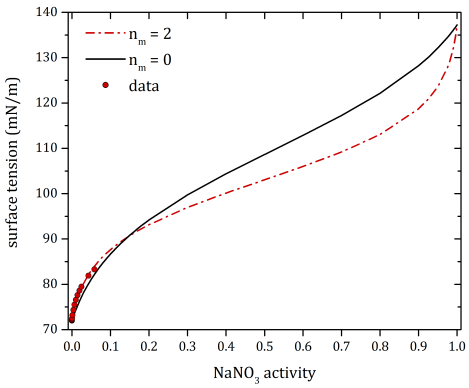

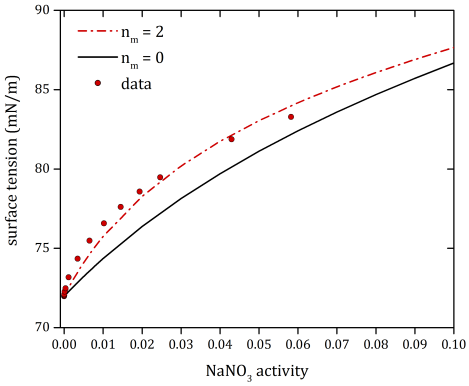

solute activity	surface tension (mN/m)	molality (mol/kg)	Data ref.
2.03E-06	72.016	0.025	Washburn, ICT
7.17E-06	72.046	0.05	
2.46E-05	72.096	0.1	
0.000119	72.276	0.25	
0.000375	72.476	0.5	
0.001148	73.176	1	
0.00344	74.346	2	
0.00651	75.476	3	
0.010232	76.576	4	
0.014531	77.606	5	
0.019353	78.576	6	
0.024647	79.476	7	
0.042944	81.876	10	
0.058205	83.276	12.2	

n_m	r	K	C	σ_s	rmse
2	-5.52	0.99	65.99	137.23	0.12
1	-5.52	0.99	65.99	137.23	0.12
0	-5.52	0.99	23.79	137.23	3.6

$(NH_4)_2SO_4$

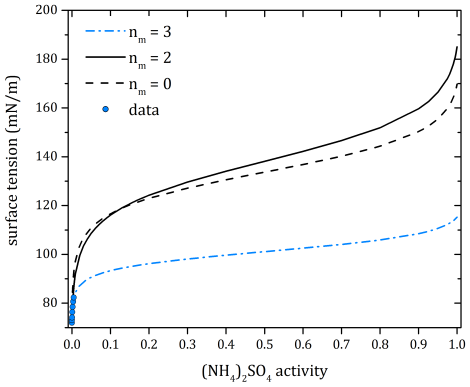

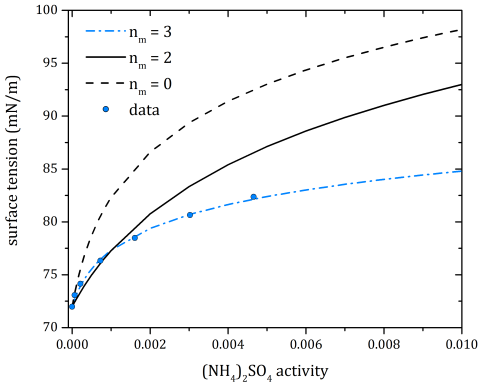

solute activity	surface tension (mN/m)	molality (mol/kg)	Data ref.
6.09E-05	73.066	0.5	Washburn, ICT
0.000209	74.146	1	
0.000724	76.326	2	
0.001611	78.476	3	
0.003027	80.646	4	
0.004656	82.356	4.8	

n_m	r	K	C	σ_s	rmse
3	-11.42	0.98	3492	115.1	0.255
2	-4.04	0.99	692.62	184.99	0.999
1	-4.04	0.99	692.62	184.99	0.999
0	-4.04	0.99	2777.86	184.99	2.57

K_2SO_4

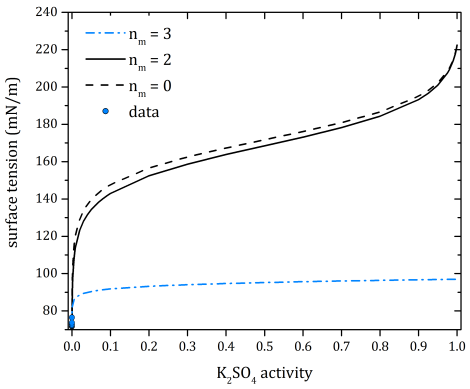

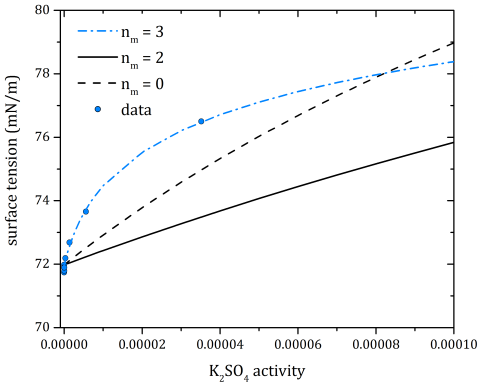

solute activity	surface tension (mN/m)	molality (mol/kg)	Data ref.
1.86E-14	71.89641	0.0002	Abramzon and Gaukhberg, vol. 66, No. 7 part 2
2.16E-13	71.89353	0.0004	
2.87E-12	71.89137	0.001	
1.98E-11	71.88706	0.002	
1.35E-10	71.89497	0.004001	
1.47E-09	71.73988	0.010004	
8.28E-09	71.79057	0.020014	
4.25E-08	71.89137	0.040056	
3.24E-07	72.19071	0.100342	
1.38E-06	72.6827	0.201241	
5.59E-06	73.65522	0.404946	
3.52E-05	76.49585	1.021905	

n_m	r	K	C	σ_s	rmse
3	-21.1	0.34	773393.2	97.01	0.293
2	-3.51	0.99	3953.27	222.4	0.999
1	-3.51	0.99	3953.27	222.4	0.999
0	-3.51	0.99	9004.11	222.4	2.57

Appendix C

Binary Solution Treatments: Alcohols and Sucrose

This appendix contains surface tension versus activity plots with surface tension data and model predictions for binary aqueous solutions of the following alcohols and polyols: methanol, ethanol, isopropanol, 1,2-ethanediol, 1,2-propanediol, 1,3-propanediol, 1,3-butanediol, 1,4-butanediol, sorbitol and glycerol. Sucrose data and model treatment with equation 2.1 are also included.

Model predictions are presented using one parameter ($n_m = 1$) or zero parameters ($n_m = 0$). The equation used for the $n_m = 3$ and $n_m = 2$ curves is equation 2.3:

$$\sigma = \sigma_w - \frac{kT}{rS_w} Ln(1 + Ka_s) \tag{C.1}$$

The equation used for the $n_m = 0$ curves is equation 2.5:

$$\sigma = \sigma_W - (\sigma_W - \sigma_S)\frac{Ln(1 + K'a_S)}{Ln(1 + K')} \tag{C.2}$$

methanol

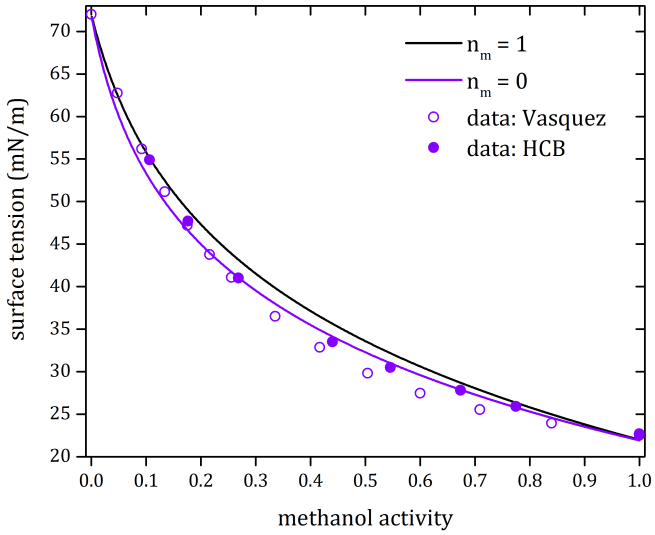

solute activity	surface tension (mN/m)	molality (mol/kg)	mole fraction	data reference
0.047669	62.77	1.657387	0.029	Vasquez, *J. Chem. Eng. Data*, 1985
0.092098	56.18	3.479426	0.059	
0.134049	51.17	5.488407	0.09	
0.175294	47.21	7.783066	0.123	
0.216039	43.78	10.41334	0.158	
0.25543	41.09	13.35709	0.194	
0.335397	36.51	20.83884	0.273	
0.416772	32.86	31.21532	0.36	
0.50395	29.83	46.89337	0.458	
0.599794	27.48	72.9642	0.568	
0.708932	25.54	124.6811	0.692	
0.839831	23.93	280.8327	0.835	
1	22.51	Inf	1	
0.106378	54.9	4.129518	0.06926	H.C.B., Wilhelmy plate
0.176379	47.7	7.848069	0.1239	
0.268299	41	14.41527	0.2062	
0.43996	33.5	34.8429	0.3857	
0.54541	30.5	56.72834	0.5055	
0.673496	27.8	104.0172	0.6521	
0.774723	25.9	180.4495	0.7648	
1	22.7	Inf	1	

n_m	r	K'	rmse
1	2.58	22.32	1.21
0	2.58	14.036	

ethanol

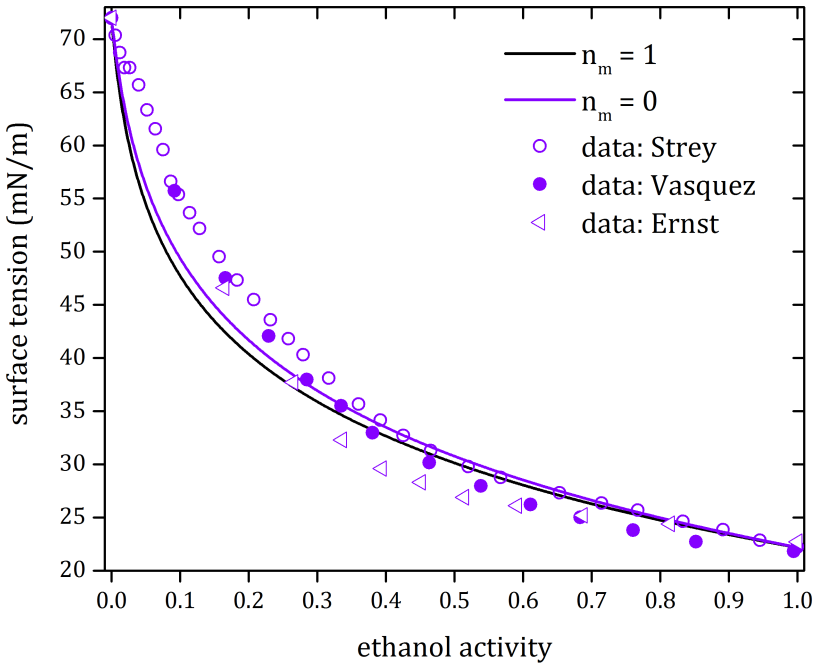

solute activity	surface tension (mN/m)	molality (mol/kg)	mole fraction	data reference
0	72	0	0	Ernst, *J.Phys. Chem.* 1936
0.1645	46.6	2.4088	0.0416	
0.265	37.7	5.4215	0.089	
0.336	32.3	9.2976	0.1435	
0.394	29.6	14.4593	0.2067	
0.451	28.3	21.6882	0.281	
0.514	26.9	32.5358	0.3696	
0.591	26.1	50.613	0.477	
0.687	25.2	86.7617	0.6099	
0.814	24.4	195.2693	0.7787	
1	22.72	Inf	1	

n_m	r	K'	rmse
1	3.5*	69.19	3.48
0	3.5*	49.01	

solute activity	surface tension (mN/m)	molality (mol/kg)	mole fraction	data reference
0	72.01	0		Vasquez, *J. Chem. Eng. Data*, 1985
0.091724	55.73	1.1425		
0.166172	47.53	2.4119		
0.229435	42.08	3.8307		
0.284936	37.97	5.4268		
0.334805	35.51	7.2357		
0.380493	32.98	9.303		
0.463153	30.16	14.4714		
0.538573	27.96	21.707		
0.610713	26.23	32.5606		
0.683148	25.01	50.6498		
0.760512	23.82	86.8282		
0.852054	22.72	195.3634		
0.994604	21.82	10000		
1	22.2	Inf		

solute activity	surface tension (mN/m)	molality (mol/kg)	mole fraction	data reference
0	71.94	0		Strey, *J. Phys. Chem. B,* 1999
0.005503	70.37	0.000999		
0.01224	68.72	0.002241		
0.018936	67.3	0.003496		
0.026782	67.3	0.004997		
0.0395	65.67	0.007495		
0.051776	63.33	0.009986		
0.063762	61.55	0.0125		
0.075221	59.6	0.01498		
0.08652	56.6	0.0175		
0.097546	55.39	0.02003		
0.114198	53.67	0.024		
0.128368	52.19	0.02752		
0.157055	49.52	0.03508		
0.183204	47.33	0.0425		
0.207609	45.49	0.04993		
0.232014	43.59	0.05788		
0.25804	41.82	0.06698		
0.279619	40.31	0.07505		
0.316643	38.11	0.09011		
0.360562	35.67	0.1102		
0.392082	34.16	0.1263		
0.425329	32.71	0.145		
0.46545	31.29	0.1702		
0.519995	29.79	0.2098		
0.567218	28.76	0.2499		
0.653414	27.32	0.3402		
0.714678	26.34	0.4208		
0.767214	25.7	0.5029		
0.833316	24.63	0.6252		
0.891841	23.84	0.7512		
0.945352	22.86	0.8772		
1	22.22	1		

isopropyl alcohol

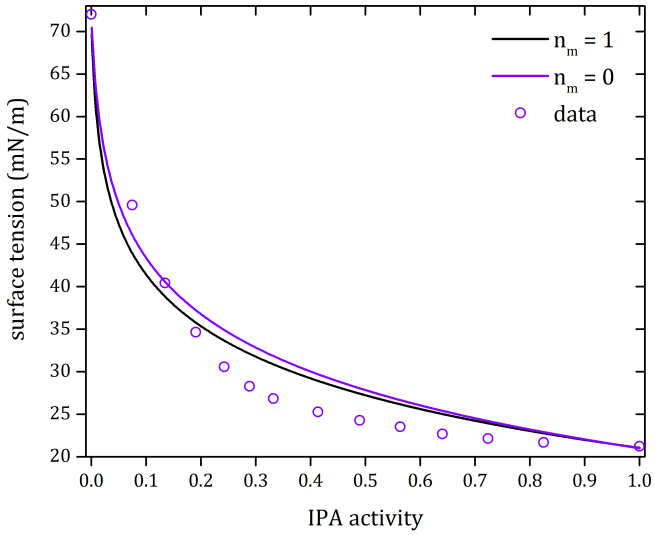

solute activity	surface tension (mN/m)	molality (mol/kg)	mole fraction	data reference
0	72.01	0	0	Vasquez, J. Chem. Eng. Data, 1985
0.07477	49.58	0.9023	0.016	
0.13479	40.42	1.8345	0.032	
0.19057	34.63	2.9207	0.05	
0.2424	30.57	4.177	0.07	
0.28861	28.28	5.5555	0.091	
0.33217	26.82	7.1403	0.114	
0.41349	25.27	11.1254	0.167	
0.4894	24.26	16.6698	0.231	
0.56347	23.51	24.932	0.31	
0.64048	22.68	38.8835	0.412	
0.72361	22.14	66.4707	0.545	
0.82543	21.69	150.0391	0.73	
1	21.22	Inf	1	

n_m	r	K'	rmse
1	4.57*	291.2	2.74
0	4.57*	166.8	

1,2 ethanediol

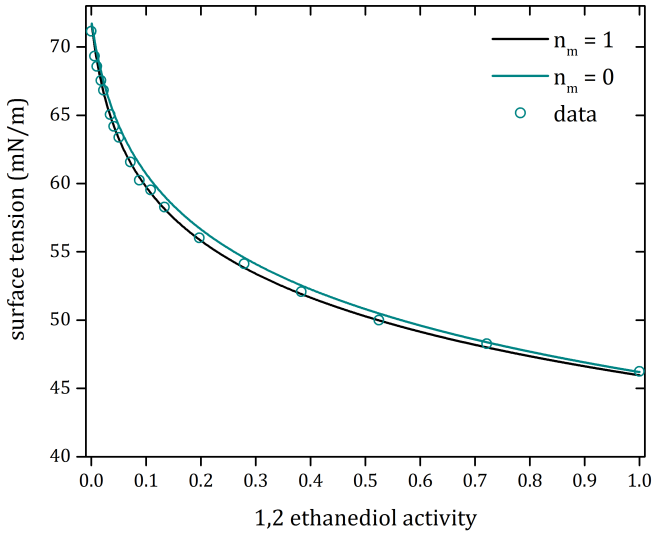

solute activity	surface tension (mN/m)	molality (mol/kg)	mole fraction	data reference
0	71.15	0	0	Nakanishi, *J. Chem. Eng. Data*, 1971
0.00597	69.33	0.4701	0.0084	
0.01038	68.58	0.8165	0.0145	
0.01779	67.54	1.3996	0.0246	
0.02248	66.84	1.7694	0.0309	
0.03444	65.04	2.7124	0.0466	
0.04099	64.19	3.2298	0.055	
0.0506	63.37	3.9915	0.0671	
0.07129	61.58	5.6429	0.0923	
0.08792	60.25	6.9852	0.1118	
0.10846	59.54	8.6683	0.1351	
0.13344	58.28	10.7596	0.1624	
0.1972	56.02	16.408	0.2282	
0.27918	54.13	24.6301	0.3074	
0.38322	52.08	37.5698	0.4037	
0.52488	49.99	63.5151	0.5337	
0.72146	48.28	143.1242	0.7206	
1	46.24	Inf	1	

n_m	r	K'	rmse
1	6.42	57.79	0.341
0	6.42	41.38	

1,2 propanediol

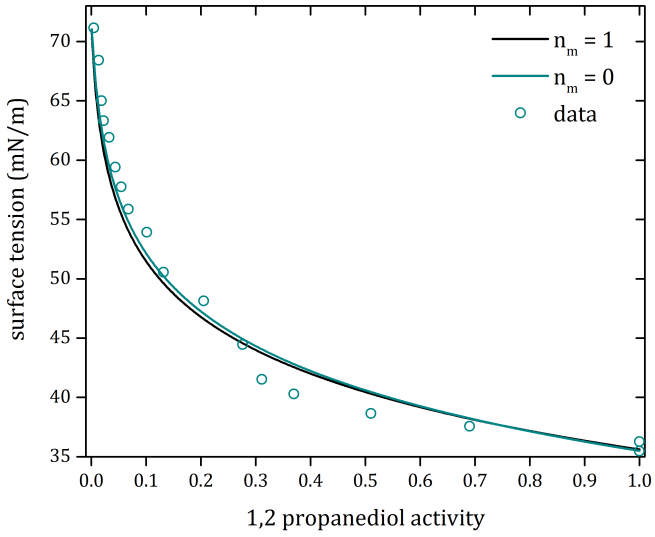

solute activity	surface tension (mN/m)	molality (mol/kg)	mole fraction	data reference
0.00475	71.15	0	0	Nakanishi, *J. Chem. Eng. Data*, 1971
0.01346	68.43	0.2397	0.0043	
0.01874	65	0.6854	0.0122	
0.02237	63.32	0.9597	0.017	
0.03266	61.92	1.1499	0.0203	
0.04367	59.41	1.6986	0.0297	
0.05443	57.75	2.3002	0.0398	
0.06762	55.88	2.9023	0.0497	
0.10142	53.92	3.6617	0.0619	
0.13199	50.56	5.7171	0.0934	
0.20532	48.13	7.7254	0.1222	
0.27627	44.46	13.2207	0.1924	
0.31144	41.53	19.6705	0.2617	
0.36967	40.28	23.3887	0.2965	
0.50997	38.64	30.5032	0.3547	
0.69033	37.56	54.8978	0.4973	
0.75	36.26	119.7869	0.6834	
1	35.46	Inf	1	

n_m	r	K'	rmse
1	5.82	173.6	1.88
0	5.82	133.6	

1,3 propanediol

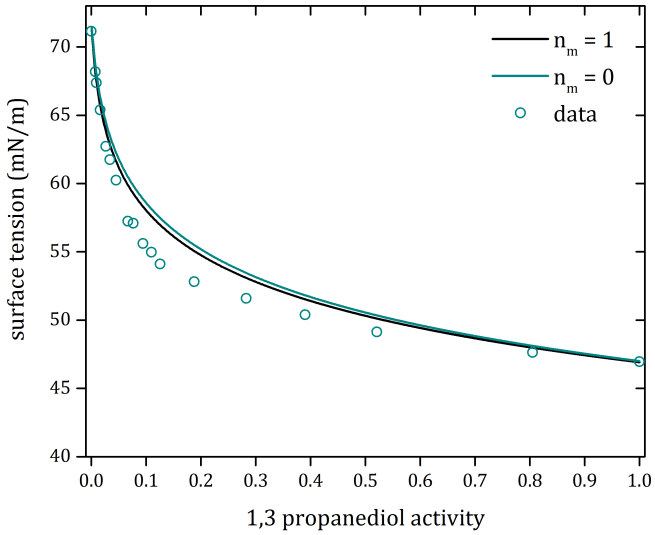

solute activity	surface tension (mN/m)	molality (mol/kg)	mole fraction	data reference
0.00748	68.18	0.3912	0.007	Nakanishi, *J. Chem. Eng. Data*, 1971
0.00939	67.38	0.4927	0.0088	
0.01635	65.38	0.868	0.0154	
0.02635	62.72	1.4229	0.025	
0.03419	61.74	1.8701	0.0326	
0.04531	60.25	2.5238	0.0435	
0.06696	57.25	3.8642	0.0651	
0.07644	57.1	4.4801	0.0747	
0.09422	55.6	5.6834	0.0929	
0.10984	54.97	6.7958	0.1091	
0.12589	54.11	7.993	0.1259	
0.18763	52.82	13.1527	0.1916	
0.28252	51.59	23.0648	0.2936	
0.39027	50.39	38.1351	0.4073	
0.52109	49.14	65.0402	0.5396	
0.80496	47.64	238.4356	0.8112	
1	46.95	Inf	1	

n_m	r	K'	rmse
1	8.28	156.8	0.986
0	8.28	121.7	

1,2 butanediol

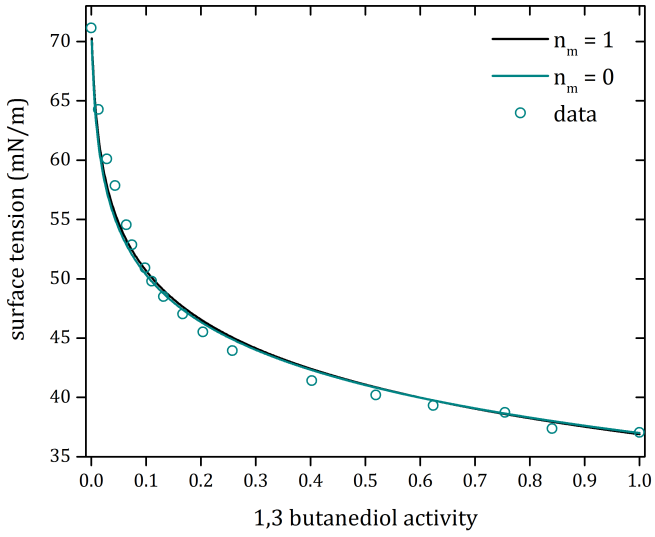

solute activity	surface tension (mN/m)	molality (mol/kg)	mole fraction	data reference
0.00748	68.18	0.3912	0.007	Nakanishi, *J. Chem. Eng. Data*, 1971
0.00939	67.38	0.4927	0.0088	
0.01635	65.38	0.868	0.0154	
0.02635	62.72	1.4229	0.025	
0.03419	61.74	1.8701	0.0326	
0.04531	60.25	2.5238	0.0435	
0.06696	57.25	3.8642	0.0651	
0.07644	57.1	4.4801	0.0747	
0.09422	55.6	5.6834	0.0929	
0.10984	54.97	6.7958	0.1091	
0.12589	54.11	7.993	0.1259	
0.18763	52.82	13.1527	0.1916	
0.28252	51.59	23.0648	0.2936	
0.39027	50.39	38.1351	0.4073	
0.52109	49.14	65.0402	0.5396	
0.80496	47.64	238.4356	0.8112	
1	46.95	Inf	1	

n_m	r	K'	rmse
1	8.28	156.8	0.986
0	8.28	121.7	

1,4 butanediol

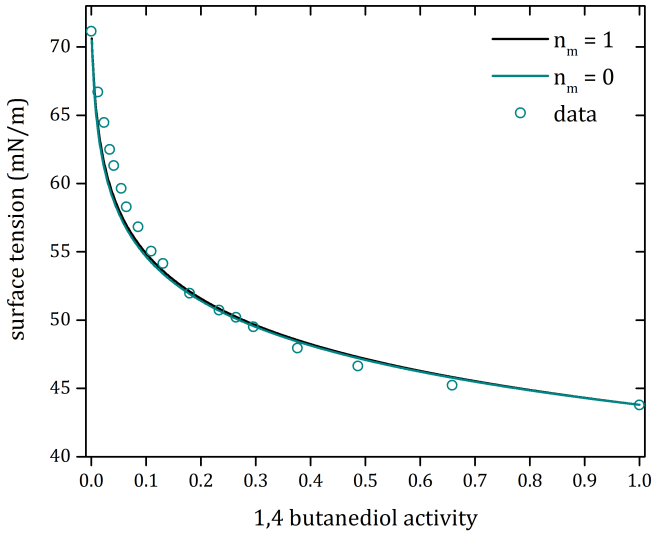

solute activity	surface tension (mN/m)	molality (mol/kg)	mole fraction	data reference
0.01304	64.27	0.3631	0.0065	Nakanishi, *J. Chem. Eng. Data*, 1971
0.02841	60.1	0.8108	0.0144	
0.04349	57.85	1.2715	0.0224	
0.06404	54.56	1.9354	0.0337	
0.07425	52.87	2.2822	0.0395	
0.09823	50.91	3.1429	0.0536	
0.11038	49.79	3.605	0.061	
0.13164	48.49	4.4599	0.0822	
0.16684	47.04	6.0156	0.0978	
0.20393	45.51	7.8698	0.1242	
0.25741	43.94	11.0057	0.1655	
0.40227	41.41	23.4673	0.2972	
0.51903	40.21	40.7828	0.4236	
0.62389	39.32	67.6617	0.5494	
0.75484	38.73	138.9486	0.7146	
0.84087	37.38	255.745	0.8217	
1	37.04	Inf	1	

n_m	r	K'	rmse
1	6.77	326.7	0.986
0	6.77	393.8	

sorbitol

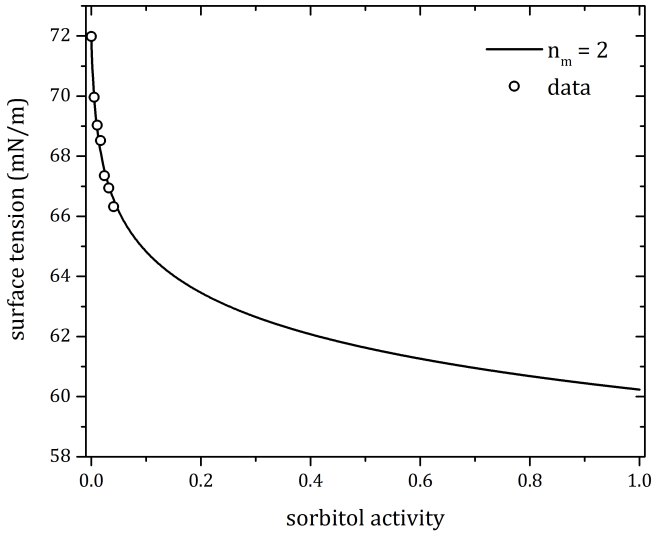

solute activity	surface tension (mN/m)	molality (mol/kg)	data reference
0.005178	69.96	0.2889	Yamada, *Int. J. Thermophys*, 1997
0.01087	69.03	0.6099	
0.017157	68.52	0.9687	
0.024138	67.35	1.3723	
0.031933	66.94	1.8298	
0.040692	66.32	2.3526	

n_m	r	K'	rmse
2	20.3	334.4	0.197

glycerol

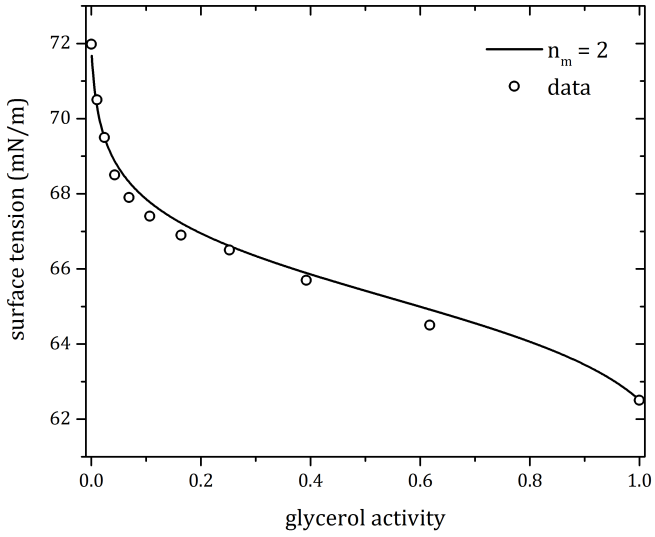

solute activity	surface tension (mN/m)	molality (mol/kg)	mole fraction	data reference
0.01048	70.5	1.2065	0.0213	Ernst, *J.Phys. Chem.* 1936
0.024216	69.5	2.7147	0.0466	
0.042784	68.5	4.6538	0.0774	
0.068781	67.9	7.2393	0.1154	
0.10659	67.4	10.8589	0.1637	
0.163647	66.9	16.2884	0.2269	
0.252307	66.5	25.3375	0.3135	
0.392425	65.7	43.4358	0.4391	
0.61744	64.5	97.7305	0.6378	
1	62.5	Inf	1	

n_m	r	K	C	rmse
1	32.5	0.91	331.07	0.0969

sucrose

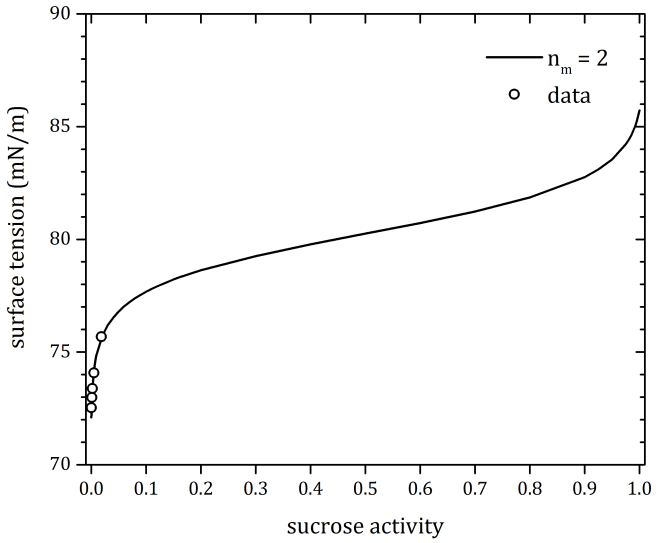

solute activity	surface tension (mN/m)	molality (mol/kg)	mole fraction	data reference
0.000367	72.53	0.9337	0.0165	Washburn, ICT
0.000998	72.98	2.1008	0.0365	
0.002205	73.38	3.6014	0.0609	
0.004824	74.08	5.6021	0.0917	
0.01821	75.68	10.2706	0.1562	

n_m	r	K	C	rmse
3	-34.7	0.99	1110.079	0.0468

Appendix D

Binary and Ternary Solution Treatments for Partially Dissociating Organic Acids

This appendix contains surface tension versus activity plots with surface tension data and model predictions for binary aqueous solutions of the following organic acids: acetic acid, formic acid, propionic acid, butyric acid, oxalic acid, malic acid, malonic acid, succinic acid, maleic acid, glutaric acid, and citric acid. Model parameters for 2, 1, and 0 parameter treatments are in Table 3.3 and 3.4.

Model predictions are presented using two parameters ($n_m = 2$), one parameter ($n_m = 1$) or zero parameters ($n_m = 0$).

The equation used for the $n_m = 3$ and $n_m = 2$ curves is equation 2.3:

$$\sigma = \sigma_w - \frac{kT}{rS_w} Ln(1 + Ka_s) \tag{D.1}$$

The equation used for the $n_m = 0$ curves is equation 3.16:

$$\sigma = \sigma_W - \frac{kT}{\bar{r}S_W} Ln\left(1 + \frac{C_{HA}K_{HA}a_{HA}}{(1 - K_{HA}a_{HA})} + \frac{C_{H^+A^-}K_{H^+A^-}a_{H^+A^-}}{(1 - K_{H^+A^-}a_{H^+A^-})}\right) \tag{D.2}$$

acetic acid

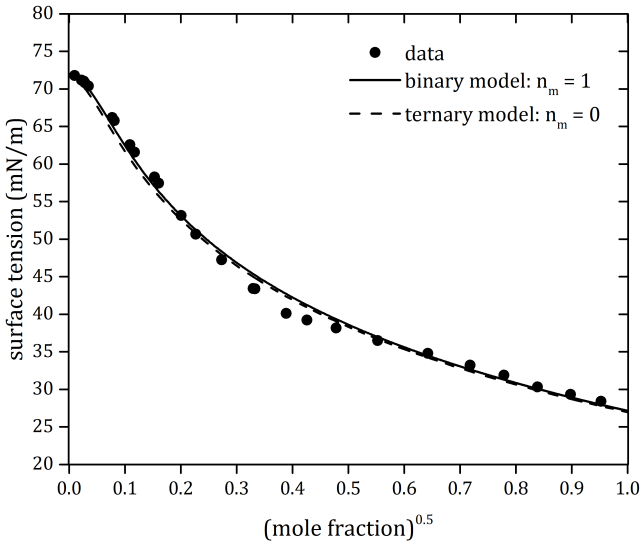

Surface tension data source	mole fraction	molality (mol/kg)	surface tension (mN/m)
Granados, 2006	0.0001	0.0055	71.79
	0.0005	0.0278	71.18
	0.0007	0.0389	71.04
	0.0008	0.0444	70.84
	0.0012	0.0667	70.37
	0.006	0.3350	66.17
	0.0066	0.3687	65.76
	0.0119	0.6683	62.57
	0.0138	0.7765	61.57
	0.0234	1.330	58.26
	0.0257	1.464	57.45
	0.0404	2.336	53.14
	0.0516	3.019	50.64
	0.0746	4.474	47.25
	0.1086	6.761	43.43
	0.1108	6.915	43.39
	0.1513	9.893	40.12
	0.1814	12.30	39.24
	0.2288	16.46	38.17
	0.3053	24.39	36.5
	0.4129	39.03	34.8
	0.516	59.16	33.23
	0.6068	85.64	31.87
	0.7035	131.7	30.32
	0.8067	231.6	29.32
	0.9076	545.1	28.42

formic acid

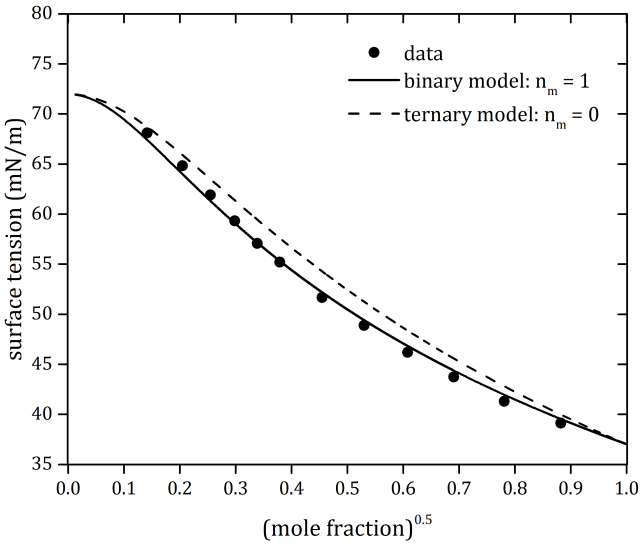

Surface tension data source	mole fraction	molality (mol/kg)	surface tension (mN/m)
Alvarez, 1997	0.02	1.133	68.11
	0.042	2.433	64.82
	0.065	3.858	61.91
	0.089	5.421	59.33
	0.115	7.211	57.07
	0.144	9.335	55.21
	0.207	14.49	51.68
	0.281	21.69	48.88
	0.37	32.59	46.18
	0.477	50.61	43.73
	0.61	86.80	41.31
	0.779	195.6	39.14

propionic acid

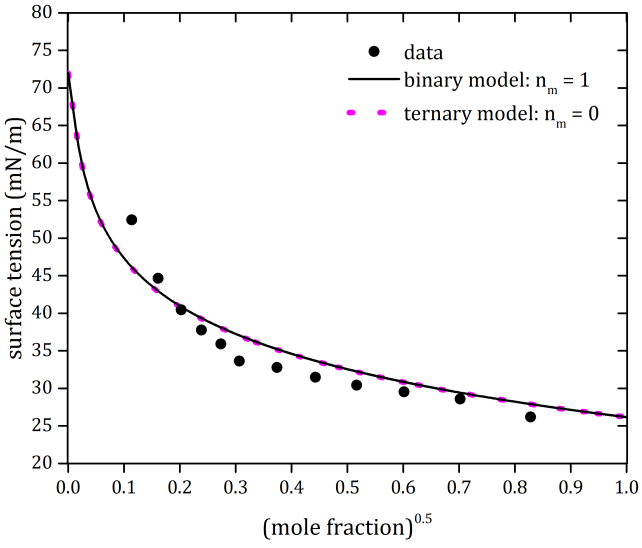

Surface tension data source	mole fraction	molality (mol/kg)	surface tension (mN/m)
Alvarez, 1997	0.013	0.730923	52.44
	0.026	1.481357	44.652
	0.041	2.372523	40.44
	0.057	3.35435	37.76
	0.075	4.499505	35.92
	0.094	5.757645	33.63
	0.14	9.03389	32.76
	0.196	13.52836	31.47
	0.267	20.21401	30.43
	0.362	31.48713	29.52
	0.493	53.96152	28.58
	0.686	121.2383	26.17

butyric acid

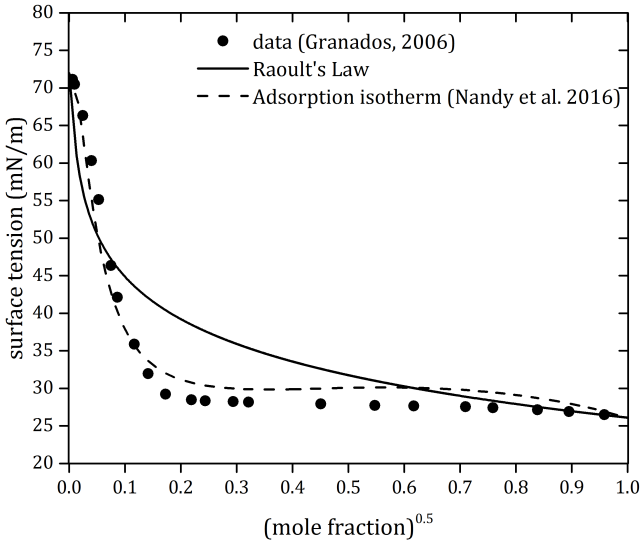

Surface tension data source	mole fraction	molality (mol/kg)	surface tension (mN/m)
Granados, 2006	0.0000	0.0022	71.12
	0.0001	0.0055	70.47
	0.0006	0.0333	66.32
	0.0016	0.0889	60.32
	0.0028	0.1558	55.12
	0.0056	0.3125	46.34
	0.0075	0.4193	42.12
	0.0136	0.7651	35.88
	0.0201	1.138	31.94
	0.0299	1.710	29.24
	0.0480	2.798	28.48
	0.0596	3.517	28.35
	0.0865	5.255	28.23
	0.1034	6.400	28.15
	0.2033	14.16	27.92
	0.2997	23.75	27.73
	0.3810	34.16	27.66
	0.5038	56.34	27.56
	0.5763	75.48	27.42
	0.7036	131.7	27.13
	0.8019	224.6	26.9
	0.9189	628.8	26.51

oxalic acid

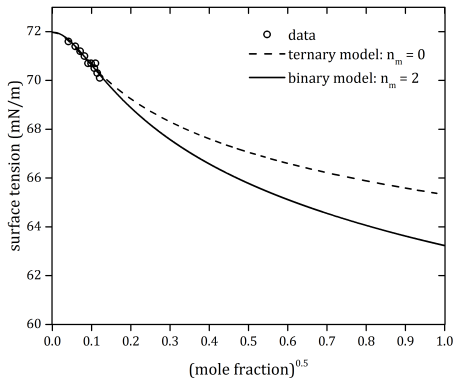

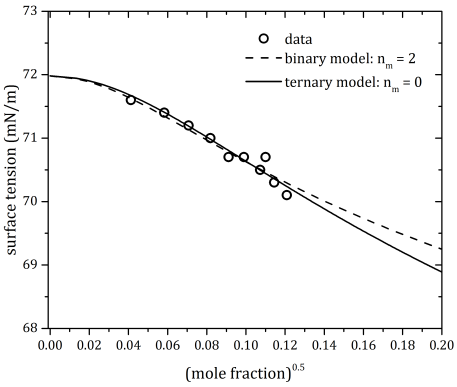

Data source	mole fraction	molality (mol/kg)	surface tension (mN/m)
Hyvarinen, 2006	0.0017	0.0945	71.6
	0.0034	0.1893	71.4
	0.0050	0.2789	71.2
	0.0067	0.3743	71
	0.0083	0.4645	70.7
	0.0098	0.5492	70.7
	0.0115	0.6456	70.5
	0.0121	0.6797	70.7
	0.0131	0.7366	70.3
	0.0146	0.8222	70.1

malic acid

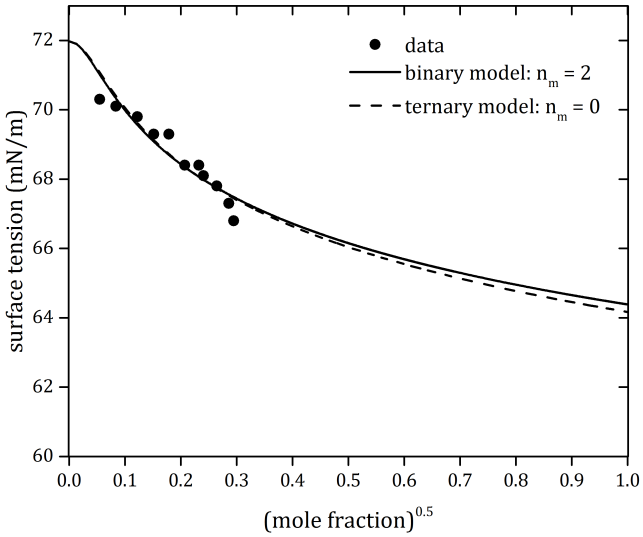

Data source	mole fraction	molality (mol/kg)	surface tension (mN/m)
Hyvarinen, 2006	0.003	0.1670	70.3
	0.007	0.3912	70.1
	0.015	0.8451	69.8
	0.023	1.306	69.3
	0.032	1.835	69.3
	0.043	2.493	68.4
	0.054	3.168	68.4
	0.058	3.417	68.1
	0.07	4.177	67.8
	0.082	4.957	67.3
	0.087	5.288	66.8

malonic acid

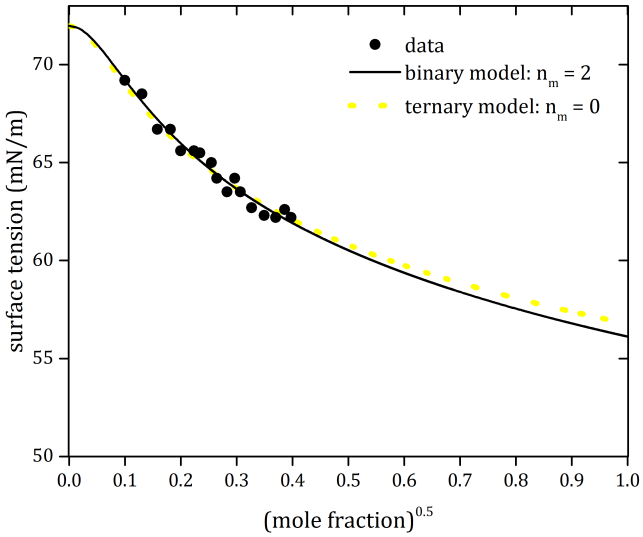

Data source	mole fraction	molality (mol/kg)	surface tension (mN/m)
Hyvarinen, 2006	0.01	0.561	69.2
	0.017	0.960	68.5
	0.025	1.42	66.7
	0.033	1.89	66.7
	0.04	2.31	65.6
	0.05	2.92	65.6
	0.055	3.23	65.5
	0.065	3.86	65
	0.07	4.18	64.2
	0.08	4.83	63.5
	0.088	5.35	64.2
	0.094	5.76	63.5
	0.107	6.65	62.7
	0.122	7.71	62.3
	0.137	8.81	62.2
	0.149	9.72	62.6
	0.158	10.41	62.2

succinic acid

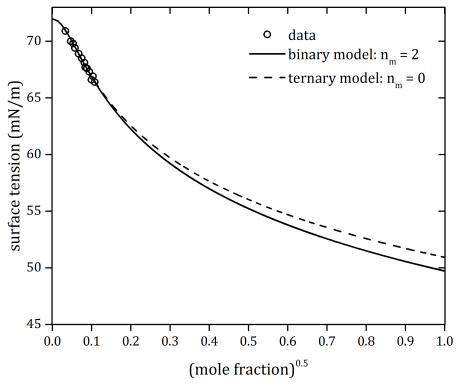

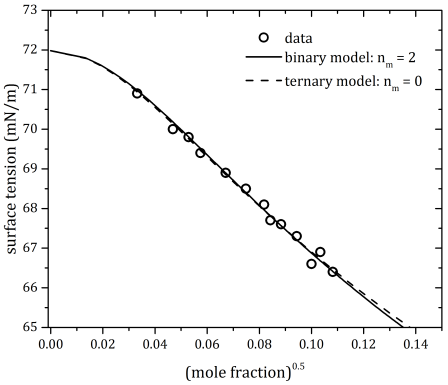

Data source	mole fraction	molality (mol/kg)	surface tension (mN/m)
Hyvarinen, 2006	0.01	0.561	69.2
	0.017	0.960	68.5
	0.025	1.42	66.7
	0.033	1.89	66.7
	0.04	2.31	65.6
	0.05	2.92	65.6
	0.055	3.23	65.5
	0.065	3.86	65
	0.07	4.18	64.2
	0.08	4.83	63.5
	0.088	5.35	64.2
	0.094	5.76	63.5
	0.107	6.65	62.7
	0.122	7.71	62.3
	0.137	8.81	62.2
	0.149	9.72	62.6
	0.158	10.41	62.2

maleic acid

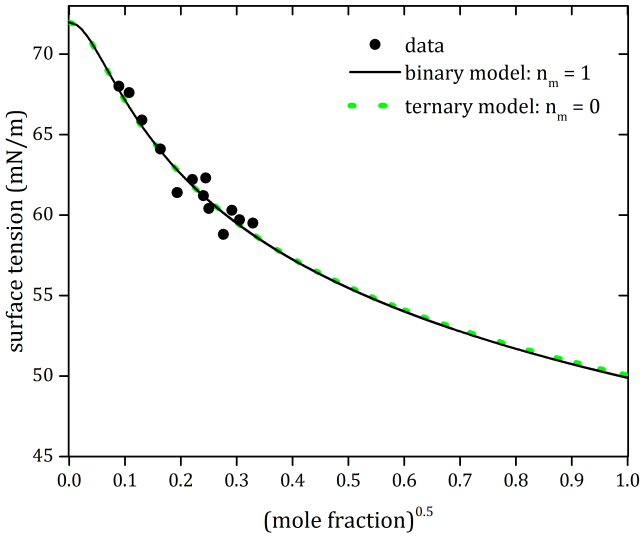

Data source	mole fraction	molality (mol/kg)	surface tension (mN/m)
Hyvarinen, 2006	0.008	0.447531	68
	0.0116	0.651284	67.6
	0.017	0.959711	65.9
	0.0267	1.522333	64.1
	0.0374	2.15611	61.4
	0.0376	2.168091	61.4
	0.0489	2.853172	62.2
	0.0579	3.410568	61.2
	0.06	3.542164	62.3
	0.0627	3.712224	60.4
	0.0764	4.590444	58.8
	0.085	5.155171	60.3
	0.0932	5.703607	59.7
	0.1083	6.739923	59.5

glutaric acid

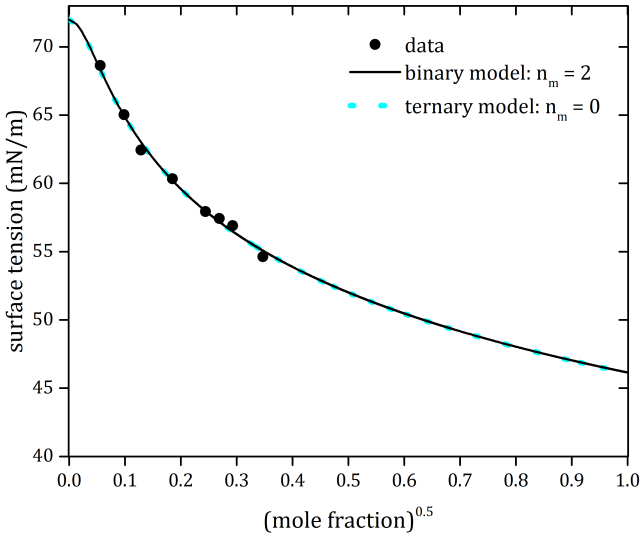

surface tension data source	mole fraction	molality (mol/kg)	surface tension (mN/m)
H.C.B., Wilhelmy plate	0.0031	0.1760	68.63
	0.0097	0.5460	65.03
	0.0166	0.9410	62.43
	0.0344	1.985	60.33
	0.0598	3.544	57.93
	0.0725	4.350	57.43
	0.0859	5.232	56.90
	0.1206	7.631	54.63

citric acid

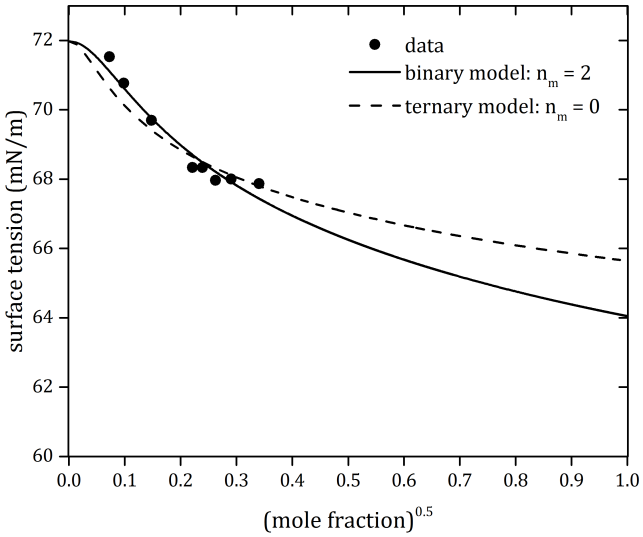

surface tension data source	mole fraction	molality (mol/kg)	surface tension (mN/m)
H.C.B., Wilhelmy plate	0.0053	0.295	71.53
	0.0096	0.54	70.77
	0.0219	1.24	69.70
	0.0488	2.85	68.33
	0.0573	3.37	68.33
	0.0688	4.1	67.97
	0.0843	5.11	68.00
	0.1160	7.28	67.87

Appendix E

MATLAB Fitting Routine for Aqueous Electrolyte Surface Tensions

%MATLAB code for surface tension model fitting routines for ELECTROLYTE binary aqueous solutions.

% (1) reads the raw data in a spreadsheet;

% (2) user sets the chemical species and the type of fitting desired (FitCase);

% (3) data and FitCase are sent to SurfaceTensionFunction_Electrolytes for the appropriate fitting, which returns parameter values and rmse;

% (4) data and model curve are plotted with plot_binaryElectrolytes

% CALLED FUNCTIONS

% SurfaceTensionFunction_Electrolytes

% plot_binaryElectrolytes

%SYMBOLS

% as: solute activity

% s: surface tension

```
% ss: pure solute surface tension
% sw: pure water surface tension
%kTbySw: kT/Sw = 41.0 J/m2̂ for water
% np: number of data points
% nm: number of model parameters
% clear commands, clear workspace, close figures
clc
clear all;
close all;
% DEFINE Range_activity, Range_surfacetension, filename, sheet
as = xlsread(filename,sheet, Range_activity);
s = xlsread(filename, sheet, Range_surfacetension);
data = [as; s];
np = length(as);
sw = 71.98;
kTbySw = 41.0;
constants = [sw kTbySw];
FitCase = 'nm = 3: r, K, ss';
switch(FitCase)
case 'nm = 3: r, K, ss'
r_start = -5;
K_start = 0.5;
ss_start = 100;
r_min = 0;
```

K_min = 0;

ss_min = 0;

r_max = Inf;

K_max = 0.99;

ss_max = Inf;

start_point = [r_start K_start ss_start];

min_point = [r_min K_min ss_min];

max_point = [r_max K_max ss_max];

modelValues = np;

model = @(params) SurfaceTensionFunction_Electrolytes(params, as, s, np);

options = optimoptions('fmincon', 'Algorithm', 'interior-point');

$$estimates, rmse$$

= fmincon(model, start_point, [],[],[],[], min_point, max_point, [], options);

r = estimates(1);

K = estimates(2);

ss = estimates(3);

C = 1 - (1 - (1 - K).*exp(r.*(sw - ss)./kTbySw))./K;

plot_binaryElectrolytes(as, s, r, K, C, ss, rmse, sw, kTbySw);

case 'nm = 2: r, K'

r_start = -5;

K_start = 0.5;

r_min = 0;

K_min = 0;

r_max = Inf;

K_max = 0.99;

ss = 150;

start_point = [r_start K_start];

min_point = [r_min K_min];

max_point = [r_max K_max];

modelValues = [np ss];

model = @(params)SurfaceTensionFunction_Electrolytes(params, data, constants,

FitCase, modelValues);

options = optimoptions('fmincon', 'Algorithm', 'interior-point');

$$estimates, rmse$$

= fmincon(model, start_point, [],[],[],[], min_point, max_point, [], options);

r = estimates(1);

K = estimates(2);

C = 1 - (1 - (1 - K).*exp(r.*(sw - ss)./kTbySw))./K;

plot_binaryElectrolytes(as, s, r, K, C, ss, rmse, sw, kTbySw);

case 'nm = 0'

r = -5;

K = 0.99;

C = 3000;

modelValues = [np K r C];

params = [];

rmse = SurfaceTensionFunction_Electrolytes(params, data, constants, FitCase,

modelValues);

plot_binaryElectrolytes(as, s, r, K, C, ss, rmse, sw, kTbySw);

end % end switchcase

```
% CALLED FUNCTIONS
% SurfaceTensionFunction_Electrolytes
function rmse = SurfaceTensionFunction_Electrolytes(params, data, constants,
FitCase, modelValues)
np = modelValues(1);
as = data(1,1:np);
s = data(2,1:np);
sw = constants(1);
kTbySw = constants(2);
switch(FitCase)
case 'nm = 3: r, K, ss'
%%
r = params(1);
K = params(2);
ss = params(3);
C = 1 - (1 - (1 - K).*exp(r.*(sw - ss)./kTbySw))./K;
FittedCurve = sw + (kTbySw./r).*log((1-K.*as)./(1-K.*as.*(1-C)));
ErrorVector = FittedCurve - s;
rmse = sqrt(sum(ErrorVector .^2)/np);
case 'nm = 2: r, K'
%%
r = params(1);
K = params(2);
ss = modelValues(2);
```

```
C = 1 - (1 - (1 - K).*exp(r.*(sw - ss)./kTbySw))./K;
FittedCurve = sw + (kTbySw./r).*log((1-K.*as)./(1-K.*as.*(1-C)));
ErrorVector = FittedCurve - s;
rmse = sqrt(sum(ErrorVector .^2)/np);
case 'nm = 1: r'
%%
r = params(1);
ss = modelValues(2);
K = modelValues(3);
C = 1 - (1 - (1 - K).*exp(r.*(sw - ss)./kTbySw))./K;
FittedCurve = sw + (kTbySw./r).*log((1-K.*as)./(1-K.*as.*(1-C)));
ErrorVector = FittedCurve - s;
rmse = sqrt(sum(ErrorVector .^2)/np);
case 'nm = 0'
%%
K = modelValues(2);
r = modelValues(3);
C = modelValues(4);
FittedCurve = sw + (kTbySw./r).*log((1-K.*as)./(1-K.*as.*(1-C)));
ErrorVector = FittedCurve - s;
rmse = sqrt(sum(ErrorVector .^2)/np);
end
```

```
% CALLED FUNCTIONS
% plot_binaryElectrolytes
function plot_binaryElectrolytes(as, s, r, K, C, ss, rmse, sw, kTbySw)
subplot(1,3,1)
plot(as, s, '*')
hold on
FittedCurve = sw + (kTbySw./r).*log((1-K.*as)./(1-K.*as.*(1-C)));
plot(as, FittedCurve, 'r')
xlabel('solute activity')
ylabel('
sigma mN/m');
subplot(1,3,2)
plot(as, s, '*')
as = 0.001:0.001:0.999;
FittedCurve = sw + (kTbySw./r).*log((1-K.*as)./(1-K.*as.*(1-C)));
hold on
plot(as, FittedCurve, 'r')
xlabel('as');
subplot(1,3,3);
text(0.3, 0.85, ['r = ', num2str(r)], 'FontSize', 12);
text(0.3, 0.8, ['K = ', num2str(K)],'FontSize', 12);
text(0.3, 0.75, ['ss = ', num2str(ss)],'FontSize', 12);
text(0.3, 0.7, ['C =', num2str(C)],'FontSize', 12);
text(0.3, 0.65, ['rmse = ', num2str(rmse)],'FontSize', 12);
```

hold off

end

Appendix F

MATLAB Fitting Routine for Aqueous Organic Surface Tensions

%MATLAB code for surface tension model fitting routines for ORGANIC binary aqueous solutions.

% (1) reads the raw data in a spreadsheet;

% (2) user sets the chemical species and the type of fitting desired (FitCase);

% (3) data and FitCase are sent to SurfaceTensionFunction_Organics for the appropriate fitting, which returns parameter values and rmse;

% (4) data and model curve are plotted with plot_binaryOrganics or plot_binaryOrganics_fullModel

% CALLED FUNCTIONS

% SurfaceTensionFunction_Organics

% plot_binaryOrganics

% plot_binaryOrganics_fullModel

%SYMBOLS

% as: solute activity

```
% s: surface tension
% ss: pure solute surface tension
% sw: pure water surface tension
%kTbySw: kT/Sw = 41.0 J/m2̂ for water
% np: number of data points
% nm: number of model parameters
% clear commands, clear workspace, close figures
clc
clear all;
close all;
% DEFINE Range_activity, Range_surfacetension, filename, sheet
as = xlsread(filename,sheet, Range_activity);
s = xlsread(filename, sheet, Range_surfacetension);
data = [as; s];
np = length(as);
sw = 71.98;
kTbySw = 41.0;
constants = [sw kTbySw];
FitCase = 'nm = 3: r, K, ss';
switch(FitCase)
case 'Reduced equation: nm = 2: r, ss(K)'
r_start = 5;
ss_start = 20;
r_min = 0;
```

```
ss_min = 0;
r_max = Inf;
ss_max = Inf;
start_point = [r_start ss_start];
min_point = [r_min ss_min];
max_point = [r_max ss_max];
modelValues = np;
model = @(params) SurfaceTensionFunction_Organics(params, data, constants,
FitCase, modelValues);
options = optimoptions('fmincon', 'Algorithm', 'interior-point');
[estimates, rmse] = fmincon(model, start_point, [],[],[],[], min_point, max_point, [],
options);
r = estimates(1);
ss = estimates(2);
K = exp(r.*(sw - ss)./kTbySw) - 1;
C = [];
plot_binaryOrganics(as, s, r, K, C, ss, rmse, sw, kTbySw, FitCase);
case 'Reduced equation: nm = 1: r(K)'
K = 100;
r_start = 5;
r_min = 0;
r_max = Inf;
start_point = r_start;
min_point = r_min;
```

max_point = r_max;

modelValues = [np K];

model = @(params) SurfaceTensionFunction_Organics(params, data, constants,

FitCase, modelValues);

options = optimoptions('fmincon', 'Algorithm', 'interior-point');

[estimates, rmse] = fmincon(model, start_point, [],[],[],[], min_point, max_point, [],

options);

r = estimates(1);

C = [];

plot_binaryOrganics(as, s, r, K, C, ss, rmse, sw, kTbySw);

case 'Reduced equation: nm = 0'

r = 5;

K = 100;

ss = 22;

modelValues = [np K r];

params = [];

rmse = SurfaceTensionFunction_Organics(params, data, constants, FitCase,

modelValues);

C = [];

plot_binaryOrganics(as, s, r, K, C, ss, rmse, sw, kTbySw, FitCase);

case 'Full equation: nm = 3: r, K, ss'

r_start = 5;

K_start = 0.5;

ss_start = 20;

r_min = 0;

K_min = 0;

ss_min = 0;

r_max = Inf;

K_max = 0.99;

ss_max = Inf;

start_point = [r_start K_start ss_start];

min_point = [r_min K_min ss_min];

max_point = [r_max K_max ss_max];

modelValues = np;

model = @(params)SurfaceTensionFunction_Organics(params, data, constants,

FitCase, modelValues);

options = optimoptions('fmincon', 'Algorithm', 'interior-point');

[estimates, rmse] = fmincon(model, start_point, [],[],[],[], min_point, max_point, [],

options);

r = estimates(1);

K = estimates(2);

ss = estimates(3);

C = 1 - (1 - (1 - K).*exp(r.*(sw - ss)./kTbySw))./K;

plot_binaryOrganics_fullModel(as, s, r, K, C, ss, rmse, sw, kTbySw, FitCase);

case 'Full equation: nm = 2: r, K'

ss = 50;

r_start = 5;

K_start = 0.5;

```
r_min = 0;
K_min = 0;
r_max = Inf;
K_max = 0.99;
start_point = [r_start K_start];
min_point = [r_min K_min];
max_point = [r_max K_max];
modelValues = [np ss];
model = @(params)SurfaceTensionFunction_Organics(params, data, constants,
FitCase, modelValues);
options = optimoptions('fmincon', 'Algorithm', 'interior-point');
[estimates, rmse] = fmincon(model, start_point, [],[],[],[], min_point, max_point, [],
options);
r = estimates(1);
K = estimates(2);
C = 1 - (1 - (1 - K).*exp(r.*(sw - ss)./kTbySw))./K;
plot_binaryOrganics_fullModel(as, s, r, K, C, ss, rmse, sw, kTbySw, FitCase);
% CALLED FUNCTIONS
% SurfaceTensionFunction_Organics
function rmse = SurfaceTensionFunction_Organics(params, data, constants,
FitCase, modelValues)
np = modelValues(1);
as = data(1:np,1);
s = data(1:np,2);
```

```
sw = constants(1);
kTbySw = constants(2);
switch(FitCase)
case 'Reduced equation: nm = 2: r, K(ss)'
r = params(1);
ss = params(2);
K = exp(r.*(sw - ss)./kTbySw) - 1;
FittedCurve = sw - (kTbySw./r).*log((1+K.*as));
ErrorVector = FittedCurve - s;
rmse = sqrt(sum(ErrorVector .^2)/np);
case 'Reduced equation: nm = 1: r(K)'
r = params(1);
ss = modelValues(2);
K = exp(r.*(sw - ss)./kTbySw) - 1;
FittedCurve =sw - (kTbySw./r).*log((1+K.*as));
ErrorVector = FittedCurve - s;
rmse = sqrt(sum(ErrorVector .^2)/np);
case 'Reduced equation: nm = 0'
r = modelValues(2);
K = modelValues(3);
FittedCurve =sw - (kTbySw./r).*log((1+K.*as));
ErrorVector = FittedCurve - s;
rmse = sqrt(sum(ErrorVector .^2)/np);
case 'Full equation: nm = 3: r, K, ss'
```

```
r = params(1);
K = params(2);
ss = params(3);
C = 1 - (1 - (1 - K).*exp(r.*(sw - ss)./kTbySw))./K;
FittedCurve = sw + (kTbySw./r).*log((1-K.*as)./(1-K.*as.*(1-C)));
ErrorVector = FittedCurve - s;
rmse = sqrt(sum(ErrorVector .^2)/np);
case 'Full equation: nm = 2: r, K'
r = params(1);
ss = modelValues(2);
K = exp(r.*(sw - ss)./kTbySw) - 1;
FittedCurve =sw - (kTbySw./r).*log((1+K.*as));
ErrorVector = FittedCurve - s;
rmse = sqrt(sum(ErrorVector .^2)/np);
end
% CALLED FUNCTIONS
% plot_binaryOrganics
function plot_binaryOrganics(as, s, r, K, C, ss, rmse, sw, kTbySw, FitCase)
subplot(1,2,1)
plot(as, s, '*')
hold on
plot(as, s, '*')
as = 0.001:0.001:0.99;
FittedCurve = sw - (kTbySw./r).*log(1+K.*as);
```

```
hold on
plot(as, FittedCurve, 'r')
xlabel('solute activity')
ylabel('
sigma mN/m')
subplot(1,2,2);
text(0.3, 0.85, ['r = ', num2str(r)], 'FontSize', 12);
text(0.3, 0.8, ['K = ', num2str(K)],'FontSize', 12);
text(0.3, 0.75, ['ss = ', num2str(ss)],'FontSize', 12);
text(0.3, 0.7, ['C =', num2str(C)],'FontSize', 12);
text(0.3, 0.65, ['rmse = ', num2str(rmse)],'FontSize', 12);
hold off
% CALLED FUNCTIONS
% plot_binaryOrganics_fullModel
function plot_binaryOrganics_fullModel(as, s, r, K, C, ss, rmse, sw, kTbySw,
FitCase)
subplot(1,2,1)
plot(as, s, '*')
hold on
subplot(1,2,1)
plot(as, s, '*')
as = 0.001:0.001:0.99;
FittedCurve = sw + (kTbySw./r).*log((1-K.*as)./(1-K.*as.*(1-C)));
hold on
```

```
plot(as, FittedCurve, 'r')
xlabel('solute activity')
ylabel('
sigma mN/m')
subplot(1,2,2);
text(0.3, 0.85, ['r = ', num2str(r)], 'FontSize', 12);
text(0.3, 0.8, ['K = ', num2str(K)],'FontSize', 12);
text(0.3, 0.75, ['ss = ', num2str(ss)],'FontSize', 12);
text(0.3, 0.7, ['C =', num2str(C)],'FontSize', 12);
text(0.3, 0.65, ['rmse = ', num2str(rmse)],'FontSize', 12);
hold off
end
```